



Martin-Luther-Universität Halle-Wittenberg

---

# Electrospinning of polymeric nanofibers and nanocomposite materials: Fabrication, physicochemical characterization and medical applications

Dissertation

zur Erlangung des akademischen Grades  
Doktor rerum naturalium (Dr. rer. nat.)

vorgelegt der

**Naturwissenschaftlichen Fakultät II - Chemie, Physik und Mathematik**

der Martin-Luther-Universität, Halle-Wittenberg

von Herrn Ashraf Shaban Asran Abdel Sayed

geb. am: 15/10/1976 in: Kairo

Gutachter:

1- Prof. Dr. Goerg H. Michler (Halle/Saale)

2- Prof. Dr. W. Mormann (Siegen)

**Halle (Saale), 9 February 2011**



## Dedicated to my family

This dissertation is dedicated to my beloved parents especially my mother whose prayers & encouragement have been always with me. I am indebted to them for their support, guidance and encouragement. I would like also to dedicate my thesis to my brother Mohammed and my sisters Ekram, Shaimaa and their lovely kids. Special dedication to my beloved sister Fayza, my wife Marwa and my son Mohammed.



## Acknowledgements

I feel indebted to many people whom, without their support, cooperation or guidance, this work would have never been completed in its present form.

First and foremost I would like to express my heartfelt gratitude towards my supervisor **Prof. Dr. rer. nat. habil. Goerg. H. Michler** for giving me the opportunity to work under his supervision and also for his academic guidance, continuous support and encouragement throughout this project. I appreciate his generosity in providing me the opportunity to attend various conferences that gave me good academic exposure. He has been very cooperative all along and gave me his precious time and advice whenever I needed it.

I am also indebted to **Prof. Dr. rer. nat. habil. Thomas Groth** at Institute of Pharmacy for giving me the opportunity to investigate the cell culture experiments at his prominent group. I have learned so much from his useful suggestions and comments during my experimental work.

I do appreciate all kind members of general materials science group especially **Dipl.-Phys. Volker Seydewitz, Dipl.-Ing. Sylvia Goerlitz** and **Dipl.-Ing. Stefanie Scholtyssek** for their assistance with the transmission electron microscopy investigations. I am grateful to **Dr. rer. nat. Reinhold Godehardt, Dipl.-Phys. Werner Lebek, Dipl.-Ing. Wolfgang Schurz, Frau Cornelia Becker** and **Frau Birgit Erfurt** for providing a quite friendly and helpful working environment and solving my day to day problems. I wish also to express my sincere gratitude to **Dr. rer. nat. Sven Henning** and **M.Sc. Imam Khasim H-R**. I would like also to thank **Dr. Andre´ Wutzler** for giving me the opportunity to conduct the FTIR, DSC and TGA experiments at the group of **Prof. Dr.-Ing. habil. Hans-Joachim Radusch**. Special thanks to **Prof. Dr. Karl-Ernst Dette** at the Faculty of Dentistry for giving me the opportunity to cooperate with his group. For funding and hosting of my research I would like to thank the **Egyptian ministry of higher education and scientific research**.

Finally, I would like to express my deepest gratitude to my beloved family who always took pride in my academic achievements and facilitated me in all the ways possible. I also want to thank my lovely wife. Without my family's love and support, this work would have never been finished. No words can express my gratitude to them.

**Last, but by no means least, I thank God.**



## **Declaration**

I certify that this work has been carried out and written up entirely by myself.  
No literature references and resources other than those cited have been used.  
The present thesis was never submitted to departments of other universities.

**Halle (Saale)**

**Ashraf Sh Asran**



# Table of contents

<b>List of Figures</b> .....	<b>iv</b>
<b>List of Tables</b> .....	<b>vii</b>
<b>List of Abbreviations</b> .....	<b>viii</b>
<b>1. Introduction and objectives</b> .....	<b>1</b>
<b>2. Background and literature review</b> .....	<b>5</b>
2.1. Preface of nanotechnology .....	5
2.2. Nanofibers.....	6
2.3. Nanofibers fabrication methods.....	6
2.3.1. Drawing .....	7
2.3.2. Template synthesis .....	7
2.3.3. Phase separation .....	7
2.3.4. Self assembly .....	8
2.3.5. Splittable bicomponent fibers.....	8
2.4. Electrostatic spinning (Electrospinning) .....	8
2.4.1. History of electrospinning .....	9
2.4.2. Electrospinning Process.....	10
2.4.3. Parameters affecting electrospinning process.....	12
2.4.4. Different morphology of nanofibers.....	12
2.4.5. Properties and potential applications of nanofibers.....	15
2.4.6. Aligned nanofibers .....	16
2.4.7. Nanofibers blends and their phase morphology .....	17
2.4.8. Nanofiber nanocomposites .....	17
2.4.9. Biomimetic nanocomposite nanofibers .....	18
<b>3. Materials and experimental Methods</b> .....	<b>20</b>
3.1. Materials .....	20
3.1.1. Materials for electrospinning fibers.....	20
3.1.2. Types of cells for cell culture .....	20
3.2. Experimental .....	22
3.2.1. Electrospinning apparatus setup .....	22
3.2.2. Hot compaction of aligned polystyrene nanofibers.....	23
3.3. Characterization methods .....	23
3.3.1. Scanning electron microscopy (SEM).....	23
3.3.2. Transmission electron microscope (TEM) .....	24
3.3.3. Image analysis .....	25
3.3.4. In situ deformation of polystyrene nanofibers.....	25
3.3.5. Thermal investigations .....	27
▪ Differential scanning calorimetry (DSC) .....	27
▪ Thermo gravimetric analysis (TGA) .....	28
3.3.6. Fourier Transform Infrared spectroscopy (FTIR) .....	28

3.3.7. Water contact angle measurements (WCA)	29
3.3.8. Zeta potential	29
3.4. Biological tests	30
3.4.1. Degradation measurements	30
3.4.2. Sterilization of nanofibrous matrices	30
3.4.3. Cells harvesting	31
3.4.4. Cells adhesion and proliferation investigation	31
<b>4. Results and discussion</b>	<b>33</b>
4.1. Electrospinning novel fibers with different morphologies for spread applications	33
4.1.1. Electrospun fibers with porous structure	33
4.1.2. Electrospun fibers with bead and ribbon-like structures	34
4.1.3. Electrospun fibers with helical and twisted structures	35
4.1.4. Electrospun fibers with rough surface	36
4.1.5. Electrospun fibers with core sheath structure	37
4.2. Mechanical properties of PS nanofibers	44
4.2.1. Morphology	45
4.2.2. Deformation of single electrospun PS nanofibers	47
4.2.3. Deformation of compacted PS nanofibers	50
4.2.4. Thermal analysis (DSC)	53
4.2.5. Discussion and conclusions	53
4.3. Electrospun PMMA/EVA nanofibers for dentistry applications (custom-made mouth guards and dentures)	57
4.3.1. Morphology of electrospun PMMA/EVA	58
4.3.2. Manufacturing of mouth guards	58
4.3.3. Phase separation of PMMA/EVA at the nano scale	61
4.3.4. Measuring the interfacial strength (bond) between soft liner (EVA) and denture base (PMMA)	63
4.3.5. The bond between EVA (soft liner) and PMMA (denture base) materials	64
4.4. Nanofibers for bone tissue engineering	66
4.4.1. Crystalline structure and morphology of HAp and the electrospun NCNFs	67
4.4.2. FTIR measurements	70
4.4.3. DSC measurements	74
4.4.4. TGA and DTGA	77
4.5. Nanofibers from blends of polyvinyl alcohol and polyhydroxy butyrate as potential scaffolds material for tissue engineering of skin	80
4.5.1. Morphology of electrospun PVA/PHB blended nanofibers	82
4.5.2. Phase morphology characterization of electrospun PVA/PHB	84
4.5.3. Water contact angle (WCA) measurements	85
4.5.4. Zeta potential	87
4.5.5. Fourier transform infrared spectroscopy (FTIR)	90
4.5.6. Differential scanning calorimetry (DSC)	91
4.5.7. TGA and first order derivatives of TGA	92

4.5.7. In vitro degradation of electrospun PVA/PHB nanofibrous scaffold.....	95
4.5.9. Adhesion and proliferation of epidermal and dermal cells on the nanofibers	97
▪ HaCaT cells .....	97
▪ Dermal fibroblasts cells .....	99
<b>5. Summary and conclusions .....</b>	<b>103</b>
<b>6. References .....</b>	<b>107</b>
<b>List of publications .....</b>	<b>I</b>
<b>Curriculum Vitae .....</b>	<b>IV</b>

## List of Figures

Fig. 1. Electrospinning apparatus.....	11
Fig. 2. A schematic diagram showing (a) cortical shell bone and a cancellous bone structures, and (b) the lowest level of hierarchical organization.....	19
Fig. 3. Electrospinning setup (a) square metal plate used as fibers collector (b) metal rotating drum used as fibers collector .....	22
Fig. 4. Schematic illustration of parallel electrodes method for aligned nanofibers preparation.....	23
Fig. 5. In situ deformation devices.....	26
Fig. 6. Electrospun PLLA/PEO (80/20) fibers have a porous structure after selective removal of PEO.....	34
Fig. 7. Electrospun Polyetherimide using N-methyl 2-pyrrolidone as a solvent .....	35
Fig. 8. Electrospun Polyethimide using chloroform as a solvent.....	35
Fig. 9. Electrospun PET/ $\gamma$ -Fe <sub>2</sub> O <sub>3</sub> (ferromagnetic iron oxide nanoparticles) nanocomposites fibers with twisted structure .....	36
Fig. 10. Electrospun PEO/ $\gamma$ -Fe <sub>2</sub> O <sub>3</sub> (ferromagnetic iron oxide nanoparticles) nanocomposites fibers with helical structure .....	36
Fig. 11. Electrospun PEI/EVA with different ratios .....	37
Fig. 12. SEM micrograph of (a) electrospun CTS nanofibers using TFA/DCM as a solvent and (b) electrospun PHB/CTS nanofibers using TFA/HFIP as a solvent .....	38
Fig. 13. Diameter distribution of electrospun (a) PHB/CTS (50/50) using HFIP/TFA as a solvent and (b) Chitosan using TFA/DCM .....	39
Fig. 14. Electrospun PHB/CTS blend nanofibers, stained with OsO <sub>4</sub> vapors for 4 days (fibers thinner than 500 $\mu$ m) .....	39
Fig. 15. Electrospun PHB/CTS blend nanofibers, stained with OsO <sub>4</sub> vapors for 4 days (fibers thicker than 500 $\mu$ m).....	39
Fig. 16. FTIR spectra of electrospun (a) pure PHB, (b) PHB/CTS (50/50) and (c) pure CTS nanofibers, the marked peaks represent the crystalline phase of PHB.....	41
Fig. 17. DSC thermograms of (a) PHB powder, (b) electrospun PHB and (c) PHB/CTS (50/50) nanofibers .....	42
Fig. 18. SEM images showing in vitro morphology changes of electrospun PHB/CTS (50/50) blend nanofibers after one week degradation in PBS solution at 37 °C.....	43
Fig. 19. SEM micrograph of electrospun PS nanofibers.....	45
Fig. 20. Diameter distribution of PS nanofibers .....	46
Fig. 21. SEM micrograph of uniaxially PS nanofibers.....	46
Fig. 22. Morphology of a pattern of hot compacted PS nanofibers .....	46
Fig. 23. TEM micrographs of deformed PS nanofibers with fibrillated crazes .....	47
Fig. 24. Distribution of craze thickness, craze fibril diameter and interfibrillar distance (long period) in deformed PS nanofibers .....	48
Fig. 25. Deformed PS nanofibers in ESEM micrographs: Local necking zones are shown by arrows.....	48
Fig. 26. TEM micrographs of deformed PS nanofibers with necking and cold drawing zones in lower (left) and larger magnification (right): image rotating due to change in magnification in TEM.....	49
Fig. 27. Deformation of hot compacted aligned PS nanofibers in SEM compacted at 85 °C with a pressure of 30 MPa for 5 min.....	51
Fig. 28. Deformation of hot compacted aligned PS nanofibers in SEM compacted at 85 °C with a pressure of 30 MPa for 5 min.....	51

Fig. 29. Distribution of craze thickness, craze fibril diameter and interfibrillar distance of deformed hot compacted PS nanofibers (hot compacted at 85 °C, 30 MPa for 5 min).....	52
Fig. 30. Schematic illustration of micromechanical deformation mechanism of PS in dependence on sample thickness .....	55
Fig. 31. Entanglements and entanglement network in amorphous polymers; $M_e$ , $l_e$ are the molecular .....	56
Fig. 32. Scheme of change in the deformation mechanism of PS with decreasing sample thickness from bulk material to nanofibers .....	56
Fig. 33. SEM micrographs of electrospun PMMA/EVA (50/50) with different concentration ratios of the solutions : (a) 15 wt %, (b) 18 wt% and (c) 20 wt% .....	59
Fig. 34. SEM micrograph showing the morphology and diameter distribution of electrospun PMMA/EVA (50/50) using $\text{CHCl}_3/\text{DMF}$ (80/20) as a solvent.....	60
Fig. 35. Photo image of polymerized PMMA on the EVA plate using PMMA/EVA (50/50) nanofiber as an interface between them .....	60
Fig. 36. TEM micrographs showing the phase separation of PMMA/EVA blend at the nano range, the fibers stained with $\text{RuO}_4$ vapours for 4 days .....	62
Fig. 37. Interfacial strength (adhesion) between heat cured PMMA and EVA plate, the surface of EVA plate is smooth.....	63
Fig. 38. Effect of the surface roughness on the bond strength .....	64
Fig. 39. TEM micrographs showing the contact layer between EVA plate and heat cured PMMA using electrospun PMMA/EVA 40 (30/70) nanofibers mat as an interface between them, the sample was stained with $\text{RuO}_4$ vapours for 4 days.....	65
Fig. 40. TEM micrograph of HAp nanorods .....	67
Fig. 41. Size diameters distribution of n- HAp nanorods.....	67
Fig. 42. TEM micrograph for electrospun PVA nanofibers .....	68
Fig. 43. Diameter distribution of (a) electrospun PVA, (b) PVA/n-HAp, (c) PVA/Col and (d) PVA/Col /n-HAp .....	68
Fig. 44. TEM micrograph of electrospun PVA/n-HAp nanocomposite nanofiber .....	69
Fig. 45. TEM micrograph of electrospun PVA/Col nanofibers .....	69
Fig. 46. TEM micrograph for electrospun (a) PVA/Col/n-HAp and (b) back scattered SEM micrograph for aligned electrospun PVA/Col/n-HAp.....	70
Fig. 47. Photograph of PVA/Col/n-HAp biocomposite nanofibrous scaffold .....	70
Fig. 48. FTIR spectra of n-HAp nanorods.....	71
Fig. 49. FTIR spectra for solutions of (a) Col, (b) Col/n-HAp and electrospun fibers of (c) PVA, (d) PVA/n-HAp, (e) PVA/Col and (f) PVA/Col/n-HAp.....	71
Fig. 50. (a) DSC curves for PVA granules,(b) electrospun PVA, (c) PVA/n-HAp, (d) Col, (e) PVA/Col and (f) PVA/Col/n-HAp.....	74
Fig. 51. Suggested hydrogen bonds between Col, n-HAp and PVA.....	77
Fig. 52. TGA thermogram for (a) Col, (b) electrospun PVA, (c) PVA/n-HAp, (d) PVA/Col and (e) PVA/Col/n-HAp.....	78
Fig. 53. First order derivatives TGA for (a) Col, (b) electrospun PVA, (c) PVA/n-HAp, (d) PVA/Col and (e) PVA/Col/n-HAp.....	78
Fig. 54. SEM micrographs of the electrospun fibers of (a) pure PHB, (b) PVA/PHB (50/50) and (c) pure PVA using HFIP as a solvent for both polymers .....	83
Fig. 55. Fiber diameter distribution of electrospun mats of (a) pure PHB and (b) PVA/PHB (50/50) blend nanofibers.....	84
Fig. 56. TEM micrograph of chemically stained PVA/PHB (50/50) nanofibers, stained with $\text{OsO}_4$ vapor for 4 days (a, b) in a lower and higher magnification (fibers have an average diameter less than 1.5 $\mu\text{m}$ ).....	85

Fig. 57. TEM micrograph of chemically stained PVA/PHB (50/50) nanofibers, stained with OsO <sub>4</sub> vapor for 4 days (fibers have an average diameter more than 1.5 μm) .....	85
Fig. 58. Zeta potential vs. pH for films of (□) pure PHB, (×) PVA/PHB (05/95), (※) PVA/PHB (10/90), (Δ) PVA/PHB (30/70) and (O) PVA/PHB (50/50) .....	87
Fig. 59. TGA thermograms for electrospun pure PVA, pure PHB and their blends with different ratios .....	93
Fig. 60. DTGA thermograms for electrospun pure PVA, pure PHB and their blends with different ratios .....	95
Fig. 61. Degradation of electrospun nanofibrous mats of PHB, PVA/PHB (05/95), PVA/PHB (10/90), PVA/PHB (30/70) and PVA/PHB (50/50), degradation were measured by weighting the nanofibers scaffolds after degradation in phosphate-buffered saline within 3 months .....	96
Fig. 62. HaCaT cell growth on the electrospun PVA/PHB nanofibers scaffolds with different blend compositions after 3, 7 and 14 days .....	98
Fig. 63. HaCaT cells surface coverage on the electrospun PVA/PHB nanofibers scaffolds with different blend compositions after 3, 7 and 14 days .....	99
Fig. 64. Dermal fibroblast growth on the electrospun PVA/PHB nanofibers scaffolds with different blend compositions after 3, 7 and 14 days .....	100
Fig. 65. Dermal fibroblast cells surface coverage on the electrospun PVA/PHB nanofibers scaffolds with different blend compositions after 3, 7 and 14 days .....	101

## List of Tables

Table. 1. List of the overall polymers used in the present thesis and their solvents .....	21
Table. 2. Polymers, solvents and optimum electrospinning parameters for all fabricated fibers used in the present thesis .....	32
Table. 3. DSC data and the characteristics observed for PHB powder, electrospun PHB and PHB/CTS nanofibers .....	42
Table. 4. Results of image analysis of deformed PS nanofibers with appearance of crazes or necking zones, respectively .....	50
Table. 5. Glass transition temperatures for bulk PS, PS nanofibers and hot compacted PS nanofibers .....	52
Table. 6. Assignments of FTIR absorption bands of pure polymers and electrospun nanofibers .....	72
Table. 7. DSC and the characteristics observed for the pure and electrospun polymer nanofibers. ....	75
Table. 8. Water contact angle, zeta potential and pH values at zero charge for spin coated films of PHB, PVA and their blend with different compositions.....	86
Table. 9. Assignments of FTIR absorption bands for electrospun pure PVA, pure PHB and PVA/PHB (50/50) blend nanofibers.....	89
Table. 10. DSC data and the characteristics observed for PVA granules, PHB powder, electrospun PVA, PHB and their blend nanofibers with different compositions.....	94
Table. 11. Summary of all prepared and investigated electrospun fibers.....	104
Table. 12. Overview on the kind of the work novelty, e.g, the type of the polymer used to produce nanofibers, obtained morphology, applications, new effect and combination of non-compatible polymers. ....	106

## List of Abbreviations

$\Delta H_f$ : Measured enthalpy of fusion from DSC thermograms  
 $\Delta H_f^0$ : The enthalpy of fusion for 100% crystalline polymer  
0-D: Zero-dimensional  
1-D: One-dimensional  
2-D: Two-dimensional  
3-D: Three-dimensional  
ATR-FTIR: Attenuated Total Reflectance -Fourier transform infrared spectroscopy  
CLSM: Confocal laser scanning microscopy  
Col: Collagen (Type I)  
CTS: Chitosan  
DCM: Dichloromethane  
DKFZ: Deutsches Krebsforschungszentrum  
DMEM: Dulbecco's modified Eagle medium  
DMF: Dimethylformamide  
DSC: Differential scanning calorimetry  
DTGA: The first order derivatives of TGA  
ECM: Extracellular matrix  
EDTA: Ethylenediaminetetraacetic acid  
ESEM: Environmental scanning electron microscope  
EVA: Poly(ethylene-co-vinyl acetate)  
EVA 40: Poly(ethylene-co-vinyl acetate), 40 % Vinyl acetate  
FDA: Fluorescein diacetate  
FEG-ESEM: Field emission gun–environmental scanning electron microscopy  
FTIR: Fourier transform infrared spectroscopy  
HaCaT: Human adult low Calcium Temperature keratinocytes  
HFIP: Hexafluoroisopropanol  
MCT: Mercury-cadmium-telluride  
MPa: Megapascal  
mV: milli Volt  
mW: milliWatts  
 $M_w$ : molecular weight  
NC: Nanocomposite  
NCNFs: Nanocomposite nanofibers  
NFs: Nanofibers  
n-HAp: nano-Hydroxyapatite  
NMP: N-Methyl-2-pyrrolidone  
OsO<sub>4</sub>: Osmium tetroxide  
PBS: Phosphate-buffered saline  
PEI: Polyetherimide  
PEO: Polyethylene Oxide  
PET: Polyethylene terephthalate  
PHAs: Polyhydroxyalkanoates  
PHB: poly-(3-hydroxybutyrate)  
PLLA: Poly-L-Lactide Acid  
PMMA: Polymethyl methacrylate  
PP: Polypropylene  
PS: Polystyrene

PVA: Polyvinyl alcohol  
PVAc: Poly(vinyl acetate)  
PVC: Poly(vinyl chloride)  
PVdF: Poly(vinylidene fluoride)  
RuO<sub>4</sub>: Ruthenium tetroxide  
SEM: Scanning electron microscopy  
T<sub>c</sub>: Crystallization temperatures  
T<sub>cc</sub>: Cold crystallization temperatures  
TCP: Tissue culture polystyrene  
TEM: Transmission electron microscopy  
TFA: Trifluoroacetic acid  
T<sub>g</sub>: Glass transition temperature  
TGA: Thermo gravimetric analysis  
T<sub>m</sub>: Melting temperature  
UV: Ultraviolet  
VAc: Vinyl acetate  
WCA: Water contact angle  
X<sub>c</sub>: Degree of relative crystallinity  
ΔH<sub>c</sub>: Heat of crystallization  
ΔH<sub>cc</sub>: Heat of cold crystallization



### 1. Introduction and objectives

Since Richard Feynman's famous statement in 1959 "There's plenty of room at the bottom", a new field of nanostructure science and technology has been opened <sup>1</sup>. However, nanotechnology has emerged in the last decade as an exciting new research field. Recently, the nano scaled materials have attracted extensive research interests due to their high anisotropy and huge specific surface area. Furthermore, the continuously increasing interest in the nanostructure materials results from their numerous potential applications in various areas particularly in biomedical sciences <sup>2</sup>. Today, nanofibers are at the forefront of nanotechnology because of their unique properties such as low density, extremely high surface area to weight ratio, high pore volume and controllable pore size that can not be found in other structures. These properties make the nonwoven nanofibers appropriate materials for wide spread applications <sup>3</sup>. Moreover, the nanofibers found to mimic the structure, chemical composition and mechanical properties of the extracellular matrix (ECM) <sup>4</sup>. Therefore, nanofibers based scaffolds are considered to be interesting materials in the field of biomedicine, particularly in skin tissue engineering, bone regeneration, wound healing, vascular grafts and drug delivery systems <sup>5-7</sup>. Herein, the present thesis aims to fabricate nano and /or micro fibers from different polymers, polymer blends and polymer nanocomposite materials. The obtained fibers will be characterized in details to check their potential for wide applications especially for material science and biomedical uses.

Electrospinning is considered to be one of the most promising processes in the field of nanotechnology due to its simplicity, low cost, high productivity, reproducibility and its potential to be scaled up to the industrial scale <sup>8</sup>. The method involves the application of a high voltage electric field to draw very thin fibres from a polymeric fluid stream (solution or melt) delivered through a millimeter-scale nozzle <sup>9</sup>. Electrospinning technique depends on various processing parameters such as solution properties (e.g., viscosity, surface tension and conductivity) and processing parameters (e.g., electric field strength, solution flow rate, needle diameter and distance between needle tip and ground collector). Therefore, changing one or all of these parameters will influence the nanofiber size, shape and morphology. Thus, by controlling those parameters well defined fibers can be produced for desirable applications. Moreover, controlling structural features of the electrospun fibers such as fiber diameter, porosity, volume ratio, surface morphology and mechanical properties are an essential issue in biomedical applications, since nanofibers

## **Introduction and objectives**

---

structure influences the adhesion, proliferation, differentiation, and growth of the cultured cells. Therefore, it is important to study the morphology and mechanical properties of the electrospun nanofibers before these fibers can be implanted into the human body. This subject is our area of interest, since the nanofibers morphology and mechanical properties will have an influence on the final implantable products. Selection of the material and electrospinning processing parameters is the main challenge in this field. In addition, measurements of the mechanical properties for the fabricated nanofibers are important to know whether these structures are strong enough to withstand the forces as a result of manufacturing technique and processing parameters. The behaviour of the cultured cells on these structures will be influenced according to their surface morphology and mechanical properties, as they grow and migrate on these non woven scaffolds. In other words, the mechanical properties of the electrospun fibers should mimic the mechanical properties of the implantation site. Therefore, characteristics of the fabricated fibers such as surface properties, morphology, thermal behaviour, micromechanical deformation, biocompatibility of these fibers with cultured cells and other properties will be studied.

### **Objectives of the thesis**

The overall objective of this research was to prepare micro- and nanofibers scaffolds from different polymeric materials and their blends using electrospinning technique. These polymers should have special properties such as biocompatibility and biodegradability for using in biomedical applications. Moreover, the produced nonwoven fibers will be characterized using different analytical methods. Finally, after fulfilments of electrospinning conditions for preparation of nonwoven scaffolds and their characterization, the utilization of this product as a biomedical material will be subjected to a complete study.

### **The studies of the thesis are sub divided into five sections:**

- **Electrospinning of fibers with different morphology for broad applications especially in medical uses**

The first section investigates the possibility of fabricating different polymers and polymer blends for future use in medical applications. Therefore, the electrospinning parameters have to be varied to produce fibers with different morphology and diameters. The variations of the morphology are important for the desired application. Thus, the optimum

parameters for electrospinning process will be determined in order to obtain fibers from different polymeric materials with varied morphology (e.g., porous, bead, ribbon-like, twisted, helical, rough or smooth and core-sheath structure). The obtained fibers found to have potential for exploitation in the use of these materials in broad applications including tissue engineering, drug delivery, optical components, filter media, and electromechanical devices.

- **Studying the micromechanical deformation of the electrospun fibers using in situ method**

The mechanical properties of the electrospun fibers are one of the most significant factors which influence the applications of these fiber mats. It was hypothesized that reducing fiber diameters through the electrospinning process leads to improve its mechanical properties. Thereby, the mechanical properties of the polymeric materials could be enhanced by the reducing the fiber diameter. In this chapter, Polystyrene was chosen as an example of a brittle polymer to investigate the influence of the electrospinning and the reduction of the fiber diameters on its micromechanical deformation behaviour using in situ deformation method during TEM imaging.

- **Increasing the contact between different polymers with low adhesion using electrospun nanofibers**

PMMA and EVA have been used in dentistry to prepare dentures or mouth guards. However debonding of the soft liner from the acrylic resin denture base is the major problem. Herein, a new method to increase the bond strength between PMMA and EVA will be checked. The aim is to increase the contact forces between soft liner (EVA) and heat-cured (PMMA) denture base using electrospun PMMA/EVA blend nanofibers. Electrospun nanofibers from PMMA/EVA blends will be prepared in the form of nonwoven membrane and used as an interface between the soft liner and acrylic resin denture base during the processing. Electron microscopy inspections (SEM, TEM) for the electrospun PMMA/EVA blends will be performed. In addition, the bond strength between two types of acrylic resin denture teeth and a pour-type denture base resin will be measured by mechanical testing. The hope was that the large surface area to volume ratio of the electrospun PMMA/EVA nanofibers significantly improves the bond strength between denture base and liner materials.

- **Biomimetic nanofibers for bone tissue engineering**

Recently, particular attention has been paid to the biomimetic approaches. Therefore, in the present section nanocomposite nanofibrous scaffolds from electrospun PVA/Col/n-HAp will be fabricated to mimic the natural bone for future applications in bone tissue engineering. The aim is to study the structural change which occurs during the electrospinning and to characterize the compositional structural and physicochemical properties of the nanofibers nanocomposites (using SEM, TEM, FTIR, thermal analysis and others). The most striking property of the as spun nanocomposite fibers is not only the composition of the natural bone, but also mimicking the hierarchical structure of extra cellular matrix (ECM) and mineral organization in natural bone at the nanoscale level. The unique physiochemical features of the electrospun PVA/Col/n-HAp nanocomposite nanofibers scaffolds will open up a wide variety of future applications for bone tissue engineering.

- **Fabrication of bi-layer hydrophilic/hydrophobic blend nanofibers for skin tissue engineering**

This section aims to produce bi-layer nanofibrous scaffolds consist of hydrophilic/hydrophobic blend (PVA/PHB) with different ratios to mimic the ECM of natural skin for tissue engineering applications. The electrospun blend nanofibers will be characterize using different analytical methods to study the properties of the blend nanofibers. In addition, cell culture of human fibroblast and keratinocyte cells will be investigate in order to develop tissue engineered skin.

## 2. Background and literature review

### 2.1. Preface of nanotechnology

Nanotechnology is the ability to measure, observe, manipulate and construct things at the nanometer scales. The “nano” term comes from the Greek word “nanos” which means dwarf. Scientists use this prefix to indicate that one nano equal to one billionth of a metre (i.e.,  $10^{-9}$  m). On the other hand, one nanometer (nm) is about 100.000 times smaller than the diameter of a single human hair, a typical atom is 1/5 nanometer (nm) in diameter and viruses vary from 25 nm to 300 nm. The earliest systematic discussion of nanotechnology is considered to be a speech given by the Nobel laureate Richard Feynman on December 29<sup>th</sup> 1959 at the annual meeting of the American physical society at the California institute of technology (Caltech). The speech was entitled “There's Plenty of Room at the Bottom”. Feynman observed that the principles of physics do not deny the possibility of manipulating things atom by atom and he gave the first invitation to enter a new field of physics <sup>1</sup>. Feynman’s talk was published in the February 1960 issue of Caltech's Engineering and Science, which many say represents the first introduction to nanotechnology. Feynman discussed the importance "of manipulating and controlling things on a small scale and how they could tell us much of great interest about the strange phenomena that occur in complex situations. Moreover, he posed challenges of the creation of a nanomotor and the scaling down of letters to the size that would allow the whole Encyclopedia Britannica to fit on the head of a pin. Feynman never used the word nanotechnology but in 1974 professor Norio Taniguchi at Tokyo Science University coined the term nanotechnology to refer to production technology to get the extra high accuracy and ultra fine dimensions on the order of 1 nm (nanometer) <sup>10</sup>.

Later in 1977 the American engineer K. Eric Drexler originates molecular nanotechnology concepts at Massachusetts Institute of Technology (MIT). Drexler imagined a sea of minuscule robots that could move molecules so quickly and position them so precisely that they could produce almost any substance out of ordinary ingredients in a matter of hours. Drexler's vision inspired a generation of chemists, physicists, computer scientists, and engineers to focus on science at the nanoscale. He realized that molecular machines could control the chemical manufacture of complex products, including additional manufacturing systems which would be a very powerful technology. In 1981 Drexler published a paper about the basic concepts of nanotechnology <sup>11</sup>. Then, in

1986 he wrote the book entitled “Engines of Creation” and introduced the term "nanotechnology" in his book <sup>12</sup> .

During the recent decade, nanotechnology research is growing extremely fast and has received considerable scientific attention in many fields of applications such as electronics, optics, aerospace, materials science and medicine <sup>13</sup> . The importance of nanotechnology lies in the fact that properties of substances change when their size is reduced to the nanometer range. Therefore, individual particles exhibit unexpected properties, with behaviours totally different from those of the bulk materials.

### **2.2. Nanofibers**

Polymeric nanofibers are an exciting new class of material having a diameter in the range of nanometer. In general, nanofibers are defined as structures having diameter of less than one micron. They are not visible under optical microscopes, as their diameter is smaller than the wave length of light, they can only be seen under the electron microscopes. Nanofibers constitute a particularly interesting and versatile class of one-dimensional (1-D) nano-scale material which includes nanotubes and nanorods. However, the flexibility of nanofibers would align it along with other highly flexible nano-materials (assumed as 0-D soft matter), as well as solid and liquid films of nano thickness (2-D) <sup>14</sup> .

Nanofibers possess unique properties that distinguish them from other non woven fibers, like extraordinary high surface area per unit mass, high porosity, layer thinness, high permeability, low basis weight, cost effectiveness, superior directional strength, etc. The unique properties of nanofibers make it promising materials for a variety of applications from medical to consumer products and industrial to high-tech applications. They can be used in several fields such as aerospace, capacitors, transistors, drug delivery systems, battery separators, energy storage, fuel cells, information technology and medical applications <sup>15</sup> .

### **2.3. Nanofibers fabrication methods**

With the rapid growth of nanoscience in recent years, nanofibers technology has been greatly accelerated to create nanoscale fibers from a broad range of polymeric materials. There are several approaches for generating fibers in a nanometer scale such as drawing, template synthesis, phase separation, self-assembly and electro static spinning (electrospinning). Although there are several methods for making fibers in a nanoscale

range, none matches the popularity of the electrospinning technique due to its simplicity, cost effective and relatively high production rate <sup>16</sup>.

### 2.3.1. Drawing

Nanofibers can be prepared by drawing method using a micropipette with a diameter of a few micrometers. The micropipette was dipped into the droplet of polymer solution or molten polymer near the contact line and then withdrawn from the liquid and moved at a speed of approximately  $1 \times 10^{-4}$  m/s, resulting in a nanofiber being pulled. The pulled nanofibers can be successfully drawn and deposited on the surface of the glass by touching it with the end of the micropipette. Thus, drawing nanofibers requires material with viscoelastic properties that can undergo strong deformations while being cohesive enough to support the stresses developed during pulling. Xing et al. have fabricated nanofibers with diameters down to 60 nm and lengths up to 500 mm from molten poly (trimethylene terephthalate) through the process of drawing <sup>17</sup>.

### 2.3.2. Template synthesis

Nano-sized fibers and nanotubes can be fabricated from many materials using template synthesis method. In this particular method, the water pressure will be applied from one side on the polymer solution. The pressure will increase and will force the polymer solution to penetrate through the membrane which contains cylindrical nanopores. The polymer solution will solidify by coming into contact with coagulation solution, gives rise to nanofibers. However, the nanofibers diameter depends mainly on the diameters of the pores of the membrane. Template synthesis can be used for nanofibers fabrication for polymers, metal, carbon and semiconductors <sup>18</sup>.

### 2.3.3. Phase separation

The main mechanism in this process is the separation of phases due to the physical incompatibility. When the homogenous polymer solution undergoes a decrease in temperature, two phases would form, the first phase is a polymer rich phase and the second one is a polymer lean-phase. By extracting the solvent from the polymer rich phase, a gelation could occur forming a network structure and the polymer lean phase will become pores structure. Various porous structures can be achieved by this method by varying the thermodynamics and kinetic parameters. Liu et al. have prepared gelatine matrices with

nanofibrous architecture by using a thermally induced phase separation technique as scaffolds for tissue engineering applications<sup>19</sup>.

### 2.3.4. Self assembly

Nanofiber self-assembly involves the use of smaller molecules as basic building blocks for building-up nanofibers. The main mechanism for self-assembly is the intermolecular forces that organize the smaller units together and determine the overall shape of the macromolecular nanofibers. Self assembly is significantly affected by many parameters and varying these parameters, a micro or nano scale fibers can be achieved. Self assembled nanofibers can be constructed through multiple processes of polymer chain annealing, crosslinking (chemically, thermally or UV crosslinking), dissolution and cleaving. Sargeant et al. have prepared peptide amphiphile nanofibers with porous titanium as a hybrid bone implant using the self assembly method<sup>20</sup>.

### 2.3.5. Splittable bicomponent fibers

Ultrafine fibers can be fabricated using bicomponent extrusion method, which consist of two incompatible polymers having different chemical or physical properties. They are extruded together using a special spinneret to form one filament in the range from 20 to 40  $\mu\text{m}$  per filament. The filament is then processed and splitted into smaller filaments which have a diameter of micro or nanoscale. The diameter of splitted fiber depends on the initial filament diameter, the smaller the initial bicomponent fiber diameter, the smaller the fiber after splitting<sup>21</sup>.

### 2.4. Electrostatic spinning (Electrospinning)

While there are a number of different processing techniques that can be used for fabrication of nanofibers, an additional unique synthetic method, electrostatic spinning (electrospinning), has received much attention lately. This process was patented by Antonin Formhals in 1934<sup>22</sup> and has recently become an attractive method for the preparation of polymeric and composite nanofibers<sup>3</sup>.

Electrospinning is a novel process for forming superfine fibers with diameters ranging from 10  $\mu\text{m}$  down to 5 nm by forcing a polymer melt or solution through a spinneret with an electric field. It is currently the most widely used method for the production of polymeric nanofibers, due to its simplicity, cost effective, and suitability to yield very long fibers from various polymers. It can be simply carried out by applying a high voltage

(several thousand volts/cm) to a capillary filled with polymer fluid (solution or melt), which is ejected out toward a counter electrode serving as the collector. The liquid jet undergoes a whipping process and splaying occurs in a region where the repulsive force from the electric charges carried by the jet becomes larger than its cohesive force. Splaying and solvent evaporation, together with a large elongation (because of the acceleration of the polymer jet by the electric force) are responsible for formation of the nanometer-sized polymeric fibers<sup>23</sup>.

Recently, electrospun fibers have attracted great attention due to their potential applications in many fields. To date, a variety of synthetic and natural polymers have been electrospun<sup>3</sup>, some important applications for these nanofibers include, but are not limited to nanocomposites<sup>24</sup>, fine filtration<sup>25</sup>, nanofibrous membrane for high performance batteries<sup>26</sup>, protective clothing<sup>27</sup>, scaffolds in tissue engineering<sup>5</sup>, drug delivery<sup>28</sup>, wound healing<sup>29</sup> and vascular grafts<sup>30</sup>.

### 2.4.1. History of electrospinning

The behaviour of the magnetic and electrostatic phenomenon has been described by William Gilbert in the beginning of the 17<sup>th</sup> century. He invented the term electricity and distinguished between the force arising from a loadstone and the force from rubbed amber<sup>31</sup>. The first recorded observation of electrospinning was known after he observed that when a droplet of water was brought near to a suitably charged piece of amber it would form a cone shape and small droplets would be ejected from the tip of the cone. In 1902 the fundamental idea of the term “electrostatic spinning or electrospinning” was patented by J.F Cooley and by W.J. Morton<sup>32, 33</sup>. They described a method of using high voltage power supplies to generate a cobweb-like deposition of fibres. Even at this early stage it was recognized that the electric stresses must be controlled properly to give fibres, also the fluid must be sufficiently viscous with a solvent volatile enough to evaporate and allow hardening.

In 1914 John Zeleny published work on the behaviour of fluid droplets at the end of metal capillaries and he attempted to mathematically model the behaviour of fluids under electrostatic forces. Further developments were made by Anton Formhals for the fabrication of textile yarns and described in a sequence of patents from 1934<sup>22</sup> to 1944<sup>34</sup>. Formhals used an electrical charge to draw very fine (micro and/or nano scale) fibers from a polymer solution. A polymer solution was introduced to the electrical field by placing one electrode into solution and the other onto a collector. Thus, charged polymer solution

jets ejected out of a metal spinneret and evaporated and formed fibers onto the collector. In 1936 electrospinning from melt polymers was patented by C.L Norton<sup>35</sup> using an air-blast to assist fibre formation.

Between 1964 and 1969 Geoffrey Ingram Taylor contributed to electrospinning by mathematically modelling the shape of the cone formed by the fluid droplet under the effect of an electric field. This cone has since been known as the Taylor cone<sup>36</sup>.

It was not until the mid-1990s with interest in the field of nanoscience and nanotechnology that researchers started to realize the huge potential of the process in nanofibers production<sup>37</sup>. Electrospinning has received much attention lately and has recently become an attractive method for the preparation of polymer nanofibers<sup>3</sup>. The as spun nanofibers possess some amazing characteristic like large surface area to volume ratio, flexibility in surface functionalities, and superior mechanical properties.

The electrospinning process offers many advantages over traditional nanofiber fabrications (e.g., drawing, template synthesis, phase separation, and self assembly) like control over morphology, porosity and the possibility to develop continuous nanofibers from various polymers for mass production. Electrospinning is currently the only technique that allows the fabrication of continuous fibers with diameters down to a few nanometers.

### 2.4.2. Electrospinning Process

The apparatus used for electrospinning consists of a high voltage power supply with positive or negative polarity, a needle spinneret which is connected to the syringe with a polymer reservoir and a conducting flat plate or rotating drum which acting as a ground collector (see Fig.1). The polymer solution or melt is held by its surface tension in the form of a droplet at the needle tip (spinneret). When an electric potential is applied between the needle of syringe and collector, then increasing the voltage, charge is induced on the fluid surface and the pendant droplet of the polymer solution at the needle tip is deformed into a conical shape (Taylor cone). This occurs at the equilibrium of the electric forces and surface tension of the polymer solution or melt. When the intensity of the electrical fields surpasses a critical value, the electrostatic force will increase the electrical repulsion between the mutual charges on the surface of the drop. Thereby, the electrostatic forces will overcome the surface tension of the polymer solution and consequently, a fine charged jet is ejected from the apex of the cone. Meanwhile, the solvent start immediately to evaporate and finally the jet solidify into fibres deposited on the collector plate.

## Background and literature review

In general, there are three main stages in the electrospinning of jet. The first one is the formation of Taylor cone in a fluid drop at the needle tip of the syringe. Then, a linear jet emerges from the bottom of the cone and moves towards the ground collector (stable region). After a few millimetres at most, a bending instability of the electrospun jet is observed due to the high electrostatic forces on the surface of the jet<sup>23</sup>.

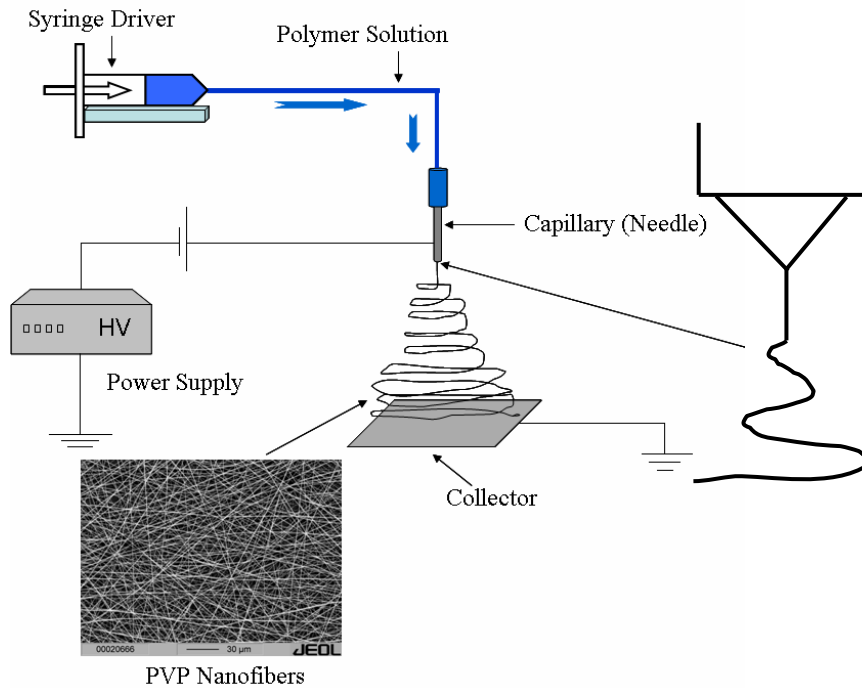


**Fig. 1. Electrospinning apparatus**

Bending instability is the region where the jet bends due to the high electrostatic forces on the surface of the jet at the tip of Taylor cone. When the pendent droplet at the needle tip is electrically charged by applying an electric field between the droplet and a ground plate, the droplet acquires a stable shape only if the electric field is not too high. This stable shape occurs only at the equilibrium between electric forces and surface tension of the droplet. Further increase of the electrical potential leads to distortion of this shape, and the droplet acquires a conical shape referred to as Taylor cone, having half of angle of  $49.3^\circ$ . Thus, Taylor cone refers to the cone observed in electrospinning from which a jet of charged particles emanates above a threshold voltage. The charged jet of the polymer is stretched and travels for a certain distance towards the ground electrode, then a bending (whipping) instability occurs and the jet transformed into superfine fibers. There are three different types of instabilities, like the so-called Rayleigh (Varicose) instability, in which the jet

breaks into micron-sized droplets. However, another mode of instability is the axisymmetric conduction instability, in which the jet resulted in a bead structure. The bending (whipping) instability is the important one in the process, which is responsible to elongate the jet and forming the nanofibers.

Bending instability of the charged jet occurs due to mutual repulsive forces between the electric charges transported by the jet. It can be defined as the region where the jet bends and stretching due to the high electrostatic forces on the surface of the jet. Bending instability was described by Sir Geoffrey Ingram Taylor in 1964<sup>38</sup>. Recently, the mechanics of the whipping jet have been analyzed by studying the instability of an electrically driven jet with increasing field strength<sup>23</sup>.

### **2.4.3. Parameters affecting electrospinning process**

The properties of the electrospun fibers (e.g., fiber morphology, average fiber diameter, porosity, uniformity and mechanical properties, etc) are dependent on several ranges of parameters such as processing parameters and solution properties. Desired electrospun fibers could be assessed systematically by varying the electrospinning parameters. The most important factors are the solution properties which are affected by solubility of the polymer in the solvent and also by vapor pressure of the solvent used. Furthermore, polymer crystallization, glass transition temperature, molecular weight and molecular weight distribution have significant influences on the electrospinnability of the solution. In addition, processing parameters include electric field strength, solution feeding rate, needle diameter and distance between needle tip and ground collector would affect of the obtained fibers<sup>14</sup>.

### **2.4.4. Different morphology of nanofibers**

Electrospinning provides a possibility to produce nanofibers with different structures and morphologies by varying the processing parameters. A number of methods have been employed in different contexts to fabricate polymeric nanofibers with different morphologies, namely, beaded, ribbon, porous, smooth and core-shell nanofibers<sup>14</sup>. The morphology of the electrospun nanofiber as well as fibers diameter can be changed by varying the electrospinning parameters to fit desired applications. Several types' fibers morphology can be realised:

### ▪ **Porous nanofibers**

Fabrication of porous nanofibers through electrospinning increases the specific surface area of the fibers. These porous nanofibers are in great demand for a wide range of applications<sup>16</sup>. The main mechanism for the formation of porous fibers is the phase separation. Highly porous nanofibers can be fabricated by the rapid phase separation during the electrospinning process using a highly volatile solvent. The more volatile solvent make a hole due to the high evaporating rate during electrospinning<sup>16</sup>. Moreover, the solvent vapor pressure has a critical influence on the process of pore formation. It was reported that decreasing the vapour pressure of the solvent used (decreasing the volatility) effectively reduced the pores formation<sup>14</sup>. Furthermore, porous nanofibers can be prepared by spinning of a blend of two different polymers. One of the polymers could be removed after fibres formation by selective dissolution in a solvent in which the other polymer is insoluble<sup>39</sup>.

### ▪ **Branched fibers**

Due to the solvent evaporation and elongation of the jet during electrospinning, the charge per unit area carried by the jet will be changed. Thereby, the shape of the jet becomes unstable because of the difference between the surface tension and the electrical forces. This instability of the jet reduces its local charge per unit surface area by ejecting a smaller jet from the surface of the primary jet or by splitting apart into two smaller jets<sup>14, 40</sup>.

### ▪ **Nanofibers with ribbon-like morphology**

Ribbon-like fibers can be obtained from several polymers under certain processing conditions. The mechanism of the formation of ribbon-like fibers is related to the solvent evaporation at the jet surface during electrospinning process. As a result, a thin polymer skin will be formed on the surface of the electrospun jet, thereby resulting in a thin layer of solid skin with a liquid core. Thereafter, the skin undergoes to an elastically buckling due to the critical pressure differential inside the ribbon. The circular cross section became elliptical and then flat, forming a ribbon-like or flattened fibers<sup>40, 41</sup>. Recently, different polymers and composites have used to create flattened or ribbon-like fibers using electrospinning technique with water and organic solvents<sup>14</sup>.

### ▪ Helical fibers

Mechanisms for the formation of the helical structures have been discussed by many researchers<sup>42</sup>. The electrospun polymeric fibers are electrically charged with the same sign; these like charges repel each other along a straight line between their centres. As a result, net coulombic elongational force will be occurred along the fiber length. When the polymer fiber deposited on a conductive surface, the charge is transferred to the surface of the polymer jet and non equilibrium between forces takes place (the contracting viscoelastic force exceeds the repulsive coulombic force). In consequently, the fiber undergoes a structural rearrangement in order to restore equilibrium and spontaneously contracts into the helical structures. Micro- and nanoscale helical structures have potential applications in many fields includes electromechanical devices, optical components and drug delivery<sup>14</sup>.

### ▪ Core-shell nanofibers

With the relatively new technique of co-axial electrospinning, core-sheath fibers can be fabricated using two different polymeric components. The co-axial electrospinning consists of a coaxial nozzle with a central tube surrounded by a concentric circular tube. The different polymer solutions are separately fed into the co-axial nozzle and ejected simultaneously. As in the conventional electrospinning, under the application of applied voltage Taylor cone is formed and a liquid jet consists of the core and a sheath material is ejected towards the ground electrode. Then, the jet will be pulled by the electric field and stretched by the bending instability. Finally, the solvent starts to evaporate leading to the formation of core-sheath micro and /or nanofibers<sup>43</sup>. Co-axial electrospinning of core – sheath structured fibers could enhance the material properties for various applications such microelectronics, optics and medicine. In addition, co-axial electrospinning offers the fabrication of hollow fibers and nanotubes using mineral oil as a core material and polymer or ceramic as a sheath material. After electrospinning, the mineral oil will be removed to created hollow fibers or nanotubes<sup>14</sup>.

### ▪ Beaded nanofibers

The formation of beads during electrospinning reduces the large surface area per unit mass of the obtained fibers. Therefore, beads considered as a defect in the electrospinning process. The mechanism of bead formation is related to the viscosity, surface tension of the polymer solution, and net charge density carried by the polymer jet<sup>44</sup>. However, the major

competition between the surface tension and viscoelastic force is the main reason of the bead formation. Basically, the surface tension of the polymer jet tries to decrease the surface area per mass, while the electric force tries to increase it. Higher surface tension leads to contraction of the radius of the jet and drives the jet towards the formation of beads. In addition, decreasing solution viscosity and net charge density favour the formation of fibers with beads. Addition of small amount of salts or polyelectrolyte to the solution increases the charge carried by the jet during the electrospinning and thereby, increase the jet stretching. As a result, fibers without beads will be created.

### **2.4.5. Properties and potential applications of nanofibers**

Polymeric nanofibers and nanocomposites materials exhibit many unique properties that distinguish them from the other conventional fibers. They possess a huge surface to volume ratio, low density, high porosity, and nano pores with highly interconnected internal structure<sup>14, 15</sup>. One of the most important property of the nanofibers is the superior mechanical behaviour that nano-sized materials possess as compared to bulk materials. The superior mechanical properties of the electrospun nanofibers (such as higher elastic modulus and strength) arise from the decrease in diameter and the higher molecular orientation of the polymer molecules. The molecular orientation is produced by the stretching of the polymer jet during Electrospinning<sup>9</sup>.

The mechanical properties of single nanofiber as well as nanofibrous scaffolds are extremely essential issue in engineering applications. In tissue engineering, the ideal scaffolds should gain some special characteristics before implantation into the human body. Scaffolds should be strong enough to withstand the forces exerted by the cells (as they grow and migrate on the scaffold). In addition, the scaffold should have suitable mechanical properties match those of the tissue that they are intended to substitute, to provide mechanical integrity for the tissue formation. So the mechanical properties of biomaterials scaffolds are one of the most significant factors in tissue engineering applications which can be improved by crosslinking of the nanofibers mats<sup>45</sup>. To improve the deficiency of the mechanical properties, a good selection of the materials should be taken into the consideration when fabricating fiber scaffolds. Furthermore, the mechanical properties can be manipulated through varying solution composition (blending) and altering the processing parameters. However, because of the small diameters of the electrospun fibers, it is a challenge to measure their mechanical properties. Although most mechanical tests have been evaluated for the scaffold or mats rather than individual fibers,

techniques for testing single nanofibers have been developed recently<sup>46</sup>. These techniques are suitable for measuring the Young's modulus, tensile strength and tensile strain at break of the single nanofiber<sup>46</sup>. Furthermore, the special properties of the electrospun nanofibers make them suitable for a wide variety of applications including, protective clothing, sensors, filter media, drug delivery, tissue engineering, nanoelectronics, wound dressing, energy & electrical applications<sup>8, 15, 37</sup>.

Electrospun micro and / or nanofibers are morphologically similar to the extracellular matrix (ECM) of natural tissues and its nanoscale fibrous structure; it can be explored in diverse areas of tissue engineering<sup>47</sup>. Natural and synthetic fibers have been widely used as promising scaffolds for tissue repair, these fibrous scaffolds are mechanically stable and capable of functioning biologically in the implant site<sup>48</sup>. However, the mechanical stability is dependent primarily on the selection of biomaterial, the architectural design of the scaffold, and the cell material interactions<sup>49</sup>. Therefore, to design an ideal scaffold, various factors should be considered, such as pore size and morphology, mechanical properties versus porosity, surface properties and appropriate biodegradability. Of these factors, the importance of mechanical properties on cell growth is particularly obvious in natural tissues such as bone, cartilage, blood vessels, tendons and muscles<sup>50</sup>. Tissue engineered constructs must exhibit tissue-like functional properties, including mechanical behaviour comparable to the native tissues they are intended to replace. Moreover, the ability to reversibly undergo large strains can help to promote and guide tissue growth.

### **2.4.6. Aligned nanofibers**

In general, the electrospun fibers are deposited as non-woven or randomly oriented fibers on the collector. However, it is desirable to control the arrangement of the electrospun fibers to form patterned structures that can be used in a wide variety of applications including biomedical engineering. Aligned electrospun nanofibrous membrane has shown considerable promise in tissue engineering to control cell proliferate in the direction of the fibre orientation. Several researchers have shown the possibility to obtain aligned fibres by using a specially designed collector consisting of patterned electrodes<sup>51</sup>. It is shown that well aligned nanofibers can be obtained by using a rotating cylindrical drum. However, the speed of the rotating drum has a main influence on the degree of the fibers alignment. Increasing the rotating speed leads to fabrication of good aligned nanofibers. In addition, the velocity of the rotating mandrel not only influences the alignment of the nanofibers, but also influences the crystallinity and mechanical properties of the obtained nanofibers. On

the other hand, if the rotating speed is too high, fibre breakage may occur<sup>51</sup>. As well as, aligned nanofibers have been fabricated by using two parallel electrodes to collect the aligned fibers in the gap between them. However, the length of the aligned electrospun fibres across a gap is limited by the gap length. The electrospun fibres would deposit across the gap from the tip of one blade to the other<sup>51</sup>.

### 2.4.7. Nanofibers blends and their phase morphology

Polymer blends have been used as a tool for tailoring products with optimized properties. They are interesting materials for a broad class of industrial products because of providing new physical and mechanical properties that the individual polymer does not possess<sup>52</sup>. However, blending polymers can lead to a wide range of phase behaviors that directly influence the associated mechanical properties and ultimate applications. Phase behaviour of the blend polymers is influenced by many factors. In short, choice of monomers, molecular architecture, composition, and molecular size<sup>53</sup>. The blend polymers show phase separation with a dispersive phase in the matrix if the polymers components are immiscible together. The dispersive phase is usually formed from the minor component, while the matrix is formed by the major component<sup>54</sup>. In case of large phase separation, the components have a weak interfacial connection results in a drastic reduction in the mechanical properties of the blend. On the other hand, phase separated nanofibers can be fabricated during electrospinning process using single polymer. The phase separation occurs during the electrospinning due to the inherent thermodynamic immiscibility<sup>55</sup>. Recently, there has been much focus on fabrication of different types of phase morphology for the electrospun fibers such as co-continuous and core-sheath<sup>56,57</sup>.

### 2.4.8. Nanofiber nanocomposites

Polymer nanocomposites are the result of combination between polymers and organic or inorganic fillers at the nanometer scale. The filler can be one-dimensional (e.g., nanotubes and fibres), two-dimensional (e.g., clay), or three-dimensional (e.g., spherical particles). The development of nanocomposite materials with improved properties has dominated the field of material science. Recently, much work has been focused on the construction of nanocomposite materials due to the structural enhancements in physical and mechanical properties for these systems<sup>58</sup>. The physical and mechanical enhancements result from the interaction between filler components and matrix (e.g., hydrogen bonds) at the nanometer scale. This interaction enables them to act as molecular bridges in the polymer matrix<sup>59</sup>.

However, the properties of these nanocomposite materials are highly dependent on how well the filler are dispersed within the polymer matrix. Achieving a uniform dispersion of the filler by conventional mixing methods is difficult as the high surface energy of the nano filler makes them very easily agglomerate. Among these methods, one of the most desirable processes for nanocomposites fabrication is electrospinning technique. It has been used to fabricate hybrid nanocomposites (organic/inorganic) nanofibers with a high dispersion of the nano fillers inside the fibers matrix <sup>60, 61</sup>. Moreover, the unique combination of high specific surface area, flexibility and superior directional strength makes nanofibers nanocomposites promising materials for wide applications including medical uses <sup>4,7</sup>.

### 2.4.9. Biomimetic nanocomposite nanofibers

Biomimicry or biomimetics is the imitating or taking inspiration from nature's forms and processes to solve human problems <sup>62</sup>. Recently, there has been an increased focus on the inspired materials because of their advanced applications especially in the fields of defense, nanotechnology, robot technology, artificial intelligence and biomedical applications <sup>63</sup>. Natural bone is an example of the natural biocomposite materials that attracted much attention from the biomimetics scientists. Bone is a nano biocomposite matrix composed of hybrid organic– inorganic components. Around 30% of bone is composed of organic compounds, of which 90 to 95% is Type I Collagen (Col). The inorganic phase composed of about 70 % mineral hydroxyapatite (HAp). The combination of both Col and HAp allows bone to be flexible and strength, thereby provide a mechanical and supportive role in the body <sup>4</sup>. Several studies have been devoted recently to mimic or closely match the composition, microstructure and properties of natural bone <sup>4, 61, 62, 64</sup>.

The main idea in mimicking natural bone is to control and fabricate the morphology and the composition of mineralized collagen fibrils, in which the nano particles of inorganic compounds (HAp) are being dispersed with preferential orientation in the organic matrices (Col), see Fig 2.

Bone in human and other mammal bodies is generally classified into two types; the first one is the cortical bone shell or compact bone, so-called due to its minimal gaps and spaces. Cortical bone constitutes the outer walls of the bones; they have thicknesses varied from about several tenths of a millimetre to about 1-2 centimetres. The second type is the trabecular bone or cancellous bone which constitutes the interior layer of the cortical bone. Cancellous bone is a highly porous tissue composed of a network of rod and plate like

## Background and literature review

---

elements<sup>65</sup> (see Fig. 2). Both cortical and cancellous bone is made of a laminate of collagen fibrils reinforced with hydroxyapatite particles of nanometric dimensions. Nanofiber nanocomposites are considered to be useful as bone regeneration scaffolds, due to their nanostructure which mimics the size of natural extracellular matrix (ECM) of bone component. Moreover, nanofibrous nanocomposite scaffolds have been demonstrated to improve cell attachment and proliferation<sup>7</sup>.

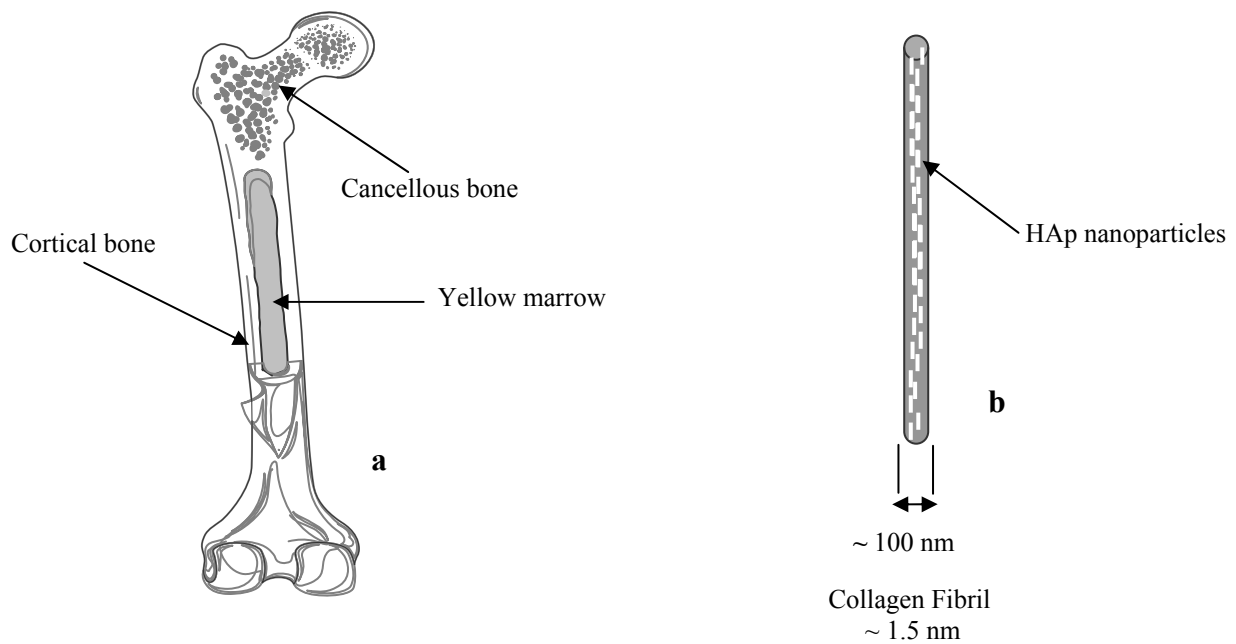


**Fig. 2. A schematic diagram showing (a) cortical shell bone and a cancellous bone structures, and (b) the lowest level of hierarchical organization**



### 3. Materials and experimental Methods

The experimental parts of this thesis can be subdivided according to the objectives into the following sections:

- 1) Fabrication of nanofibers and nanocomposite fibers through electrospinning.
- 2) Characterization of the as spun fibers using different methods.
- 3) Applications of the obtained fibers scaffolds as a materials for biomedical applications (Skin tissue engineering and dentistry applications).

#### 3.1. Materials

##### 3.1.1. Materials for electrospinning fibers

In this work, many polymers and solvents were used to fabricate different electrospun micro and /or nanofibers. In addition, blends from different polymers and polymer nanocomposites were also fabricated by electrospinning in order to get micro and nanofibers scaffolds for diverse applications. The list of the used polymers and their solvents is shown in Table.1. All solvents were purchased from Sigma–Aldrich (Deisenhofen, Germany) except Dichloromethane was purchased from Carl Roth GmbH, Germany and they were of analytical grade and used without any further modifications.

##### 3.1.2. Types of cells for cell culture

Human Fibroblasts and HaCaT (Keratinocytes) cell line were used to measure cell adhesion and surface coverage after different days of culture using electrospun PHB and PVA/PHB nanofibers with different ratios. Primary fibroblasts were purchased from Cell Lining GmbH (Berlin, Germany). HaCaT cell lines were a kind gift from Prof. Dr. N. Fusenig from the German Cancer Research Centre (DKFZ), Heidelberg, Germany.

**Table. 1. List of the overall polymers used in the present thesis and their solvents**

Polymer type	Specification	Solvents*
PLLA	Poly(L-Lactic acid), Cargill $M_w = 200$ kg/mol, Dow Chemical, Germany	Chloroform and Dichloromethane
PEI	Polyetherimide, (Utem 1000, General Electric, Schenectady, NY,U.S.A.), granted by Prof. Dr. Groth, Institute of Physics, Martin Luther University	Chloroform and N-Methyl-2-pyrrolidone
PEO/ $\gamma$ -Fe <sub>2</sub> O <sub>3</sub>	Polyethylene Oxide with an average $M_w = 600,000$ , Sigma Aldrich, Germany Fe <sub>2</sub> O <sub>3</sub> : Ferromagnetic nanoparticle concentration is 0.01 wt % in CHCl <sub>3</sub>	Chloroform
PET/ $\gamma$ -Fe <sub>2</sub> O <sub>3</sub>	Ferromagnetic nanoparticle concentration is 0.01 wt % in CHCl <sub>3</sub>	Trifluoroacetic acid
EVA 40	Poly(ethylene-co-vinyl acetate), Vinyl acetate 40 wt. % from Sigma Aldrich, Germany	Chloroform/Dimethylformamide and N-Methyl-2-pyrrolidone
PMMA	Polymethylmethacrylate, PalaXpress Kaltpolymerisat powder, Heraeus Kulzer GmbH, granted by Prof. Dr. med. dent. Karl-Ernst Dette, Faculty of Dentistry, Martin Luther University Halle	Chloroform/Dimethylformamide
Chitosan	Chitosan from crab shells highly viscous, Sigma-Aldrich, Germany,	Trifluoroacetic acid/Dichloromethane
PHB	Polyhydroxybutyrate, $M_w = 4.4 \times 10^2$ kg/mol from Sigma-Aldrich, Germany	Chloroform and Hexafluoro-2-propanol
PHB/Chitosan	As above	Trifluoroacetic acid/ Hexafluoro-2-propanol
Polystyrene	Polystyrene, $M_w = 120$ kg/mol from BASF, Germany	Chloroform /Tetrahydrofuran
PEI/EVA	As above	Chloroform/Dimethyl formamide
PVA	Polyvinyl alcohol, Average $M_w = 85,000$ - $124,000$ and 87-89% hydrolyzed from Sigma Aldrich, Germany	De-ionized Water and Hexafluoro-2-propanol
Collagen	Rat tail Type I Col (6.3 mg/ml dissolved in 1 M acetic acid) was kindly provided by Faculty of Medicine, Halle Wittenberg, Germany	1 M acetic acid in De-ionized Water
PVA/Collagen	As above	1 M acetic acid/ De-ionized Water
Hydroxyapatite	Commercial grade Ostim® from aap Implantate AG, Germany	De-ionized Water

\* All solvents were purchased from Sigma–Aldrich (Deisenhofen, Germany) except Dichloromethane was purchased from Carl Roth GmbH, Germany

### 3.2. Experimental

#### 3.2.1. Electrospinning apparatus setup

The instrument setup used in this work was a vertical spinning configuration (see Fig. 3a) Electrospinning was carried out at room temperature using applied voltages in the range from 3 to 22 kV, driven by a high voltage power supply Heinzinger PNC (Heinzinger Electronic GmbH, Rosenheim, Germany). The polymer solution was filled in a 1 ml syringe attached with a blunt steel needle of 0.8 or 1 mm inner diameter. A square steel plate covered with aluminium foil was placed 10-15 cm away from the needle tip acting as a counter electrode. In addition, the polymer solution is forced with constant flow rate during electrospinning process using an infusion pump. The polymer solution feeding rate was varied from 100  $\mu\text{l/h}$  to 1 ml/h depending on the polymer type. For morphological investigations, a glass plate was placed over the counter electrode as collecting substrate. Then, the electrospun fibers on the glass substrate coated with a thin layer of gold in a sputtering machine to conduct the surface for better imaging. The electrospun fibres mats were collected either directly on the aluminium foil as a nonwoven membrane or on grounded stainless steel network to obtain web scaffolds. On the other hand, in order to get uniaxially aligned nanofibers, a rotating drum was used as a ground collector ( Fig.3b) <sup>14</sup>. Moreover, uniaxially aligned nanofibers were prepared by the parallel electrodes method (Fig. 4) <sup>51</sup>. Two parallel electrodes were fixed as a ground collector through a conductive wire to collect the uniaxially fibers for studying the mechanical deformation behaviors insitu during the imaging with TEM.



**Fig. 3. Electrospinning setup (a) square metal plate used as fibers collector (b) metal rotating drum used as fibers collector**

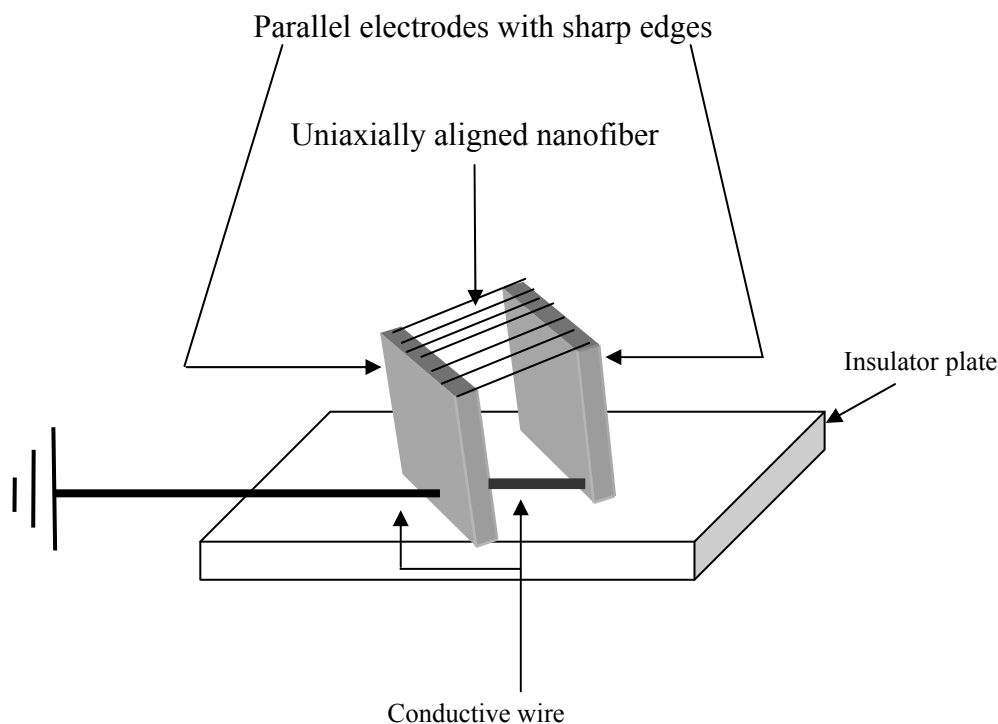


**Fig. 4. Schematic illustration of parallel electrodes method for aligned nanofibers preparation**

### **3.2.2. Hot compaction of aligned polystyrene nanofibers**

Multilayer aligned polystyrene (PS) nanofibers membranes were prepared and compacted at different temperatures using a hot compaction technique (Labo press 200 T hot compaction). The hot compaction process applied to the aligned nanofibers mats at a temperature that is below the glass transition temperature of PS ( $T_g$  about 105 °C). Compactions were at two different temperatures ( 85 °C and 90 °C) with a pressure of 20 MPa for 5 min.

## **3.3. Characterization methods**

### **3.3.1. Scanning electron microscopy (SEM)**

Over the last two decades, scanning electron microscopy (SEM) has been used in polymer research to get a better understanding of structure property correlations in polymers. Moreover, SEM considered being the most popular of the microscopic techniques because of the ease of specimen preparation, and the general simplicity of image interpretation<sup>54</sup>. It is a type of electron microscope that images the sample surface by scanning it with a high energy beam of electrons. Morphological details at length scales from the visible (0.1mm)

up to a few nm can be detected by using SEM. In general, the electrons interact with the atoms of the samples that make up the sample producing signals contains information about surface topography of the sample. Therefore, the surface must be conducting; the sample can easily be made conductive by coating the sample surface with a thin layer of heavy metal (e.g. gold) in a sputtering machine. Such a coating also contributes to reduce the surface charging and makes SEM photographing possible. Furthermore, the observation must be performed in a vacuum to prevent scattering of the electrons by stray air molecules. Basically, the coated sample is placed into the SEM chamber and the air is pumped out of the chamber creating a vacuum. Then, high energy electrons beam is emitted by electron gun positioned at the top of the set-up which travels down the column through a series of magnetic lenses in order to focus the beam to a very fine spot. The focused beam hits the sample surface producing secondary electrons which are attracted and collected by a detector and then translated into signals. These signals are then amplified, analyzed, and translated into images for the surface topography of the sample<sup>54</sup>. During 1980s, environmental scanning electron microscope (ESEM) has been invented to allow the samples to be observed in low-pressure gaseous environments and high relative humidity. It is operating in 'wet' mode and it is not necessary to coat the nonconductive samples before imaging<sup>54</sup>.

In the present work, samples for electron microscopy were prepared by direct electrospinning of the polymers, nanocomposites and polymer blends on the slide glasses then followed by Au sputtering to  $\sim 20$  nm thickness for better conductivity during imaging. The size and morphology of the electrospun fibers were investigated by a scanning electron microscope (JSM 6300 JEOL). The mechanical deformation behaviours of PS nanofibers were measured by using field emission gun–environmental scanning electron microscopy (FEG-ESEM, Philips ESEM XL 30 FEG).

### 3.3.2. Transmission electron microscope (TEM)

In general, transmission electron microscope (TEM) operates on the same basic principles as the light microscope but uses a highly energetic beam of electrons as "light source" that passes through the specimen instead of light. The lower wavelength of the electron beam makes it possible to get a resolution a thousand times better than with a light microscope. It can be used to visible objects to the order of a few angstroms ( $10^{-10}$  m). Basically, the electron gun at the top emits a stream of monochromatic electrons that travel through vacuum in the column of the microscope. The electromagnetic lenses used to focus the electrons into a very thin beam. Then the electron beam travels through the sample

specimen and scattered from the specimen at different angles depending on the density of the material used. The unscattered electron signals are magnified by a series of electromagnetic lenses and hit a fluorescent screen, which gives rise to a shadow image of the sample displayed in varied darkness according to the density of the material present<sup>54</sup>. In the present work, the morphology of the electrospun polymeric fibers, nanofiber blends, nanoparticles, and nanofiber nanocomposites were investigated by conventional transmission electron microscopy (TEM) (JEOL 200CX operated at 200 kV). Samples were prepared by directly depositing electrospun fibers onto Cu-grids 3 mm diameter covered with an ultrathin carbon layer. The spatial dispersion of the nanoparticles within the electrospun fibers were also conducted using the same method.

For phase characterization and miscibility of the binary polymers in the electrospun blend nanofiber, a conventional transmission electron microscopy (TEM) (JEOL 200CX operated at 200 kV) was used to image the phase morphology after selective staining. Samples were prepared directly by depositing nanofibers onto Cu-grids 3 mm diameter covered with an ultrathin carbon layer. The grid was then placed into a sealed chamber with Osmium tetroxide ( $\text{OsO}_4$ ) or Ruthenium tetroxide ( $\text{RuO}_4$ ) vapors for different time. The selective stain attacks the functional group of one polymer (e.g. hydroxyl group) giving it a darker contrast compared to the other region<sup>54</sup>.

### 3.3.3. Image analysis

The fibers size distribution were determined by measuring over 200 fibers selected randomly from the SEM or TEM images using image analysis software (Analysis, Soft Imaging System Co., Germany). In addition, the scaffold porosity has been measured from the SEM images using analysis software (Image J, National Institute of Health, USA), according to the method of Ghasemi-Mobarakeh et al.<sup>66</sup>.

### 3.3.4. In situ deformation of polystyrene nanofibers

To study the mechanical deformation structures of the electrospun PS nanofibers, aligned nanofibers were prepared in a miniaturized straining holder from Gatan Inc, USA., for a TEM (JEOL, JEM 4010, 400 kV in the Max-Plank-Institute of Microstructure Physics in Halle/S). In addition, a miniaturized straining holder from Kammrath & Weiß GmbH for an ESEM has been used to study the micromechanical deformation of PS nanofibers. Straining devices, shape and size of the specimen used are shown in Fig. 5.

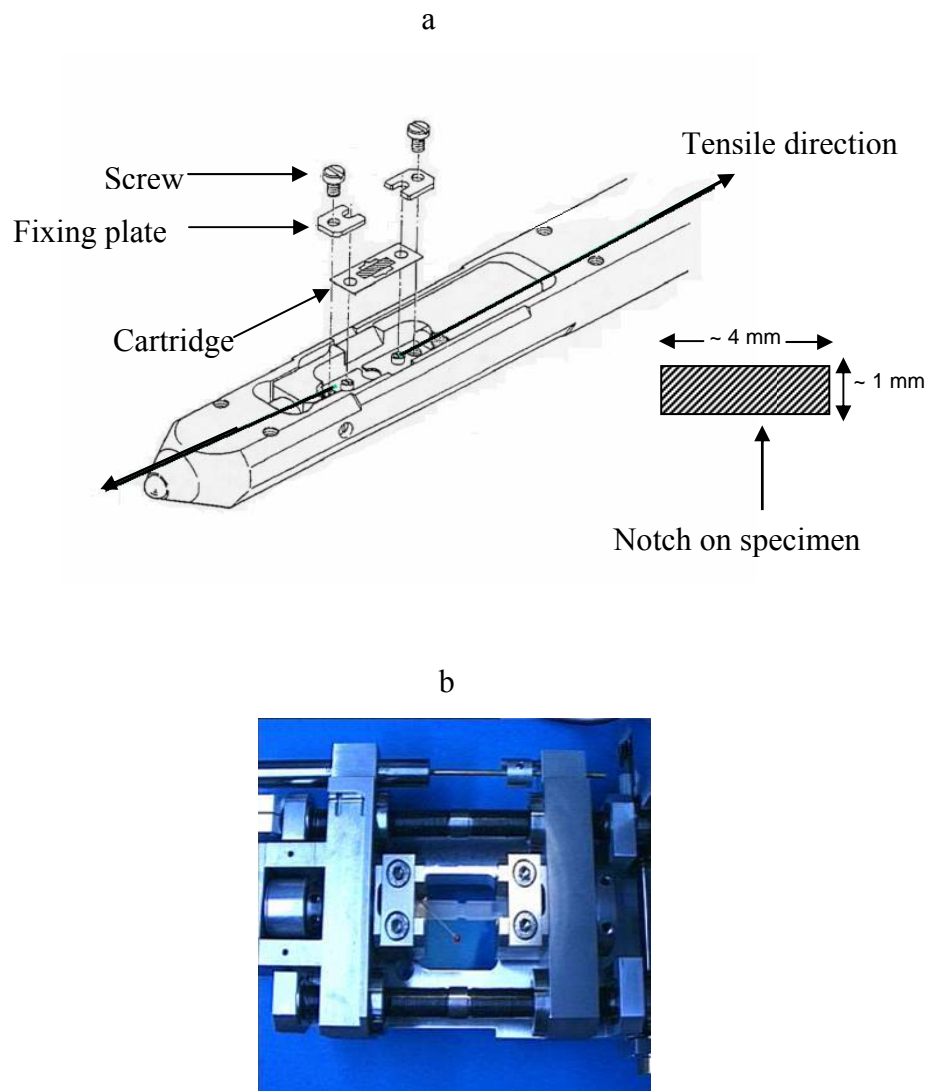


**Fig. 5. In situ deformation devices**

- (a) Scheme of the miniaturized straining holder from Gatan Inc., for a TEM (JEOL, JEM 4010, operated at 400 kV)
- (b) Straining holder from Kammrath & Weiß GmbH for ESEM

### 3.3.5. Thermal investigations

It is an important issue to check the thermal characteristics of the electrospun nanofibers, nanofiber blends and nanocomposite nanofibers after electrospinning in order to compare them with their pure polymers. The glass transition temperature, melting temperature, enthalpy of fusion, degree of crystallinity and thermal degradation are a sign of structural change which might be occurred after electrospinning and / or blending. Therefore, differential scanning calorimetry (DSC) and thermo gravimetric analysis (TGA) were investigated to get some information about the thermal behaviour of the electrospun fibers after electrospinning. Also to check the homogeneity and miscibility of the polymer blends through the degree of crystallinity.

#### ▪ Differential scanning calorimetry (DSC)

Thermal characteristics such as glass transition temperature, melting temperature, degree of crystallinity and thermal degradation of the pure polymers and their electrospun fibers were investigated using DSC. Thermal measurements have been done in heat flux mode under nitrogen as purge gas using the instrument DSC Mettler Toledo 820, Giessen, Germany. About 5 mg of the samples were heated and cooled in the temperature range from 25 °C to 250 °C at a rate of 10 K/min. Firstly, the samples were heat treated from 25 °C to 250 °C, and then cooled to 25 °C for complete crystallization of the matrix. The specimens were heated again to 250 °C without prior cooling to obtain the DSC endotherms. In case of PHB and their blends with PVA, the samples were heated and cooled in the temperature range from -30 to 200 °C at a rate of 10 K/min. The sample firstly heated from -30 to 200 °C and kept at 200 °C for 2 min to eliminate any thermal history, and then cooled to -30 °C for complete crystallization of the matrix. The specimens were heated again from -30 to 200 °C without prior cooling to obtain the DSC endotherms. For all samples, the heat evolved during non-isothermal crystallization was recorded as a function of time. Furthermore, crystallization temperatures ( $T_c$ ) and heat of crystallization ( $\Delta H_c$ ) were determined from exothermal peaks in cooling run. In addition, cold crystallization temperatures ( $T_{cc}$ ), heat of cold crystallization ( $\Delta H_{cc}$ ) and melting temperature ( $T_m$ ) were obtained from the second endothermic heating runs. On the other hand, the degree of relative crystallinity ( $X_c$ ) was estimated from the endothermic area using equation 1.

$$X_c = \Delta H_f / \Delta H_f^o \quad (\text{equation 1})$$

Where  $\Delta H_f$  is the measured enthalpy of fusion from DSC thermograms and  $\Delta H_f^o$  is the enthalpy of fusion for 100% crystalline polymer.

The degree of crystallinity of PHB in the blends was calculated by assuming that the  $\Delta H_f^o$  value of 100% crystalline PHB is  $146 \text{ J g}^{-1}$ <sup>67</sup> and  $\Delta H_f^o$  of 100% crystalline PVA is  $156 \text{ J g}^{-1}$ <sup>68</sup>.

### ▪ Thermo gravimetric analysis (TGA)

Thermo gravimetric analysis (TGA) was performed using TGA /SDTA 851 (Mettler-Toledo GmbH, Germany) under a nitrogen flow. About 5 mg of sample was heat-treated from room temperature to  $750^\circ\text{C}$  at a heating rate of  $20^\circ\text{K/min}$ . All the graphs were plotted for temperature against the heat flow mW (Y-axis). DSC and TGA not only give information about thermal behavior of the polymer blend, but also can provide information about the compatibility of the polymer blend. In addition, it can be used to estimate the influence of the blending on the crystallinity, hence mechanical properties of the obtained electrospun fibers. The first order derivative of TGA refers to the temperatures at which the maximum decrease of mass occurs.

### 3.3.6. Fourier Transform Infrared spectroscopy (FTIR)

The principle of FTIR spectroscopy is to submit the sample to an infrared beam and the absorption of this radiation will promote the excitation of its molecular vibrations by depositing quanta of energy into vibrational modes<sup>69</sup>. The chemical bonds absorb the infrared energy at specific frequencies (or wavelengths) corresponding to its molecular modes of vibration in the region of the electromagnetic spectrum<sup>70</sup>. This absorption corresponds specifically to the bonds present in the molecule and the resulting spectrum is characteristic of the molecules structures present in the sample. FTIR is an effective analytical tool for identification of the compounds structure. It represents a fingerprint of the sample because each specific chemical group has a specific frequency or wave number. Moreover, FTIR technique is one of the powerful tools to obtain information on polymer blend systems, such as crystallinity, existence of specific interaction such as hydrogen bonds and so on<sup>71</sup>. In the present study, FTIR spectroscopy was carried out to analyze any complex structural changes that might have occurred due to the electrospinning and

blending. Also to elucidate the interaction (hydrogen bonding) in the blend nanofibers which is in consequently affect on the crystallinity and compatibility of blend fibers<sup>61</sup>. The spectra of the pure polymers and electrospun fibers were obtained using an FTIR Spectrometer S2000, Perkin-Elmer, Germany equipped with a fixed 100  $\mu\text{m}$  diameter aperture and a mercury-cadmium-telluride (MCT) detector was used to analyze the absorbance in the wave number range of 500- 4000  $\text{cm}^{-1}$  with a resolution of 2  $\text{cm}^{-1}$ .

### 3.3.7. Water contact angle measurements (WCA)

Water contact angle or the measure of wettability is an important factor which can help to evaluate the possible effect of a biomaterial on cell adhesion and growth. Thin films of PVA, PHB and their blends with different ratios (dissolved in HFIP) were prepared onto glass substrates by spin coating (at 350 rpm) with 'SPIN150-NPP Spin coater by SPS-Europe B.V' (Putten, Netherlands). The static values of water contact angle on the prepared films were measured in a humidity chamber with the Contact Angle Unit OCA-15+, Dataphysics Instruments, (Filderstadt, Germany). The sample and needle of the device were enclosed with a chamber containing a Petri dishes have a wetted salt of sodium hydrogen sulfate (ROTH, Germany) to control the humidity of the chamber (relative humidity of about 50% $\pm$ ). At least three measurements on different film locations were averaged for data analysis.

### 3.3.8. Zeta potential measurement ( $\zeta$ )

Zeta potential is related to the quantity and dissociation of charged groups on the material surface. Thereby, increasing or decreasing in the surface charged groups will result in a higher or lower zeta potential value<sup>72</sup>. Surface zeta potential is an important feature of material surface and its interaction in biological environments. It is highly dependant on environmental pH value and if plotted versus pH, will be positive at low pH and lower or negative at high pH.

Streaming potential measurements were performed using a SurPASS (Anton Paar, Graz, Austria) to monitor the surface charge. Films of PVA/PHB with different blend compositions were prepared by solution casting of 1.5 wt% PHB and PVA in HFIP. Two films were attached on the sample holder and introduced into the flow cell. The zeta potential ( $\zeta$ ) was determined by adjusting the gap of the flow cell to a distance where a flow rate between 100 and 150 ml/ min at a maximum pressure of 300 mbar was reached. A flow check was performed to achieve a constant flow in both directions. 1 mM

## Materials and experimental methods

---

potassium chloride was used as electrolyte while 0.1 N hydrochloric acid was used for pH titration. Before starting a measurement the pH value of the electrolyte solution was adjusted to pH 10.5 using 1 N sodium hydroxide. Finally, an automated titration program performed the measurement from pH 10.5 to pH 2.25 using titration steps of 0.03  $\mu$ l from pH 10.5 to pH 5.0 and 0.25  $\mu$ l from pH 5.0 to pH 2.25.

### 3.4. Biological tests

#### 3.4.1. Degradation measurements

The measurement of degradation rate in a specific biological environment is an important factor in tissue engineering. The growing cells have to replace the scaffolds and build the new ECM structure. Electrospun nanofibrous scaffolds from PHB and PVA/PHB with different compositions were cut into square shapes weighting  $\sim$  3-6 mg and placed in wells of 12 well plates. Wells were filled with phosphate-buffered saline (PBS; 2.7 mM KCl, 137 mM NaCl, 1.4 mM  $\text{KH}_2\text{PO}_4$ , 4.3 mM  $\text{Na}_2\text{HPO}_4$  dihydrate, pH 7.4). The samples were incubated at 37°C to mimic the biological environments of the body. The PBS buffer was changed every 3-4 days, and samples were taken out after 1, 3, 6, 9 and 12 weeks and washed with micro-pure water then dried to constant weight. They have been weighted with a precise balance and weight loss was measured. The degradation rate was determined by the ratio of the weight loss to the initial weight of samples as shown in equation number 2.

$$S = \frac{W_0 - W_t}{W_0} \times 100 \quad \text{(equation 2)}$$

where S is the degradation rate,  $W_0$  is the initial sample weight and  $W_t$  is the weight of dried samples.

#### 3.4.2. Sterilization of nanofibrous matrices

The nanofibrous scaffolds were backed up by transparent polypropylene (PP) sheets for better handling during cell culture. The transparent PP sheets were washed before the experiments for 2 hours in a solution mixture composed of ethanol/acetone (50/50) to remove any contaminations on the surface. Then, the nanofibrous scaffolds supported with PP films and they were cut into discs with a diameter of 14 mm. The prepared mats were placed in 24 well-plates and supported with glass rings to avoid them floating in medium.

## Materials and experimental methods

---

Thereafter, they were sterilized for 1 hour with 70% pure ethanol followed by 3 times rinsing with sterilized PBS before cell seeding.

### 3.4.3. Cells harvesting

Human Fibroblasts and HaCaT (Keratinocytes) cell line were used to measure cell adhesion and surface coverage after different days of culture. Both cell types were cultured in Dulbecco's modified Eagle medium (DMEM, Biochrom AG, Germany) supplemented with 10% v/v fetal bovine serum (FBS, Biochrom AG, Germany), 1% Pen/Strep/Fungizone (AAs, PromoCell, Heidelberg, Germany), and 1% L-glutamine (Sigma, Germany) and were incubated in humidified incubator at 37°C with 5% CO<sub>2</sub> (NuAire Corp., Plymouth, Minnesota, USA). For the experiments, cells from confluent cultures were harvested with 0.25% Trypsin /0.02% EDTA solution (PromoCell, Heidelberg, Germany) and resuspended in culture medium DMEM with 10% FBS and seeded on the nanofibrous scaffolds at a density of  $2.5 \times 10^4$  cells/ml for HaCat cells and  $1.5 \times 10^4$  for human fibroblast.

### 3.4.4. Cells adhesion and proliferation investigation

Sterilized PVA/PHB blend nanofibrous scaffolds of different compositions were placed into 24-well tissue culture plate for studies of cell attachment and growth. Plain tissue culture polystyrene (TCP) was used as a control. HaCaT cells were seeded at a concentration of 25000 cells/ml while human dermal fibroblasts were seeded at a density of 15000 cells/ml. Dulbeccos Modified Eagle Medium (DMEM) supplemented with 10% fetal bovine serum (FBS) and 1% antibiotic/antimycotic solution (all obtained from Biochrom AG, Berlin, Germany). Samples were incubated at 37°C, 5% CO<sub>2</sub> for the times indicated. The medium was exchanged every 48h. Attachment, distribution and growth of cells were visualized by vital staining with fluorescein diacetate (FDA, Sigma, Deisenhofen, Germany) and imaging with confocal laser scanning microscopy "CLSM 710" (Carl-Zeiss, Oberkochen, Germany).

FDA staining was performed exchanging the medium by 1 ml DMEM plus 5µl FDA stock solution (5 mg/ml acetone), followed by an incubation for 5 min at 37°C, 5% CO<sub>2</sub>. Thereafter, staining medium was replaced by DMEM only and 15 images of each scaffold were taken by CLSM at an excitation wavelength of 485 nm and an emission of 520 nm. Percentage of surface coverage of samples with cells was calculated by image processing software 'ImageJ, NIH', and compared as quantitative measurement.

## Materials and experimental methods

**Table. 2** Polymers, solvents and optimum electrospinning parameters for all fabricated fibers used in the present thesis

Fibers	Solvent	Concentration (Wt %)	Volt (kV)	Distance (cm)*	Flow rate (mL/h)	Needle diameter (mm)**
PLLA/PEO (90/10) with porous structure	CHCl <sub>3</sub>	4	14	15	1	0.8
PEI (bead structure)	NMP	20	10-12	8	0.1	1
PEI (Ribbon-like structure)	CHCl <sub>3</sub>	15	12	8	0.1	1
PET/ $\gamma$ -Fe <sub>2</sub> O <sub>3</sub> ***	TFA	12	10	8	0.1	1
PEO/ $\gamma$ -Fe <sub>2</sub> O <sub>3</sub> ***	CHCl <sub>3</sub>	2	10	8	0.2	1
PEI/EVA	NMP	20	14	15	0.1	1
CTS	TFA/DCM (70/30)	2.5	20	15	0.1	0.8
PHB	HFIP	3	16	15	0.1	0.8
PHB/CTS (50/50)	HFIP/TFA (50/50)	3	16	15	0.1	0.8
PS	THF/DMF	20	16-20	15	0.1	0.8
PVA	H <sub>2</sub> O	7	16	15	0.1	0.8
PVA/Col	H <sub>2</sub> O	7	16	15	0.1	0.8
PVA/n-HAP	H <sub>2</sub> O	7	16	15	0.1	0.8
PVA/Col/n-HAp	H <sub>2</sub> O	7	16	15	0.1	0.8
PMMA/EVA	CHCl <sub>3</sub> /DMF (80/20)	18	16-20	15	0.1	0.8
PVA/PHB	HFIP	3	16	15	0.1	0.8

\* Distance from the needle tip to the ground collector

\*\* Inner needle diameter

\*\*\* The concentration of Fe<sub>2</sub>O<sub>3</sub> in the total solution is 250 ppm



### 4. Results and discussion

#### 4.1. Electrospinning novel fibers with different morphologies for spread applications

##### 4.1.1. Electrospun fibers with porous structure

It is well known that electrospinning technique depends on various processing parameters such as solution properties and instrument setup. Therefore, choosing the solvent and type of the polymer are important factors that influence the solution properties, (e.g., viscosity, surface tension and conductivity) which in turn, influence the electro-spinnability, surface morphology and diameters of the obtained fibers <sup>73</sup>. However, in order to control the morphology and diameters of the obtained fibers, the overall parameters of electrospinning process should be taken into consideration. Recently, many researchers showed that surface morphology of the biomaterial scaffolds play a vital role in controlling cell adhesion, proliferation, shape, and function <sup>74</sup>. Herein, this chapter aims to develop and fabricate different electrospun polymeric materials with different structures and morphology that can be applied in many fields, especially in biomedical uses. In this chapter, solution parameters including polymer type, concentration, solvent vapour pressure, viscosity and composition of the solution (polymer blend) were studied. In addition, the process parameters including electric field strength, conductivity, solution flow rate, distance between the capillary and the collector, and needle diameter were also investigated. The results showed the possibility to produce fibers with a variety of surface morphologies including porous, beaded, ribbon-like, helical and uniform structure. In addition, the fiber size diameters were also varied by changing the electrospinning parameters.

In the present work, Poly (L-lactic acid) (PLLA) has been electrospun using solvents with different vapour pressures to investigate the influences of the solvent vapour pressure on morphology, diameter, crystallinity and mechanical properties of the electrospun fiber scaffolds. The results showed that the vapour pressure of the solvent and /or mixture solvents play an important role in the fiber diameters and their crystallinity. Furthermore, the fiber crystallinity increased by lowering the vapor pressure of the used solvent. In addition, the mechanical properties (tensile strength and young's modulus) are strongly dependent on morphological features such average fiber diameter. The smaller the average diameter the higher the tensile strength and Young's modulus <sup>75</sup>.

Fig. 6 shows the electrospun PLLA fibers with a highly porous structure. The as spun fibers were fabricated by inducing phase separation between PLLA and PEO (80/20 wt/wt)

## Electrospinning novel fibers with different morphology for spread application

during electrospinning. Then, the fibers were soaked in water for 5 days for selective removal of PEO fraction. Thereby, a highly porous structure with a controllable pore size and interconnected pores were obtained. Such kind of biocompatible, biodegradable, and highly porous fibers with high surface area can be applied as drug carrier for drug delivery systems<sup>76</sup>. Moreover, the fibers porosity allows favorable cell adhesion, propagation, and growth and hence makes them potential candidates for tissue engineering applications.

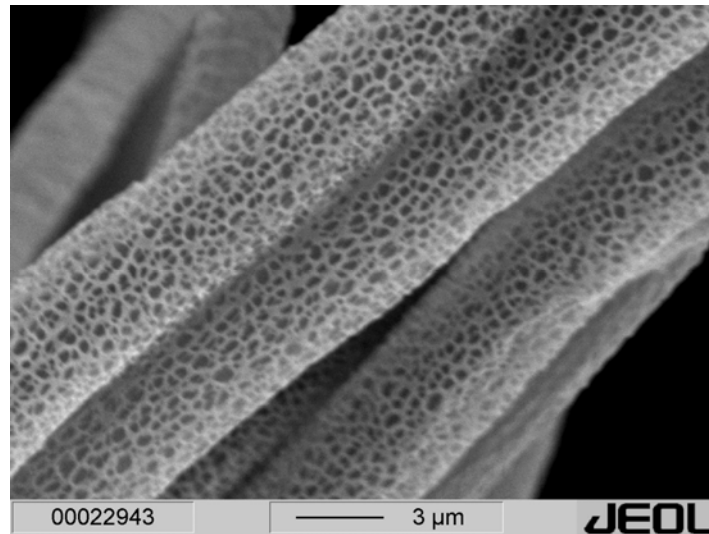


**Fig. 6. Electrospun PLLA/PEO (80/20) fibers have a porous structure after selective removal of PEO**

### 4.1.2. Electrospun fibers with bead and ribbon-like structures

Polyetherimide (PEI) is an amorphous thermoplastic that features high strength and rigidity at elevated temperatures with good flame retardant and chemical resistance. It is commonly specified for aerospace, automotive, and packaging applications. Recently, PEI have been used as a membrane for medical applications<sup>77</sup>. In the present work, beaded fibers from electrospun PEI were fabricated using N-Methyl-2-pyrrolidone (NMP) as a solvent. Ribbon-like fibers were obtained due to the high boiling point and higher surface tension of the solvent used. NMP has a boiling point of  $\sim 202^{\circ}\text{C}$ , meaning that a long time is required to evaporate the solvent during electrospinning. Moreover, the surface tension of NMP is  $\sim 30$  dyne/cm which has the main influence to form the bead structure of the resultant fibers. The surface tension tries to decrease the surface area per mass unit of the electrospun jet and will contract its radius to form such beads along the fiber axis (Fig. 7). On the other hand chloroform has a boiling point of about  $61.2^{\circ}\text{C}$  and a surface tension of  $\sim 26.67$  dyne/cm which is low compared with NMP. In this case, the solvent starts to

## Electrospinning novel fibers with different morphology for spread application

evaporate immediately after the ejection of the electrospun jet and will form a thin polymer skin on the surface of the jet. Then the skin undergoes to an elastically buckling, and the circular across the fiber section will be elliptical and then flat to form a ribbon-like shape (Fig. 8). Electrospun PEI fibers with bead or ribbon-like structures might be used in the future as a scaffold for tissue engineering applications<sup>77</sup>.

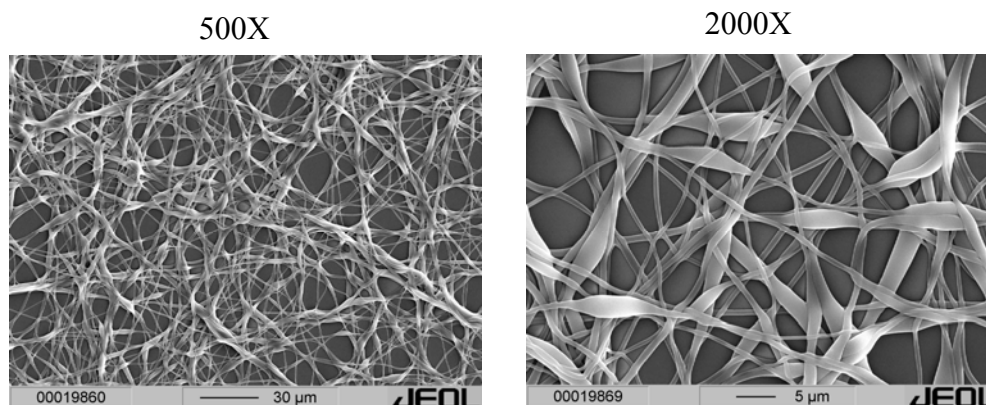


Fig. 7. Electrospun Polyetherimide using N-methyl 2-pyrrolidone as a solvent

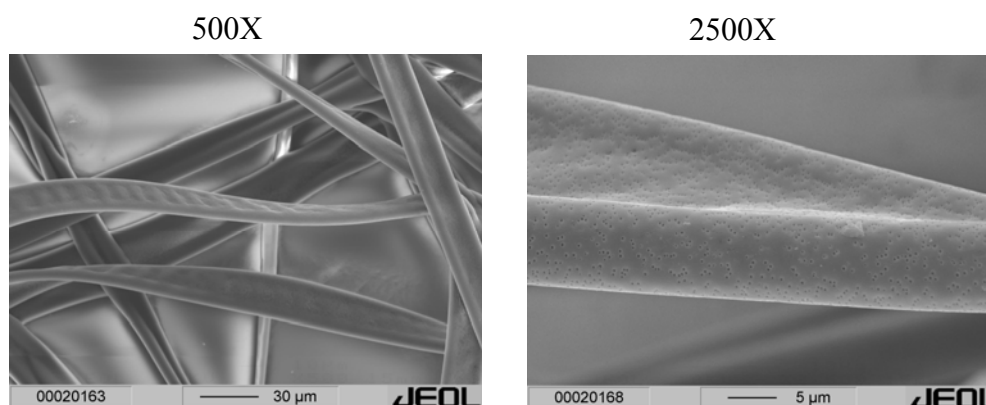


Fig. 8. Electrospun Polyethimide using chloroform as a solvent

### 4.1.3. Electrospun fibers with helical and twisted structures

The electrochemical property of conductive  $\gamma$ -Fe<sub>2</sub>O<sub>3</sub> played an essential role in the formation of the helical structure as helical fiber was not achieved from neat polymer<sup>14</sup>. The charge carried by  $\gamma$ -Fe<sub>2</sub>O<sub>3</sub> were transformed to the surface of the collected fibers on the ground collector. Thereby, an imbalance between the forces occurred to compel the rearrangement of the fibers (to retain the force equilibrium) and finally a helical or twisted structure could be obtained as shown in Fig. 9 and 10 a, b. The electrospun PET/ $\gamma$ -Fe<sub>2</sub>O<sub>3</sub> showed a twisted structure which arises from the presence of  $\gamma$ -Fe<sub>2</sub>O<sub>3</sub>. On the other hand, PEO/ $\gamma$ -Fe<sub>2</sub>O<sub>3</sub> exhibited a helical structure with some deformed fibers. The high amount of

## Electrospinning novel fibers with different morphology for spread application

forces carried by electrospun jet leads also to stretch the fibers in the electrospinning direction and the fibers will be deformed. The deformed fibers possess internal plastically stretched fibrils parallel to the fiber direction (see Fig. 10 b). Both electrospun fibers containing ferromagnetic nanoparticles could be potential candidates for micro electronics, smart textiles and biomedical applications.

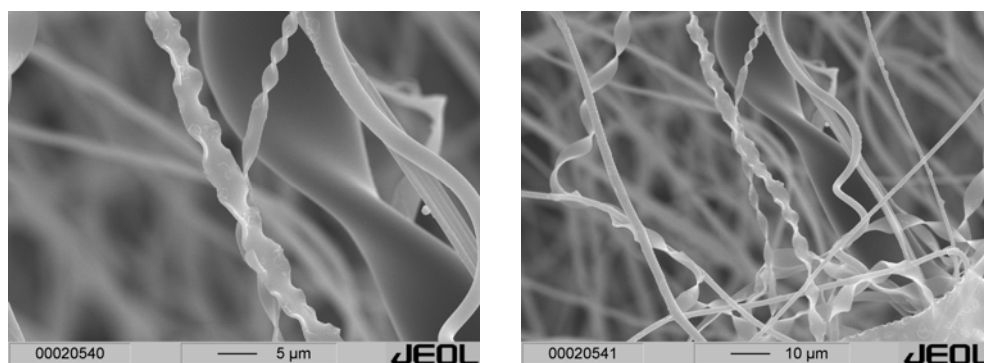


**Fig. 9. Electrospun PET/  $\gamma$ -Fe<sub>2</sub>O<sub>3</sub> (ferromagnetic iron oxide nanoparticles) nanocomposites fibers with twisted structure**

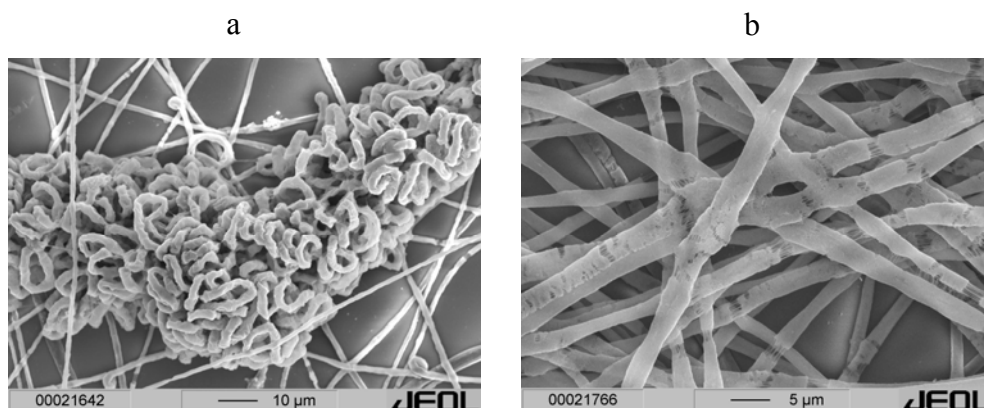


**Fig. 10. Electrospun PEO/  $\gamma$ -Fe<sub>2</sub>O<sub>3</sub> (ferromagnetic iron oxide nanoparticles) nanocomposites fibers with helical structure**

### 4.1.4. Electrospun fibers with rough surface

Polyethylene co-vinyl acetate (40% vinyl acetate) (EVA) were blended with PEI and they were electrospun using NMP as a solvent for the blend polymers. The influences of polymer composition on the fibers morphology were studied. The results showed that pure EVA solution (dissolved in NMP) is not able to form fibers, they produce only drops. This might be attributed to the less entanglement of the EVA macromolecules which is not sufficient to form continuous fibers. Addition of about 20 wt% PEI will promote the fiber structure formation, but they showed a high amount of spherical beads along the fibers. The spherical beads were transformed gradually to cylindrical structure by increasing the

## Electrospinning novel fibers with different morphology for spread application

PEI fraction (see Fig. 11). Furthermore, addition of small amount EVA (5 wt%) to PEI not only enhance the fiber homogeneity, but also provide a rough morphology to the fiber surface. The electrospun biocompatible PEI/EVA scaffolds might be useful candidate for biomedical application. It can be used in skin tissue engineering, drug delivery system and vascular graft application<sup>77</sup>.

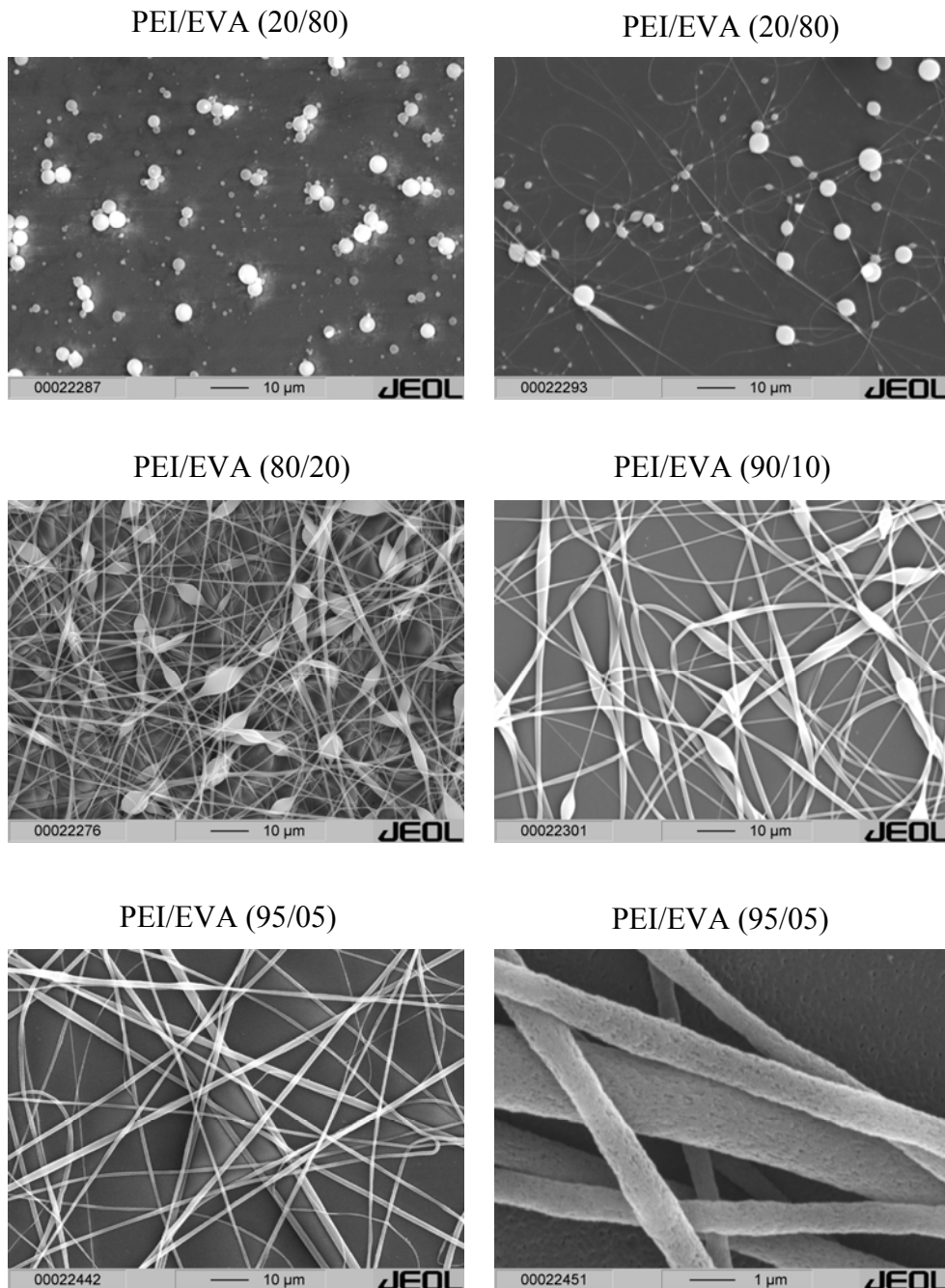


Fig. 11. Electrospun PEI/EVA with different ratios

### 4.1.5. Electrospun fibers with core sheath structure

- Morphology and phase structure of the blend PHB/Chitosan nanofibers :

## Electrospinning novel fibers with different morphology for spread application

Chitosan (CTS) and their derivatives were investigated as one of candidate materials for vastly diverse applications, including but not limited to waste management, food processing, biotechnology, tissue engineering and regenerative medicine<sup>78, 79</sup>. Moreover, much attention has been devoted recently to fabricate CTS nanofibers for medical applications<sup>80</sup>. Likewise, electrospun PHB nanofibers have been reported as scaffolds for medical applications<sup>81, 82</sup>. However, the major problem associated with the PHB applications is its high degree of crystallinity and brittleness<sup>83</sup>. An approach to overcome the high crystallinity of PHB is to make miscible blends of PHB with another kind of polymer such as CTS<sup>84</sup>. Nevertheless, electrospun PHB/CTS blend nanofibers have not been investigated in the literature. Fig. 12 (a, b) shows the SEM micrographs of electrospun chitosan and PHB/Chitosan (50/50) nanofibers, respectively. It is shown that both fibers have a homogenous structure without any sign of beads formation. The as spun chitosan has an average diameter of about 160 nm and PHB/Chitosan (50/50) has an average diameter of about 426 nm (see Fig. 13 a, b). Moreover, phase structure of chemically stained PHB/CTS nanofibers revealed that both polymers have a good distribution in the macromolecular region without any sign of phase separation (Fig. 14). Such kind of homogeneity and miscibility of the polymer blends is an important factor not only for reducing the high crystallinity of PHB, but also to facilitate the degradation rate of the obtained fibers scaffolds. On the other hand, fibers with diameters thicker than 500 nm exhibited a core sheath structure. The chitosan fraction agglomerated at the fiber surface as a sheath and PHB formed the fibers core (see Fig. 15).

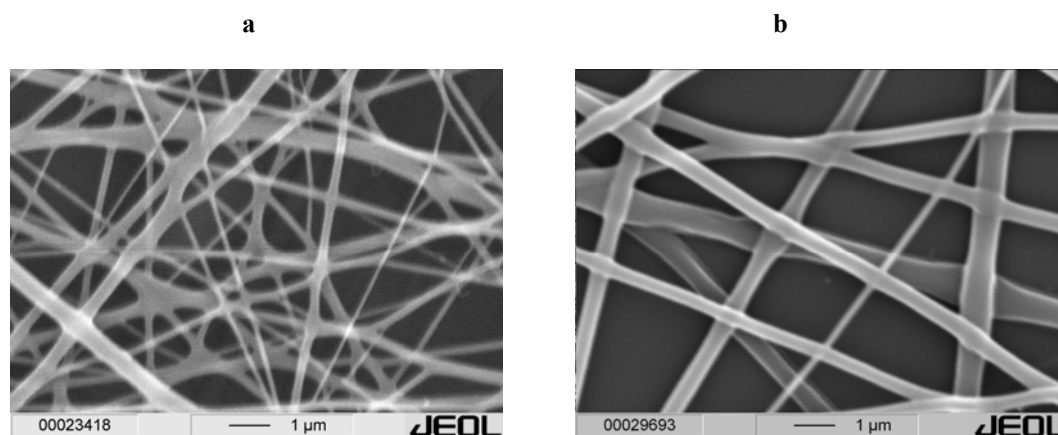


**Fig. 12.** SEM micrograph of (a) electrospun CTS nanofibers using TFA/DCM as a solvent and (b) electrospun PHB/CTS nanofibers using TFA/HFIP as a solvent

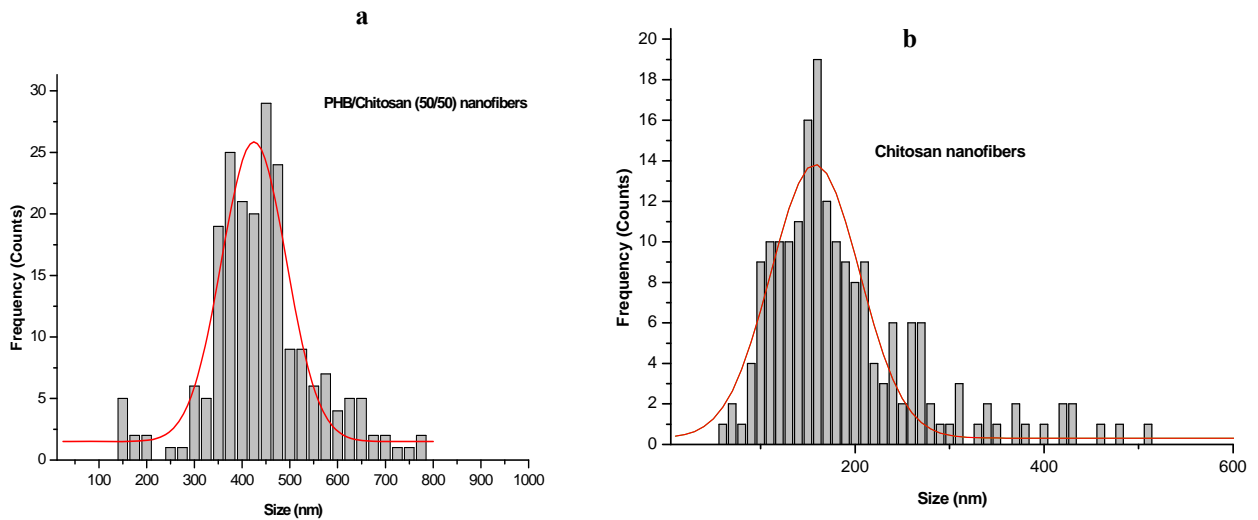


**Fig. 13. Diameter distribution of electrospun (a) PHB/CTS (50/50) using HFIP/TFA as a solvent and (b) Chitosan using TFA/DCM**

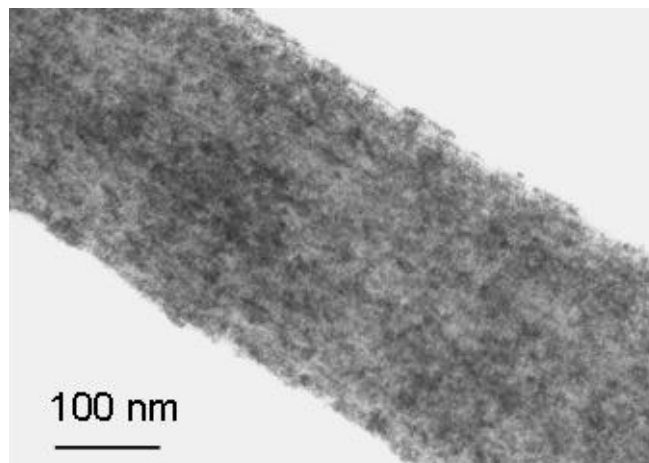


**Fig. 14. Electrospun PHB/CTS blend nanofibers, stained with OsO<sub>4</sub> vapors for 4 days (fibers thinner than 500 μm)**

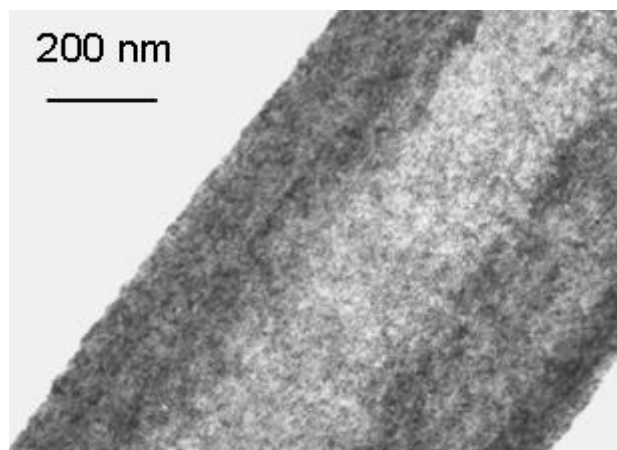


**Fig. 15. Electrospun PHB/CTS blend nanofibers, stained with OsO<sub>4</sub> vapors for 4 days (fibers thicker than 500 μm)**

### ▪ FTIR spectra of electrospun PHB/CTS blend nanofibers :

The sensitivity of FTIR spectrum to crystallization of PHB was demonstrated by Bloembergen et al.<sup>85</sup>. In the present study we investigated the influence of CTS on PHB after electrospinning. Electrospun PHB/CTS nanofibers have not been prepared before. Fig. 16 shows the FTIR spectra for electrospun PHB, CTS and PHB/CTS (50/50). The spectrum of PHB has a prominent characteristic absorption centered at about  $1720\text{ cm}^{-1}$  assigned to the stretching vibration of the carbonyl groups. In addition, the bands observed at about  $980$ ,  $1227$ ,  $1277$  and  $1720\text{ cm}^{-1}$ , attributable to the crystalline phase of PHB and band at  $1180\text{ cm}^{-1}$  arises from the amorphous phase. Moreover, the band observed at about  $1380\text{ cm}^{-1}$  is assigned to symmetric wagging of the  $\text{CH}_3$  group. CTS has characteristic absorptions centered at about  $3348\text{ cm}^{-1}$  attributed to the hydroxyl stretching ( $\nu_{\text{O-H}}$ ) and the N-H stretching, and two bands observed at about  $1652\text{ cm}^{-1}$  and  $1557\text{ cm}^{-1}$  were attributed to the amide I ( $\nu_{\text{C=O}}$ ), amide II and the N-H deformation arising from the amide and/or amine groups<sup>86</sup>. However, the carbonyl band observed at about  $1720\text{ cm}^{-1}$  in pure PHB shifted to about  $1727\text{ cm}^{-1}$  in case of electrospun PHB/CTS. The wave number of the carbonyl group was increased due to the disturbance of the crystalline portion after addition of CTS<sup>87</sup>. Moreover, the bands centered at  $980$ ,  $1227$  and  $1277\text{ cm}^{-1}$  attributable to the crystalline phase of PHB were disappeared in the electrospun PHB/CTS blend nanofibers. Furthermore, the band observed at about  $1672\text{ cm}^{-1}$  assigned for  $\text{NHCOCH}_3$  bonding of CTS and band at about  $1528$  was for the  $\text{NH}_2$  group. The results from FTIR demonstrated that PHB was interconnected with CTS through hydrogen bonds in the macromolecular region. Moreover, the crystalline related bands were disappeared in the blend fibers; CTS suppressed the crystallinity of PHB in the blend nanofibers through the interaction between them (hydrogen bonds). The interaction act as bridges between the polymers and consequently reduces the crystallinity and facilitated the miscibility of the polymers in the blend nanofibers.

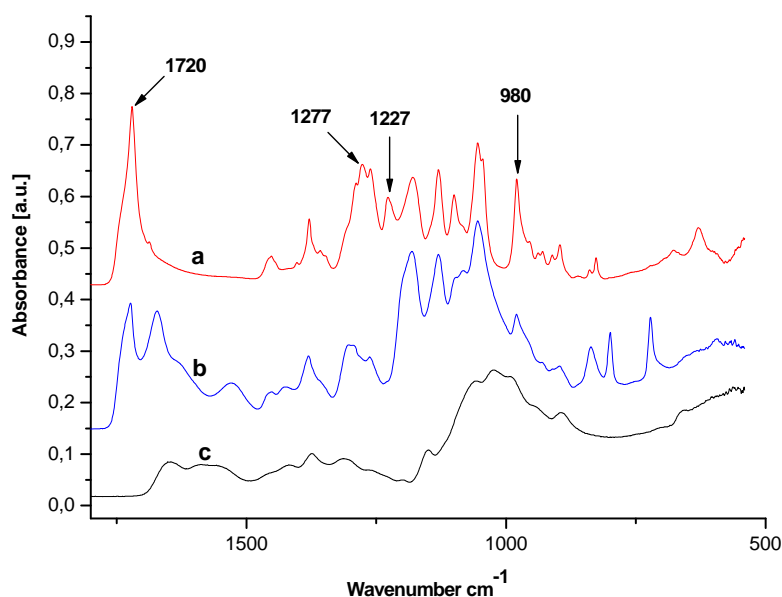


**Fig. 16.** FTIR spectra of electrospun (a) pure PHB, (b) PHB/CTS (50/50) and (c) pure CTS nanofibers, the marked peaks represent the crystalline phase of PHB

▪ **Crystallization behaviour of electrospun PHB/CTS nanofibers :**

The results from DSC and the characteristics observed for PHB powder, electrospun PHB and PHB/CTS (50/50) nanofibers were showed in Fig. 17 and summarized in Table. 3. The melting thermogram of PHB exhibited two endothermic peaks at about 147 and 159.6 °C, arising from melting of crystalline PHB. The double melting peaks of PHB can be attributed to the melting of the re-crystallized component which can occur during the melting process<sup>88</sup>. Moreover, the double melting peaks of PHB powder were slightly increased after electrospinning due to the macromolecular orientation of the polymer molecules in the fiber direction during Electrospinning<sup>89</sup>. Thus, the degree of crystallinity of electrospun PHB found to be increased compared with PHB powder. On the contrary, the double melting peaks are slightly decreased in case of electrospun PHB/CTS (50/50) blend nanofibers. Furthermore, the degree of crystallinity of PHB in the blend PHB/CTS (50/50) significantly decreased after electrospinning (see Table. 3). CTS molecule has a large amount of amine groups in its side chains that provide ability to form a large number of intermolecular hydrogen bonds with carbonyl groups of PHB. The suppression of PHB crystallization found in the PHB/CTS (50/50) blend may be caused by the formation of intermolecular hydrogen bonds between the carbonyl groups of PHB and the amine and /or

## Electrospinning novel fibers with different morphology for spread application

hydroxyl groups of CTS. The decrement of the degree of crystallinity of PHB in the nanofibers blend was also found by FTIR spectroscopy.

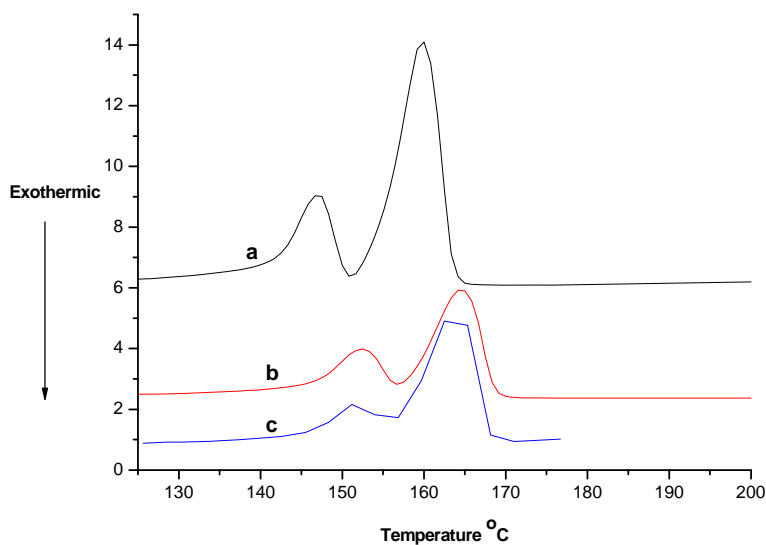


**Fig. 17. DSC thermograms of (a) PHB powder, (b) electrospun PHB and (c) PHB/CTS (50/50) nanofibers**

**Table. 3. DSC data and the characteristics observed for PHB powder, electrospun PHB and PHB/CTS nanofibers**

Sample	$T_{m1}$ (°C)	$T_{m2}$ (°C)	$T_c$ (°C)	$\Delta H_m$ ( $J \cdot g^{-1}$ )	Crystallinity (%)
PHB Powder	147.2	159.68	76	97	66.5
PHB Nanofibers	152.2	164.50	81.4	98.5	67.5
PHB/CTS Nanofibers	150	163	70.6	27.56	37.7

### ▪ Degradation morphology of PHB/CTS (50/50) blend nanofibers

The morphology changes during in vitro degradation were examined by using scanning electron microscopy. For degradation study, electrospun PHB/CTS nanofiber specimens were immersed in simulated body fluid (PBS solution) at 37 °C for one week. Thereafter, the specimens were dried in a drying oven and then coated with Au in sputter coating machine before observation through SEM. The nanofibrous scaffolds showed a remarkable degradation after one week (see Fig. 18). It is known that PHB has a low degradation rate because of its high crystallinity<sup>90</sup>. However, in the present study PHB/CTS nanofibers started to degrade one week after the test and the degradation increased by increasing the time. The reason for the fast degradation is the lower degree of crystallinity for the blend nanofibers. PHB/CTS blend nanofibers exhibited a degree of crystallinity of about 37.7 compared with about 67.5 for pure PHB nanofibers (Table. 3). The crystallisation plays an important role in the PHB hydrolytic degradation, which happened in the amorphous region at an earlier stage<sup>91</sup>. Moreover, an important factor that enhanced the degradation rate was that the nanofibers had a higher ratio of surface-to-volume than bulk materials. The characteristics of the fabricated nanofibrous scaffolds (e.g., high surface area to mass ratio, high porosity, biocompatibility and biodegradation with faster degradation rate) might be promising scaffold materials for tissue engineering application.

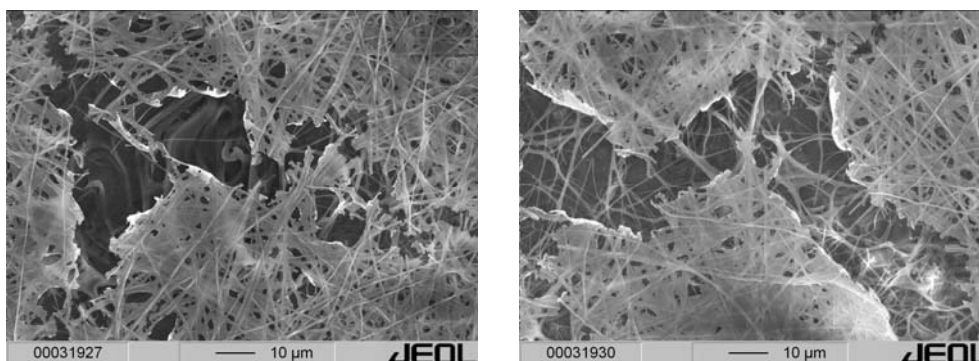


**Fig. 18. SEM images showing in vitro morphology changes of electrospun PHB/CTS (50/50) blend nanofibers after one week degradation in PBS solution at 37 °C**



### 4.2. Mechanical properties of PS nanofibers

Reneker and Chun demonstrated that the electrospun nanofibers have a good macromolecular orientation which is produced by the stretching of the polymer jet during Electrospinning<sup>9</sup>. Thereby, the high molecular orientation of polymer molecules in the electrospun fibers will enhance their mechanical properties (e.g., higher elastic modulus and strength) as compared to bulk materials. Recently, many attempts have been gained using in situ imaging of single nanofiber to study its mechanical deformation and relating the deformation observed to the stress–strain characteristics of the nanofibers<sup>92</sup>.

Polystyrene (PS) is a thermoplastic amorphous, stiff polymer with limited flexibility. It is considered to be one of the most versatile, easily fabricated and cost-effective plastics<sup>93</sup>. PS is used in many different applications including packaging for food, disposable cutlery, plastic models, packing materials, insulation, and disposable beverage cups<sup>94</sup>. Recently, PS nanofibers and nanocomposites have been fabricated by electrospinning technique for different applications<sup>95,96</sup>. One of the most disadvantages of PS is its brittleness; in tension the strain at break is only a few percentages. However, PS macromolecules can be deformed to a very high degree if they are arranged in very thin fibers or films. This effect is well known from the fibrils inside crazes, the typical deformation zones in PS.

Crazes are long deformation zones in perpendicular direction to the loading direction, up to some 100  $\mu\text{m}$  long and about 10  $\mu\text{m}$  thick. They possess an internal structure of nanovoids with plastically stretched fibrils about 10-30 nm thick. The fibrils are stretched up to more than 300 %<sup>97</sup>, the limit of deformation of the entanglement network<sup>98</sup>. In this section, PS was chosen as an example of brittle material to study the effect of the electrospinning process on the mechanical deformation behaviour of the single nanofiber. Moreover, the aim of this study was also to check if PS nanofibers reveal a transition from the typical crazing behaviour to ductile deformation with decreasing fiber thickness.

### 4.2.1. Morphology

Fig.19 shows SEM micrographs of electrospun PS nanofibers with random orientation. It is visible that the individual PS nanofibers are relatively uniform in thickness without any sign of bead formation. The diameters of the electrospun PS nanofiber vary from 150 nm to 800 nm (see Fig 20) with a well pronounced maximum at a diameter of about 380 nm. Fig. 21 shows a SEM micrograph of PS nanofibers uniaxially aligned in one direction. Such patterns of parallel nanofibers have been used to perform tensile tests and also to produce hot compacted specimen. Result of the hot compaction is a compacted pattern of fibers with many free spaces or holes between them, see Fig. 22. Fig. 22 a shows uniaxially aligned PS nanofibers compacted at 85 °C with a pressure of 20 MPa for 5 min and Fig.22 b. shows nanofibers compacted at 85 °C with 30 MPa for 5 min. The best temperature for compaction found to be at ~ 85 °C with a pressure of 20 MPa and 30 MPa. Many of the original nanofibers were connected to thick fiber bundles up to some  $\mu\text{m}$  thickness, but there were visible also some thin individual nanofibers. In case of compaction at 90 °C (which is near to  $T_g$  of PS), the nanofibers adhered together and formed a membrane without any sign of fibril structure (Fig.22 c).

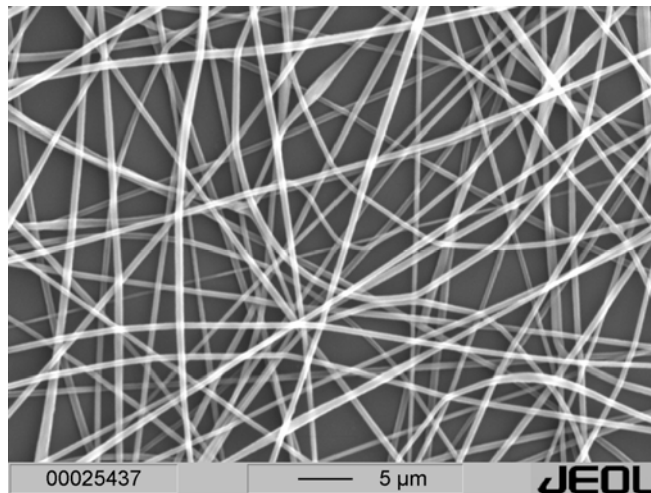


**Fig. 19. SEM micrograph of electrospun PS nanofibers**

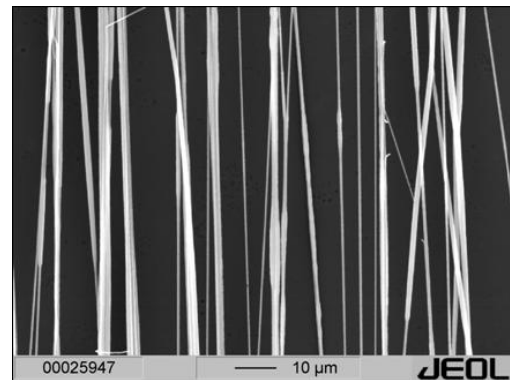
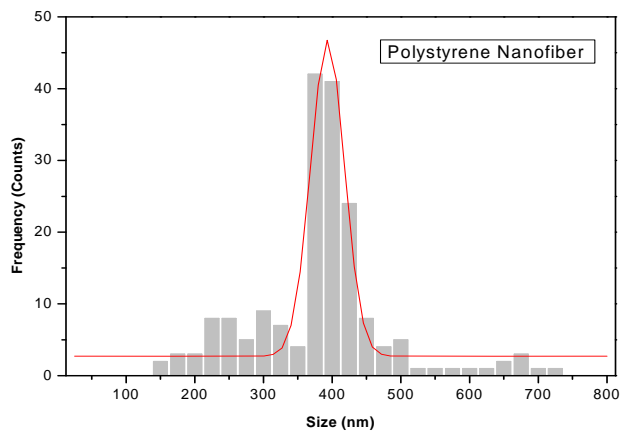


Fig. 20. Diameter distribution of PS nanofibers Fig. 21. SEM micrograph of uniaxially PS nanofibers

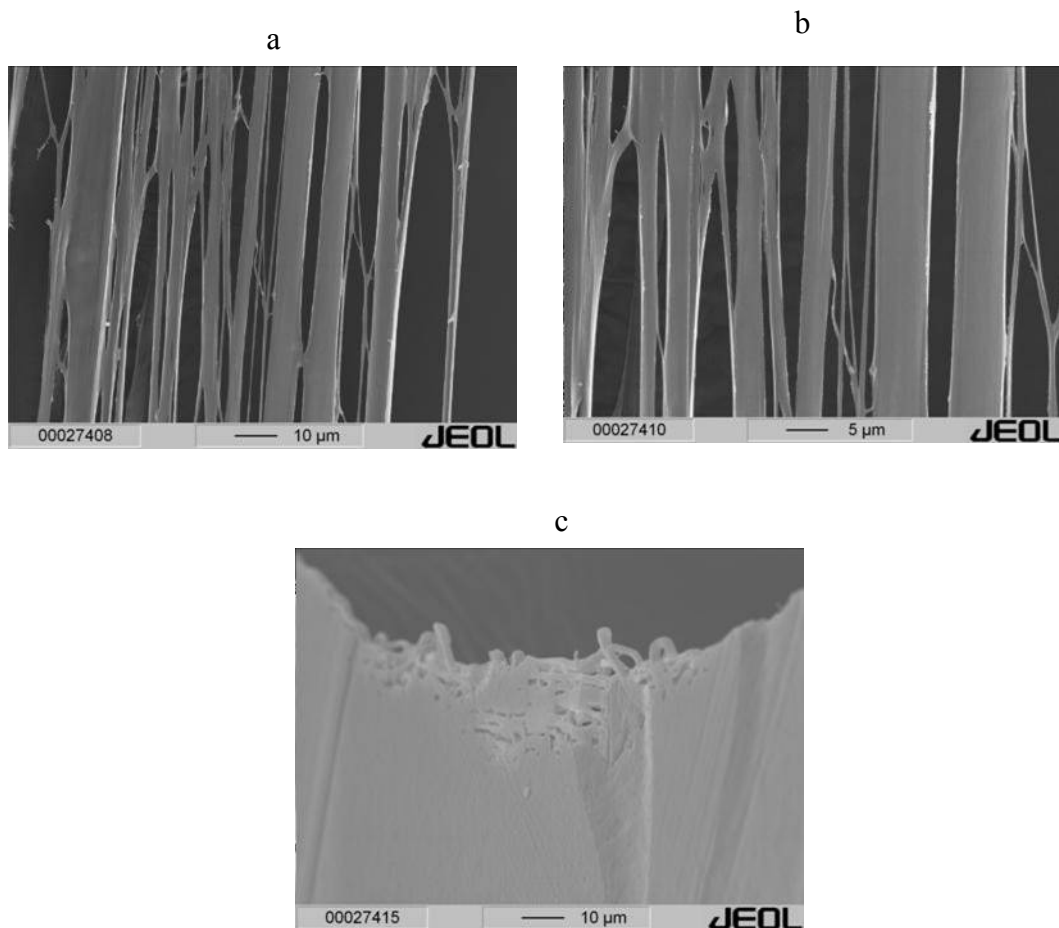
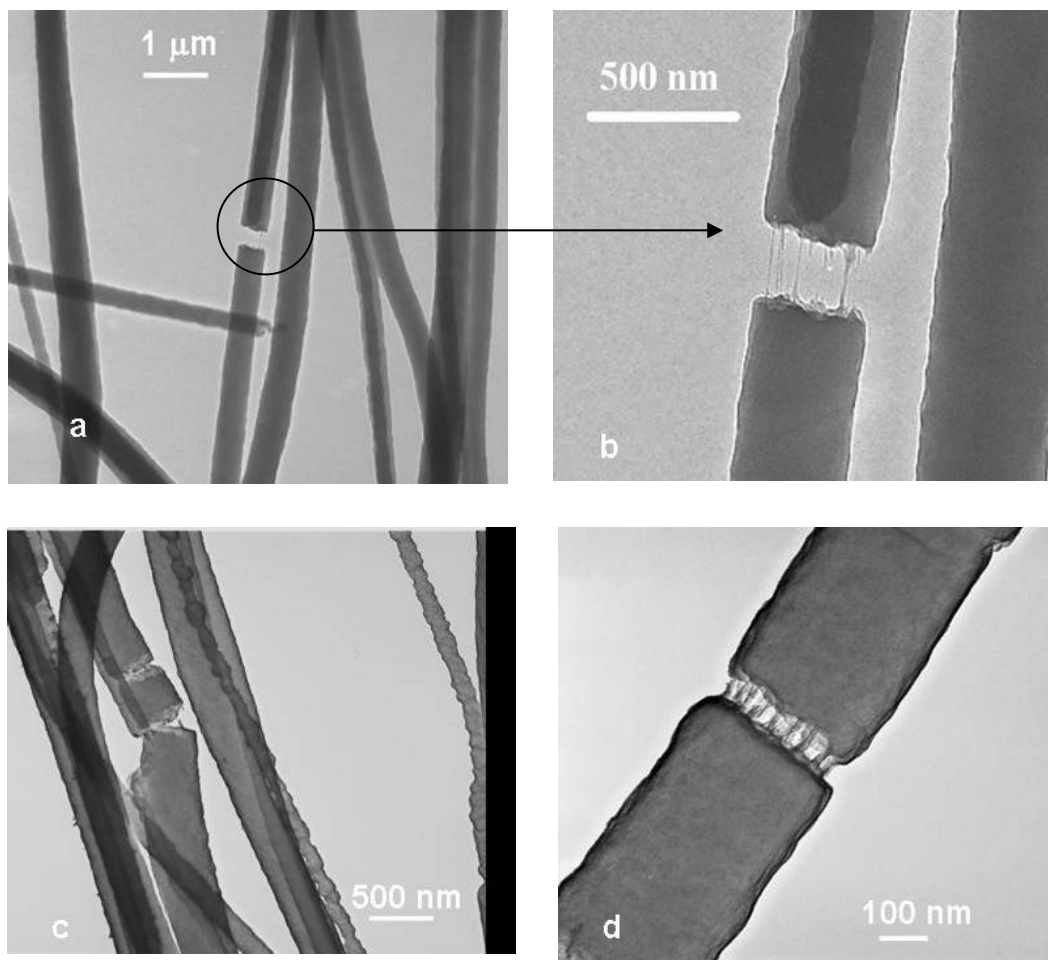


Fig. 22. Morphology of a pattern of hot compacted PS nanofibers  
(a) Compacted at 85 °C with a pressure of 20 MPa for 5 min  
(b) Compacted at 85 °C with a pressure of 30 MPa for 5 min  
(c) Compacted at 90 °C, 30 MPa for 5 min

### 4.2.2. Deformation of single electrospun PS nanofibers

Fig. 23 shows the deformation structures of PS nanofibers mechanically deformed in situ in a TEM. It is shown that the fibers exhibited some places with the appearance of typical crazes before breaking. The craze thickness (elongation of crazes in direction of fibril length) is about 120 nm, the craze fibrils are  $\sim 20$  nm thick and the interfibrillar spacing between craze fibrils (long period) is about 25 nm (Fig. 24). Appearance of crazes in similar structure has been detected in all PS fibers with diameters above 225 nm.



**Fig. 23.** TEM micrographs of deformed PS nanofibers with fibrillated crazes

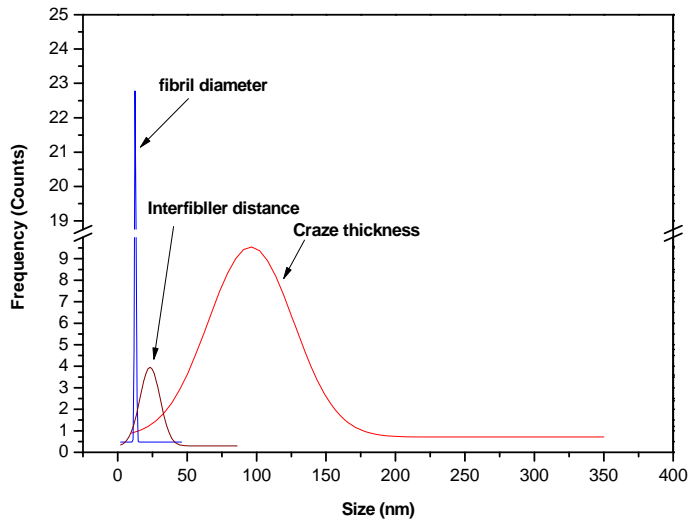


**Fig. 24. Distribution of craze thickness, craze fibril diameter and interfibrillar distance (long period) in deformed PS nanofibers**

Fig. 25 shows ESEM micrographs of deformed and partially ruptured PS nanofibers. It is an interesting result that some fibers showed thinner parts due to necking and cold drawing. The same effect was visible after deformation in the TEM (see Fig. 26).

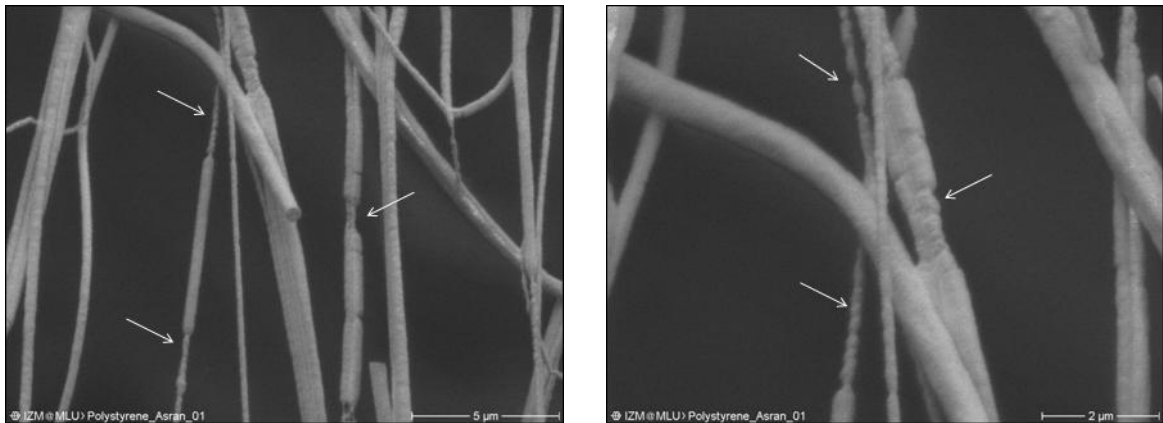


**Fig. 25. Deformed PS nanofibers in ESEM micrographs: Local necking zones are shown by arrows**

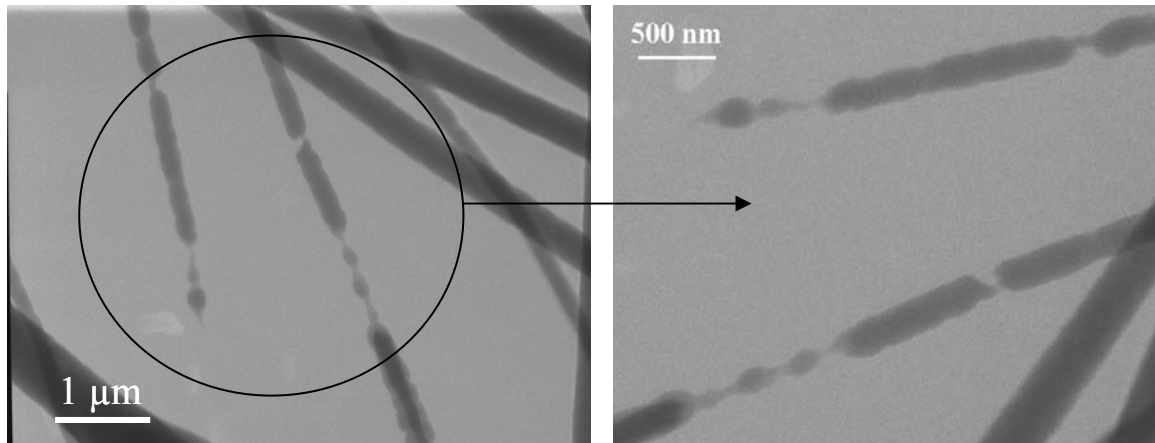


**Fig. 26. TEM micrographs of deformed PS nanofibers with necking and cold drawing zones in lower (left) and larger magnification (right): image rotating due to change in magnification in TEM**

A detailed inspection revealed that fibers with necking and cold drawing appear only in the fibers thinner than 225 nm, see Table. 4. The fiber diameter contracted from  $\sim 225$  nm to nearly 60 nm in the neck regions. The length of the neck zone was in the range from 100 nm to 200 nm and partly some necking zones follows one after the other. Partly there were thin cold drawing zones with a total length of these zones of some  $\mu\text{m}$ . It is a surprising result that the transition in the micromechanical behaviour appeared at thicknesses of the PS fibers between 220 and 230 nm, i.e. with a sharp limit. PS fibers thicker than this limit showed only craze deformation and PS fibers thinner than that revealed only necking and cold drawing.

**Table. 4. Results of image analysis of deformed PS nanofibers with appearance of crazes or necking zones, respectively**

No	Fiber Diameter (nm)	Craze Thickness (nm)	Craze Fibril Diameter (nm)	Observation
1	391	223	8	Crazing No Necking
2	614	93	25	Crazing No Necking
3	364	57	18	Crazing No Necking
4	363	58	12	Crazing No Necking
5	378	56	13	Crazing No Necking
6	237	112	23	Crazing No Necking
7	226	90	17	Crazing No Necking
8	264	99	23	Crazing No Necking
No	Fiber Diameter (nm)	length of necking zone (nm)	Neck width (nm)	Observation
9	220	123	52	Necking
10	218	155	52	Necking
11	198	168	65	Necking
12	165	109	88	Necking
13	155	189	57	Necking

### 4.2.3. Deformation of compacted PS nanofibers

PS nanofibers in parallel packaging, which have been compacted under pressure at higher temperature below the glass transition temperature of bulk PS ( $T_g = 105\text{ }^\circ\text{C}$ ) revealed in the deformation tests that the deformation mechanism is only crazing. The compacted material consists mainly of thicker PS fibers (Fig. 27) showing crazes in the thicker fibers of the compacted pattern. The thick compacted fibers, which consist of several individual parallel fibers, show coarse crazes with large nanovoids and irregularly arranged fibrils with thickness from 25 nm up to 200 nm (see Fig. 27. a, b and Fig. 28 c,d). The thick compacted

## Mechanical properties of nanofibers

fibers deform with formation of crazes propagating from one surface to the opposite one, but with interruption of the regular craze fibrillation due to the interfaces between the individual nanofibers. In general, the compacted material deforms such as thicker PS single fibers and also as bulk material.

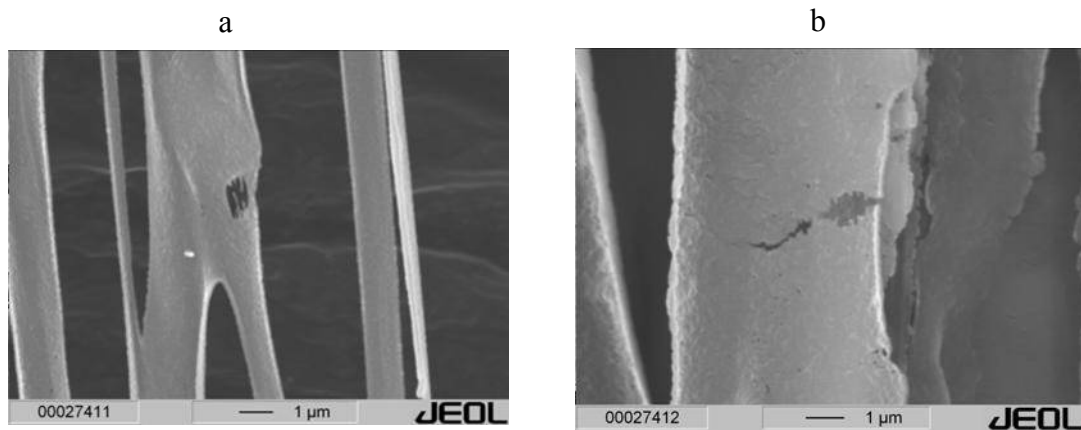


**Fig. 27. Deformation of hot compacted aligned PS nanofibers in SEM compacted at 85 °C with a pressure of 30 MPa for 5 min**

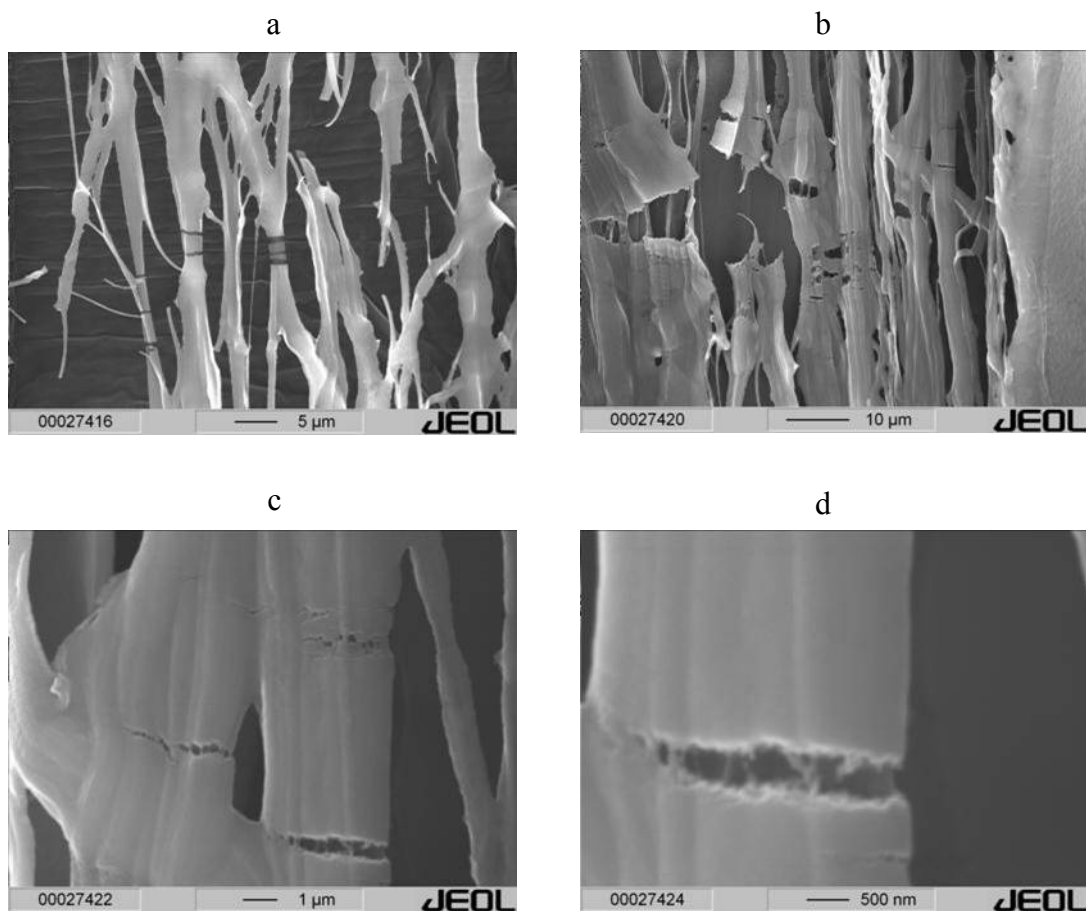


**Fig. 28. Deformation of hot compacted aligned PS nanofibers in SEM compacted at 85 °C with a pressure of 30 MPa for 5 min**

## Mechanical properties of nanofibers

The thick fibers show crazes at lower elongations and determine the deformation character. Thinner fibrils with thickness below the thickness limit of about 220-225 nm have no influence on the deformation mechanism. As mentioned before, the structure of the crazes in compacted PS nanofibers appear coarser than in the single nanofibers, see Fig. 29 (and compare with Fig. 24). The reason is partly in the higher stress level in compacted material and partly also in the limited resolution power of the SEM inspection (Fig. 27 and Fig. 28) compared with TEM inspection (Fig. 23). The SEM micrographs reveal only the thicker craze fibrils and not, as in TEM inspection, also all the thinner ones.

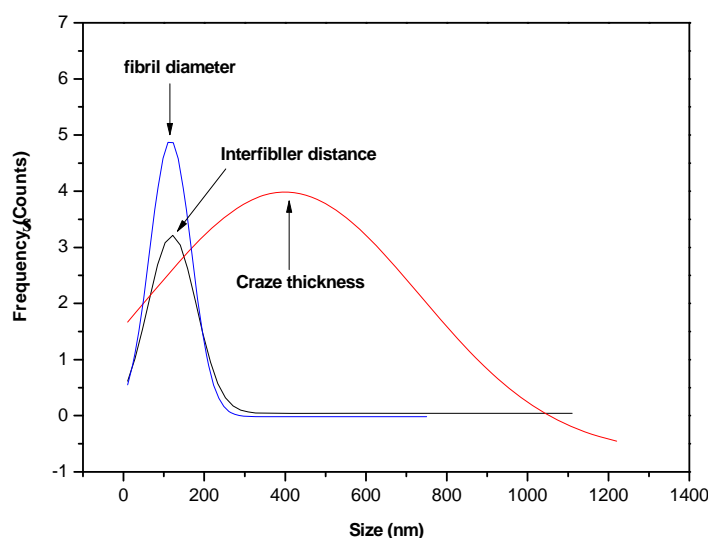


**Fig. 29. Distribution of craze thickness, craze fibril diameter and interfibrillar distance of deformed hot compacted PS nanofibers (hot compacted at 85 °C, 30 MPa for 5 min)**

**Table 5. Glass transition temperatures for bulk PS, PS nanofibers and hot compacted PS nanofibers**

Sample No	Sample description	T <sub>g</sub>
Polystyrene I	Granules	105
Polystyrene II	Nanofibers	101
Polystyrene III	Compacted nanofibers at 82 °C, 30 MPa for 5 min	99
Polystyrene IV	Compacted nanofibers at 90 °C, 30 MPa for 5 min	98

### 4.2.4. Thermal analysis (DSC)

The result of determination of the glass transition temperature of the different materials from DSC analysis is summarized in Table 5. Compared to the glass transition temperature of granules of PS (the same as in bulk PS) the fibers show lower values.

### 4.2.5. Discussion and conclusions

Bulk PS material deforms with the only formation of crazes. The features of crazes, stretched fibrils between elongated nanovoids, are illustrated in Fig. 30 a. From the starting point, e.g. a notch or defect at the surface as a stress concentration point, the craze propagates into the bulk material and usually decreases in thickness. Under additional increase in loading, the craze fibrils rupture and a crack propagates very quickly through the craze. The very fast crack propagation is the typical feature of the brittle fracture of PS. Hot compacted PS with thick fibers or strands of PS nanofibers revealed the same micromechanical behaviour with fibrillated crazes starting from the surface and propagating into the material. Crazes appear also in the thicker nanofibers (thicker than about 230 nm), but with the difference that the crazes penetrate the whole fiber thickness. The average fibril thickness of 10-25 nm and the fibril distances (long period) of 30-60 nm, i.e. the diameter of the nanovoids between fibrils of 10-40 nm, correlate very well with the typical features of crazes in bulk PS<sup>98</sup>. The craze length is limited by the fiber thickness, i.e. in the range of a few 100 nm, see Fig. 30 b. A very interesting transition in the deformation behavior appeared in fibers thinner than 225 nm. Here, the plastic deformation started with necking of the fiber and thinning up to a thickness of about 50-80 nm. The necking zone is partly localized and partly expanded up to some  $\mu\text{m}$ , similar a cold drawing zone, see Fig. 30 c. The reduction of the fibril thickness from about 200 nm up to 60-80 nm in the necking zone can be used to estimate a local plastic strain of up to few 100 %. This value correlates with the maximum elongation of the entanglement network in PS of about  $\lambda_{\text{max}} = 400\%$ <sup>99, 100</sup>, see Fig. 31. Such high elongations are also realized in the craze fibrils of bulk PS with the typical fibril thickness of 10-30 nm after stretching. The fibrils are deformed up to some 100 % and, therefore, the starting thicknesses of the PS parts before deformation were in the range of 30-60 nm. These results showed that plastic yielding in bulk PS starts, if there are material strands between nanovoids thinner than about 60 nm. In such thin strands exists only some entanglement meshes in perpendicular to the deformation direction. Therefore, there are no constraints acting and an easier deformation in length direction is possible<sup>101</sup>. Nanofibers, on the other hand, start to necking, if they are thinner than 220 nm. The reason of this larger thickness compared with

## Mechanical properties of nanofibers

---

the thickness of craze fibrils could be found in the free surface of the nanofibers and, therefore, the reduced glass transition temperature  $T_g$  (see Table 5). This effect could increase molecular mobility and ductility of the material in a modified surface layer around the fibers. If we assume such a modified surface layer with increased mobility in the same thickness than the PS strands in the crazes, i.e. of about 60 nm, an unmodified core in a thickness range of about  $(220 - 2 \times 60 = 220-120)$  100 nm remains. To explain this discrepancy we can find an additional effect in the macromolecular orientation in the fibers. It can be assumed that the macromolecules were partly oriented in fiber direction with a change from spherical macromolecular coils as in the bulk to an oriented shape in the fibers. Oriented PS films showed a higher crazing stress in orientation direction<sup>98</sup>. In a consequence, with increasing loading the yield stress can be reached earlier than cavitation stress (or crazing stress) and necking occurs. Both effects, the free surface of the nanofibers with increased molecular mobility (and reduced glass transition temperature  $T_g$ ) and the macromolecular orientation with increased crazing stress, enhance the ductility limit of the nanofibers to the larger values of about 200 nm (compacted to about 60 nm of PS strands in crazing mechanism). The change in deformation mechanism with decreasing specimen thickness of PS from crazing in bulk material to multiple craze formation in thick nanofibers and necking or cold drawing in thinner nanofibers is sketched in Fig. 32.

To conclude, the usually typically brittle PS can be modified using electrospinning technique so that a transition from crazing behaviour to micronecking and ductile behaviour appeared. The increased ductility of very thin PS fibers could be used to produce ductile PS networks for different applications for instance networks as flocculants in the treatment of waste water<sup>102</sup>, ion exchanger<sup>103</sup>, for organic electronic applications<sup>104</sup>, for optical application<sup>105</sup>, and scaffolds for biomedical applications<sup>106</sup>

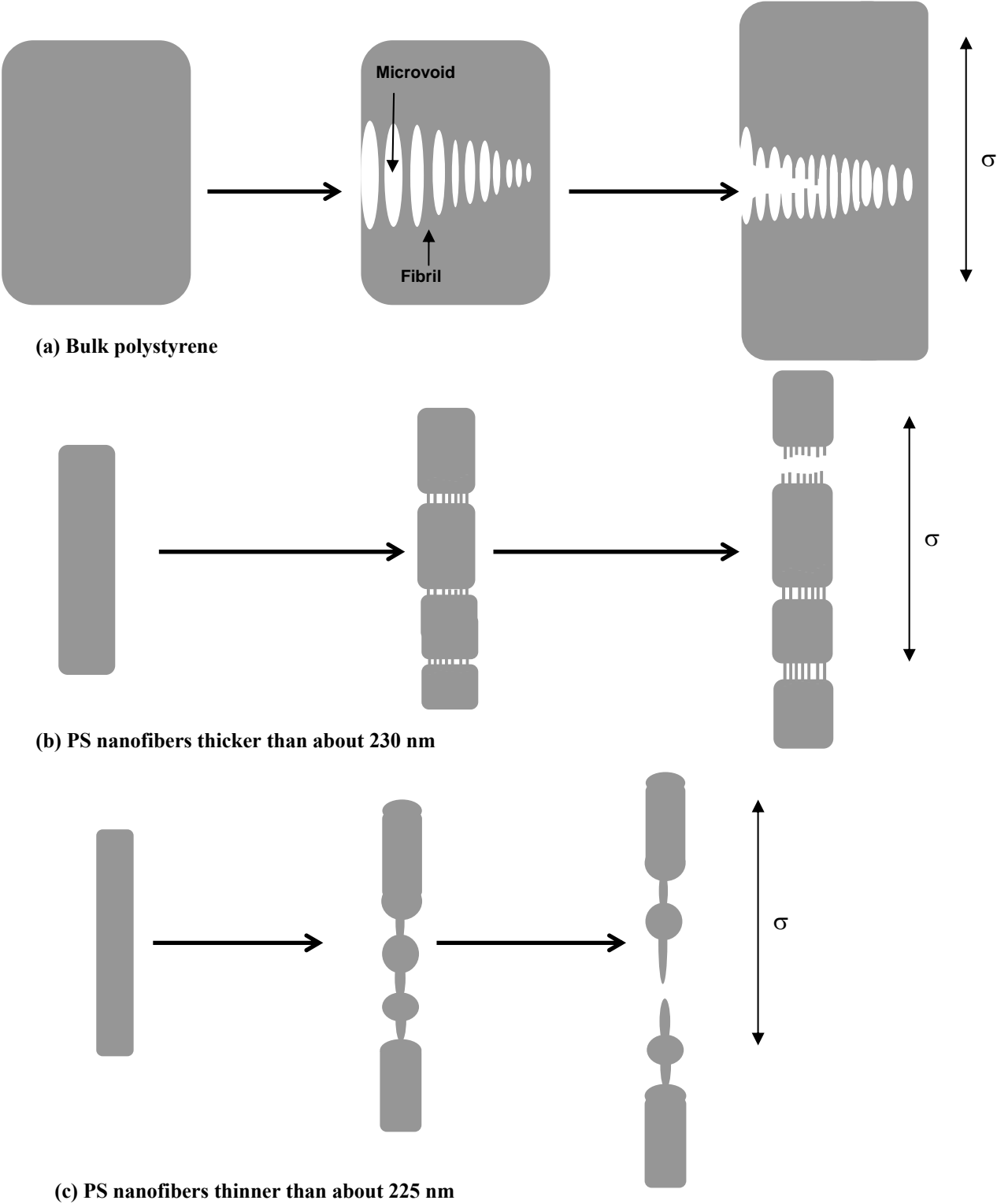


Fig. 30. Schematic illustration of micromechanical deformation mechanism of PS in dependence on sample thickness

- a) Bulk polystyrene
- b) PS nanofibers thicker than about 230 nm
- c) PS nanofibers thinner than about 225 nm

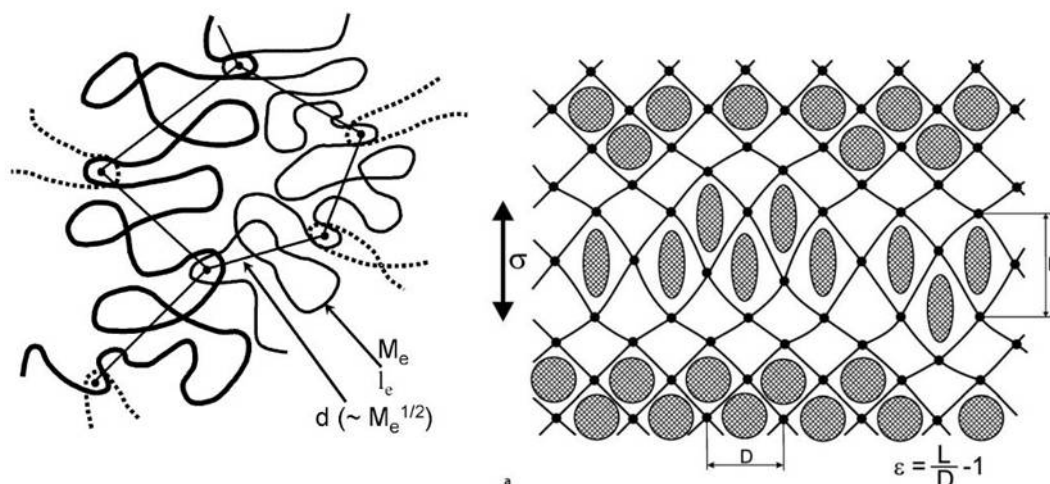


Fig. 31. Entanglements and entanglement network in amorphous polymers;  $M_e$ ,  $l_e$  are the molecular weight and the length of the macromolecular segments between entanglements, respectively;  $d$  is the distance between entanglements;  $\lambda_{\max} = \frac{L}{D}$  is the maximum elongation of the network under an applied loading stress (from reference<sup>54</sup>).

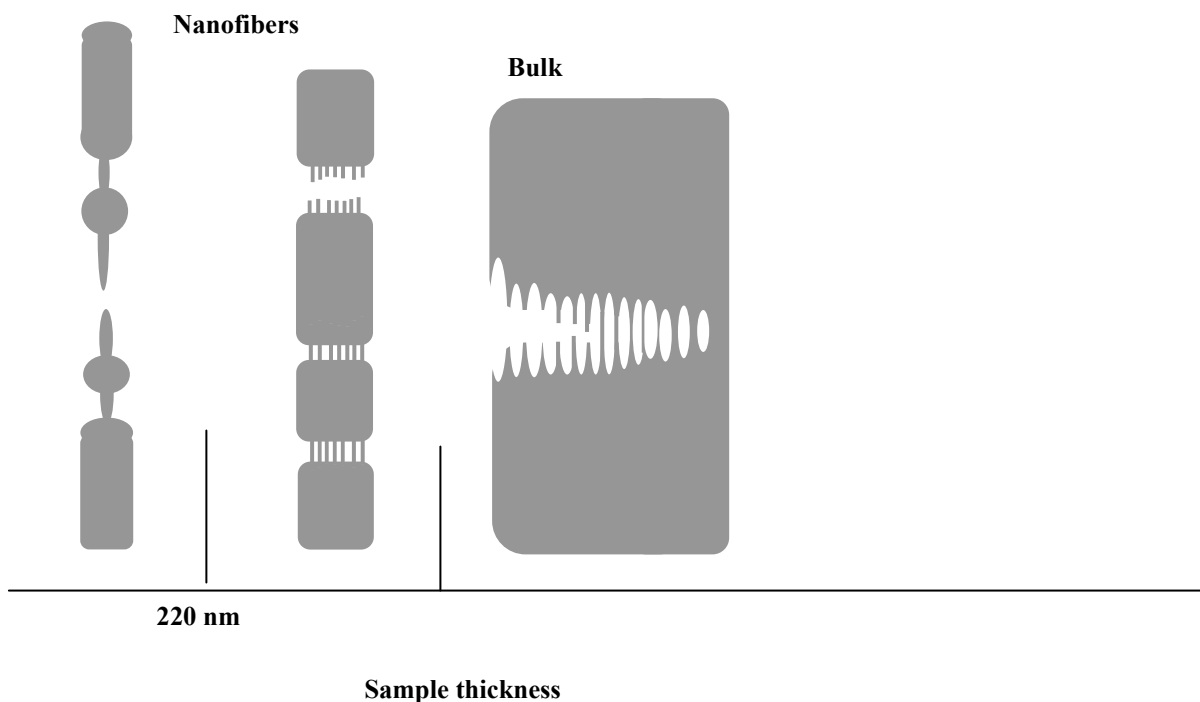


Fig. 32. Scheme of change in the deformation mechanism of PS with decreasing sample thickness from bulk material to nanofibers



### **4.3. Electrospun PMMA/EVA nanofibers for dentistry applications (custom-made mouth guards and dentures)**

Mouthguards are worn by participants are active in some fields of sport to reduce damage to the orofacial complex, as well as to protect teeth against chipping, fractures, displacement, and avulsion caused by impacts. The most commonly used and cheaper type is the mouth formed mouthguard which is made by the user after softening it in hot water and forming it in the mouth with pressure from fingers, tongue, and cheek <sup>107</sup>. The second type is the custom made mouthguard which is individually fitted to the wearer and requires a dental impression, dental models, and a forming process based on either pressure or vacuum <sup>108</sup>. Generally, this type of mouthguard has the advantage of better fit and greater comfort and is, therefore, more effective. Polyethylene-co-vinyl acetate (EVA) is the most common material exhibits desirable properties for fabrication of custom made mouthguard <sup>109</sup>. It is a non-toxic material with minimal moisture absorption, elasticity, ease of manufacture and adequate mechanical properties <sup>107, 110</sup>. Next to special medical grade rubber (EVA), denture liners are also fabricated from silicone-type compounds <sup>111</sup>. Poly (methyl methacrylate) (PMMA) is one of the plastics commonly used as dental-base materials because of its biocompatibility, relatively ease of manipulation, and low toxicity <sup>112</sup>. In addition, PMMA has been used for bone cements, contact and intraocular lens, screw fixation in bone, filler for bone cavities and skull defects and vertebrae stabilization in osteoporotic patients <sup>113</sup>. All acrylics in denture use are based on PMMA, with two distinct types, heat cured and autopolymerized. Polymeric materials processed from powders of predominantly polymerized poly (methyl- methlacrylate) (PMMA) and a liquid monomer are widely used in dentistry and orthopaedics <sup>114</sup>.

The major problem in denture was, and still is, the adhesive failure between the denture base and the liner <sup>115</sup>. Bond failure creates a potential surface for bacterial growth <sup>116</sup>. Therefore, frequent clinical evaluation and periodic replacement of the soft denture liner is required. Nowadays, the challenge is to find some other ways to increase the bonding strength between denture base and soft liner. It was suggested that surface roughness can improve the adhesion between the denture base and soft liner materials. But some authors stated the opposite effect of roughening <sup>117</sup>. The purpose of the present study is to increase the adhesion between EVA resilient lining material and heat-cured acrylic resin (PMMA) denture base material. The idea is to produce an interfacial layer by electrospinning of PMMA/EVA blends. PMMA/EVA blends with different ratios (30/70), (50/50) and

(70/30) are produced. The large surface area will act as bridges between denture base and soft liner materials.

### **4.3.1. Morphology of electrospun PMMA/EVA**

The SEM micrographs left in Fig (33) show the morphology of electrospun PMMA/EVA (50/50) blends with different concentrations (15, 18 and 20 wt %) in solution of  $\text{CHCl}_3$ . It is shown that the 15 wt% concentration exhibited fibers with beads along the fiber direction; the beads have a length of  $\sim 70 \mu\text{m}$  and a width of  $\sim 41 \mu\text{m}$ . The bead structure appeared at 15 wt% because of the low viscosity of the electrospun solution. Therefore, it is important to modify the fiber morphology and to decrease the fiber diameter in order to increase the surface area to volume ratio. Increasing the concentration of the polymer solutions to 18 and 20 wt% improves the electrospinnability, and the bead structure disappears. The fiber morphology found to be better at 18 wt% but the fiber diameter is still non homogenous with a broad diameter distribution (Fig.33 b and c). Electrospinnability and fibres morphology can be enhanced by addition of DMF to the polymer solution. DMF increases the dielectric property of the electrospun solution and thereby improves the fiber morphology (the ratio of DMF to  $\text{CHCl}_3$  was 20:80). Furthermore, the diameter of the obtained PMMA/EVA blend fibers decreased to  $\sim 1.1 \mu\text{m}$  with narrow diameter distribution (see Fig. 34).

### **4.3.2. Manufacturing of mouth guards**

PMMA/EVA blend nanofibers are deposited directly on the surface of EVA plates (80-95 % purity with about 20-34 % vinyl acetate). The time of electrospinning was varied from 15 min to 4 hours. EVA plates were heated and pressed against the nanofibers layers using a thermo pressure machine. Then, 5-20% PMMA prepolymer added at the surface of the EVA plate and distributed homogeneously. The denture composite is made by the polymerization of the PMMA prepolymer at the interface of EVA-plates (covered with PMMA/EVA nanofibers) under elevated temperature and pressure. Thereafter, the material mixture was pressed to a plate of about 4 mm thickness (see fig 35).

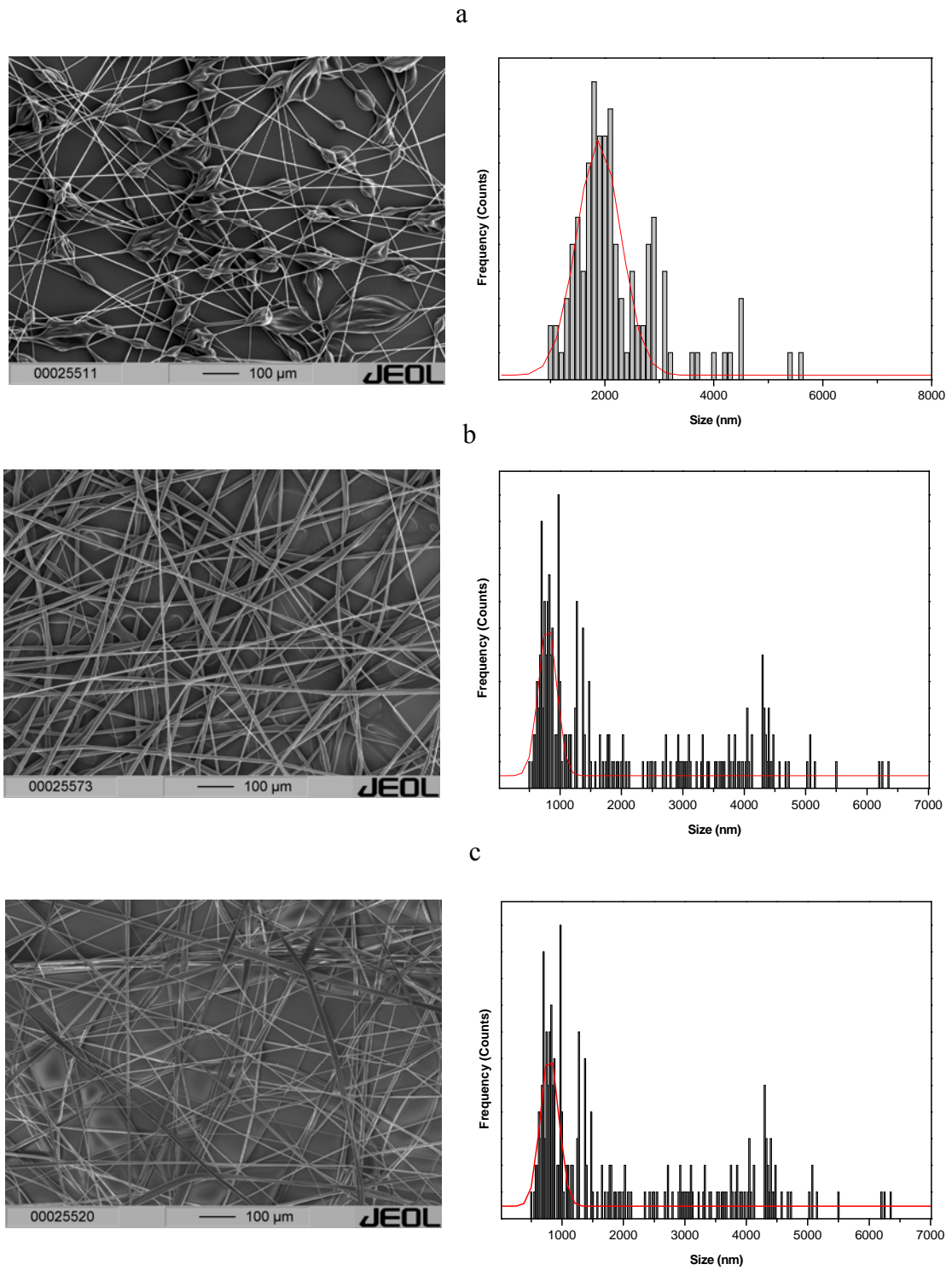


Fig. 33. SEM micrographs of electrospun PMMA/EVA (50/50) with different concentration ratios of the solutions : (a) 15 wt %, (b) 18 wt% and (c) 20 wt%

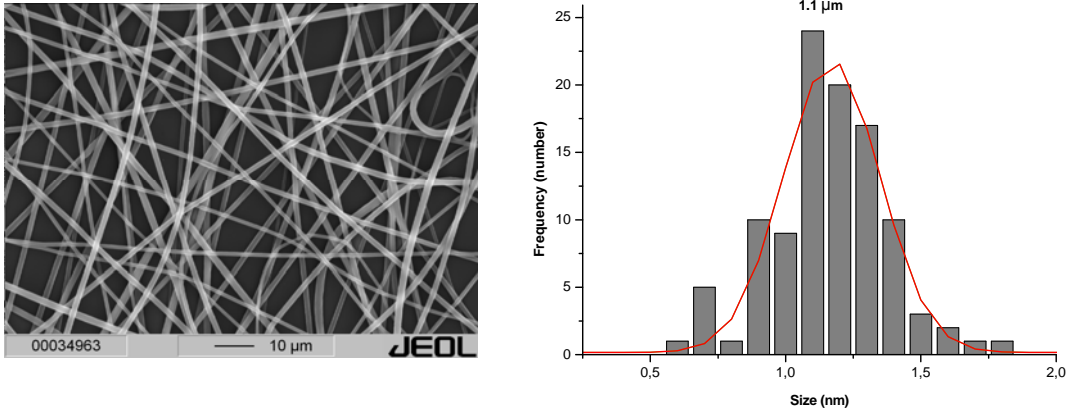


Fig. 34. SEM micrograph showing the morphology and diameter distribution of electrospun PMMA/EVA (50/50) using CHCl<sub>3</sub>/DMF (80/20) as a solvent

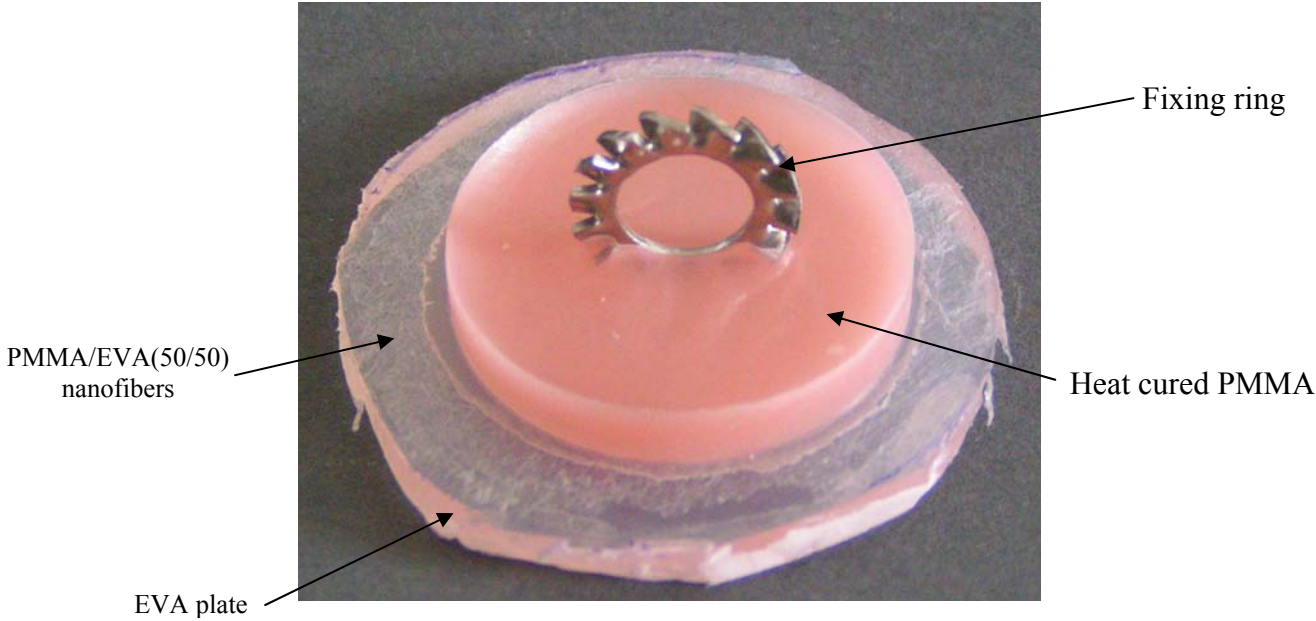


Fig. 35. Photo image of polymerized PMMA on the EVA plate using PMMA/EVA (50/50) nanofiber as an interface between them

### 4.3.3. Phase separation of PMMA/EVA at the nano scale

The phase behaviour and phase separation of the PMMA/EVA blend nanofibers have been investigated using TEM inspection after staining the electrospun fibers with RuO<sub>4</sub> vapours for 4 days. Fig. (36) shows the TEM micrographs of the electrospun PMMA/EVA (30/70) and (70/30) with 40 wt% VAc content to illustrate the phase behaviour of the binary polymers for different concentrations. It is shown that the blend PMMA/EVA (30/70) exhibits homogenous distribution of the polymers without micro phase separation. The homogeneity of the distribution of PMMA at the fibres matrix might be attributed to its low concentration. On the other hand, the PMMA/EVA blend (70/30) shows two different cases of phase behaviour. The thinner fibers (thinner than 750 nm) show homogenous distribution of the binary polymers in the blend and there is no visible micro phase separation. Decreasing the fiber diameter improves the macromolecular distribution of the polymer blend in the fiber matrix. So, the blend exhibits homogenous distribution of both polymers at the nano scale range. On the contrary, the thicker fibers (thicker than 750 nm) show separated phases between PMMA and EVA. This could be attributed to the non miscibility of both PMMA and EVA at the micro scale. It is revealed that the diameter of the fibers influences the micro phase separation. The thinner fibers have a better macromolecular distribution. Thereby, the miscibility of the polymer blends will be improved and the micro phase separation disappears.

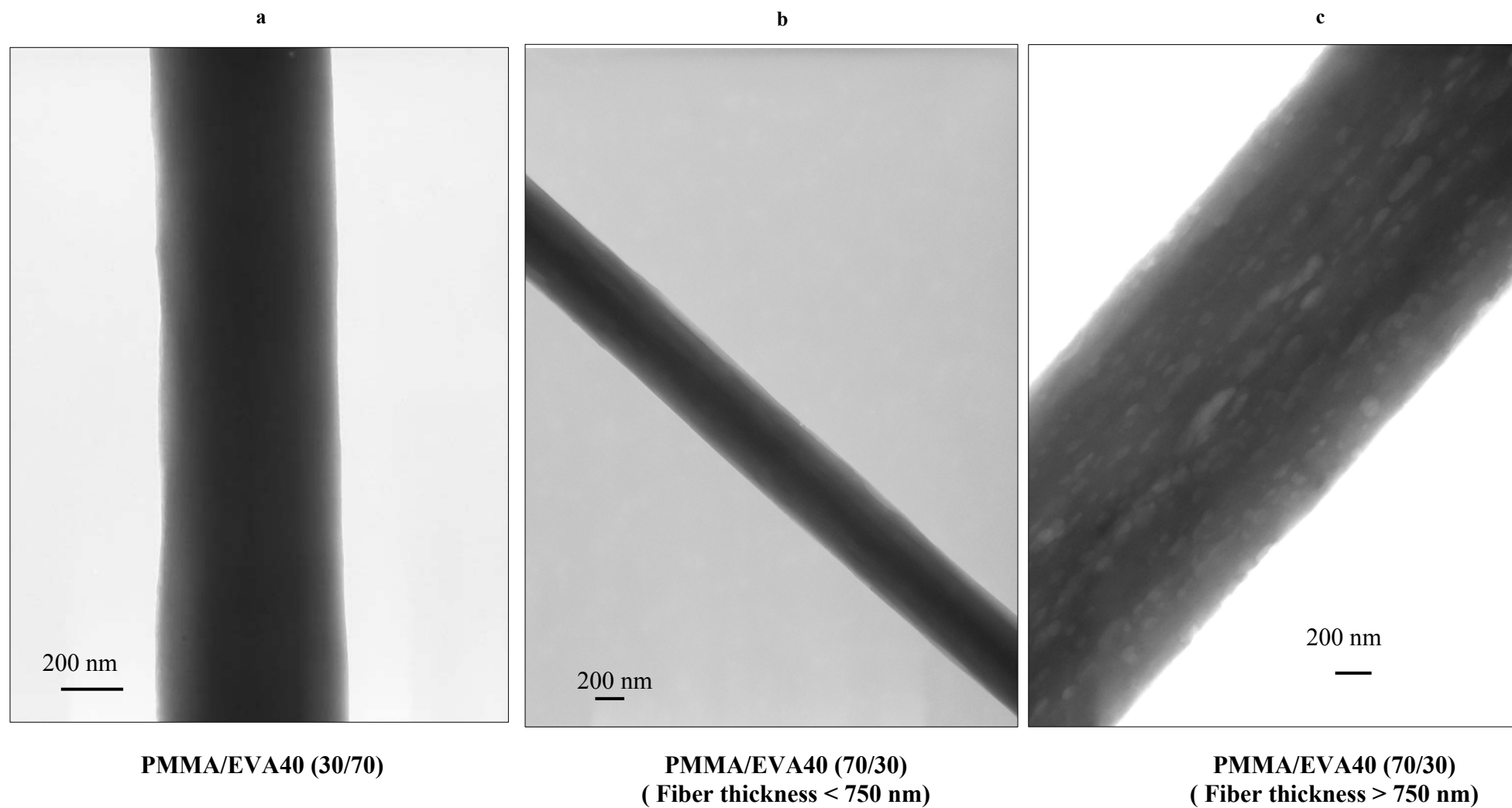


Fig. 36. TEM micrographs showing the phase separation of PMMA/EVA blend at the nano range, the fibers stained with RuO<sub>4</sub> vapours for 4 days

### 4.3.4. Measuring the interfacial strength (bond) between soft liner (EVA) and denture base (PMMA)

Tensile and peel bond strength between denture base and soft liner materials have been investigated after using electrospun PMMA/EVA nanofibers as an interface between them. The ability of the material to withstand peeling depends on the strength of the bond developed between soft lining and denture base materials. Fig. 37 shows results of the tensile strength tests for the samples prepared using electrospun PMMA/EVA (50/50) nanofibers as an interface between soft liner and denture base acrylic resin. The results show that the time of electrospinning (the thickness of the electrospun fiber mats) influences the bond strength with a significant increase in the bond strength between soft liner and denture base with increasing electrospinning time to 4 hours. The required force to detach the bond between denture base and soft liner is ~490 N. The surface property of the soft liner plays an important role for adhesion of the electrospun fibers on its surface. It is found that roughness of the EVA sheets increases the bond strength due to the good penetration of the electrospun fibers in the surface of EVA sheets. The required force to detach the bond between denture base and soft liner material is ~620 N compared with ~490 N without roughening the EVA surface (Fig. 38).

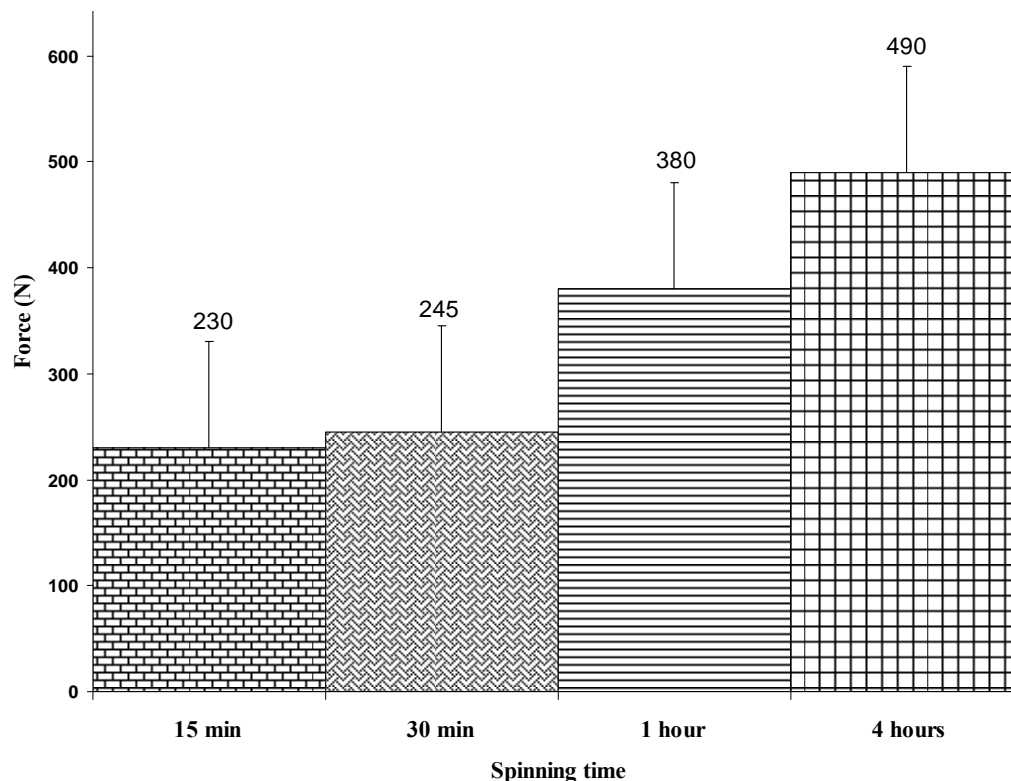
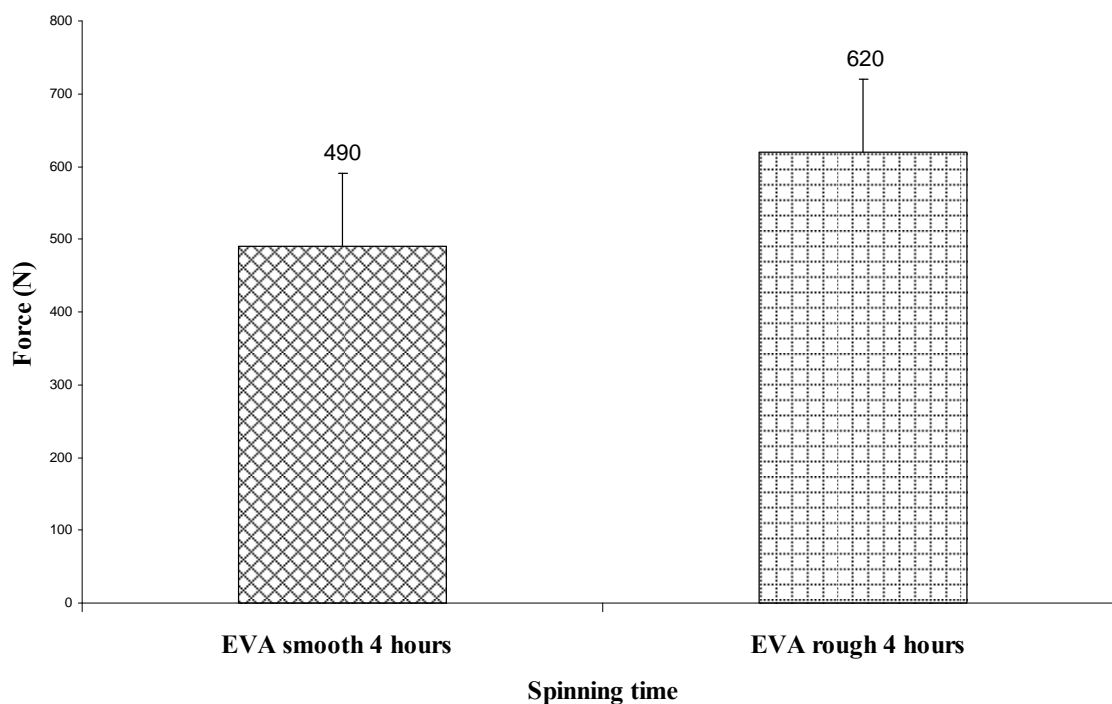


Fig. 37. Interfacial strength (adhesion) between heat cured PMMA and EVA plate, the surface of EVA plate is smooth



**Fig. 38. Effect of the surface roughness on the bond strength**

### **4.3.5. The bond between EVA (soft liner) and PMMA (denture base) materials**

To check the contact between denture base and soft liner materials, the contact layer has been investigated using TEM of the prepared denture after staining with RuO<sub>4</sub> vapours for 4 days. Fig. 39 shows the TEM micrograph of the stained denture which exhibiting the good contact between the three components (PMMA/EVA blend nanofibers, EVA plate and heat cured PMMA). The denture composite showed no phase separation between EVA plate and heat cured PMMA after using the electrospun nanofibers mat as an interface between them. Meaning that, the high surface area of the electrospun nanofibers provides a huge number of nano contacts acting as bridges between the denture liner and base materials. Moreover, the good interaction attributed to the miscibility of the blend composite which arises from the unlimited number of intermolecular hydrogen bonds. Such a huge number of hydrogen bonds are the responsible for the strong interactions between denture liner and denture base. The results showed that electrospun nanofibers might be used as dry adhesive to increase the contact between polymers that are not compatible and lacking adhesion together. In addition, the results provide a good and practical solution for the debonding problem in denture and mouth guards' applications. The results of this work has been submitted as a patent <sup>118</sup>.

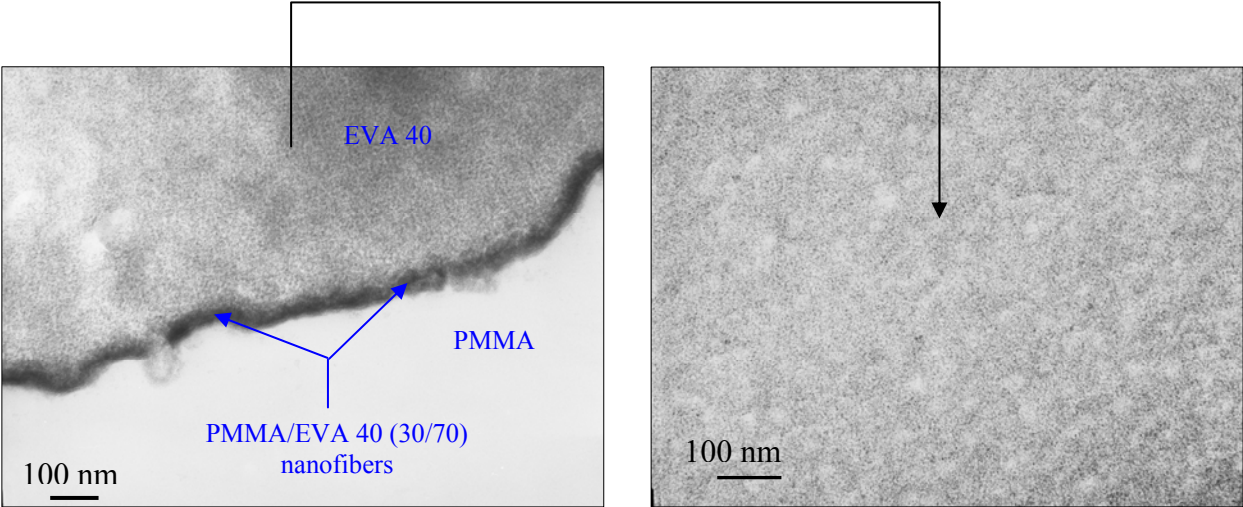


**Fig. 39.**TEM micrographs showing the contact layer between EVA plate and heat cured PMMA using electrospun PMMA/EVA 40 (30/70) nanofibers mat as an interface between them, the sample was stained with RuO<sub>4</sub> vapours for 4 days



### 4.4. Nanofibers for bone tissue engineering

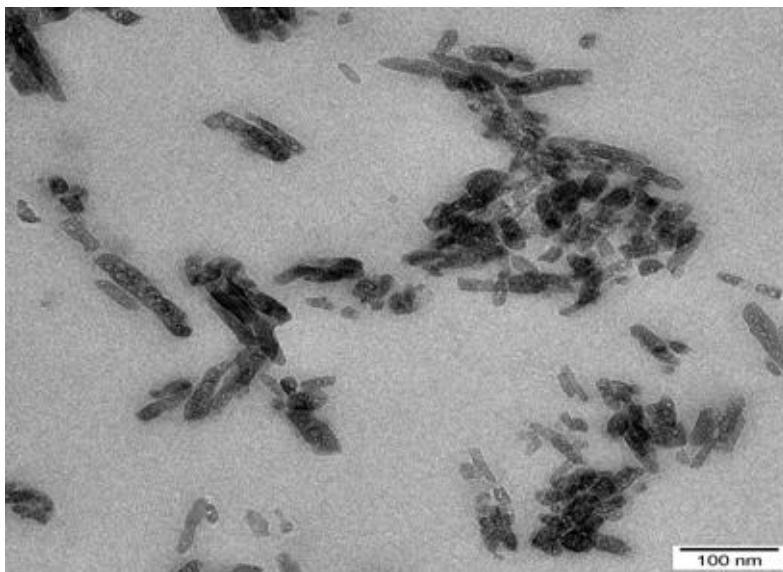
The requirement for new bone materials to replace or restore the function of traumatised, damaged, or lost bone is a major clinical need <sup>119</sup>. Large bone fracture, defects, loss, infections and tumor resections are serious problems for bone surgery <sup>120</sup>. One strategy for dealing with serious bone damage is to develop tissue engineered bone substitutes <sup>121</sup>. Mimicking the architecture of an extracellular matrix (ECM) is one of the major challenges for tissue engineering <sup>122</sup>. Col and HAp have potential in mimicking natural ECM and replacing diseased skeletal bones <sup>123</sup>. Furthermore the combination of both a ceramic and a polymer within one material result in composites, having the ductility of the polymer and the bioactivity of the calcium phosphate phase. Kikuchi et al. synthesized HAp and Col composite which could be applied for better bioactive bone graft materials <sup>124</sup>. Recently, studies on three-dimensional scaffold materials have become a key element of bone tissue engineering <sup>125</sup>. It has become a rapidly expanding research area since it offers a new and promising approach for bone repair and regeneration of fractured or diseased bones.

PVA is a synthetic polymer, has gained popularity as a scaffold supporting material for tissue engineering, because it endows mechanical stability and flexibility to the conventional scaffolds made of natural polymers. It has been selected as the polymer additive to produce electrospun nanofibrous mat because of its good fiber forming, biocompatibility, and chemical resistance properties <sup>126</sup>. Moreover, PVA hydrogels have been used in a number of biomedical applications including soft contact lenses <sup>127</sup>, implants <sup>128</sup>, drug-delivery matrices <sup>129</sup>, temporary skin covers or burn dressings <sup>130</sup> and artificial organs <sup>131</sup>. This is because of their inherent non-toxicity, non-carcinogenicity, good biocompatibility, and desirable physical properties such as rubbery or elastic nature and high degree of swelling in aqueous solutions <sup>132</sup>.

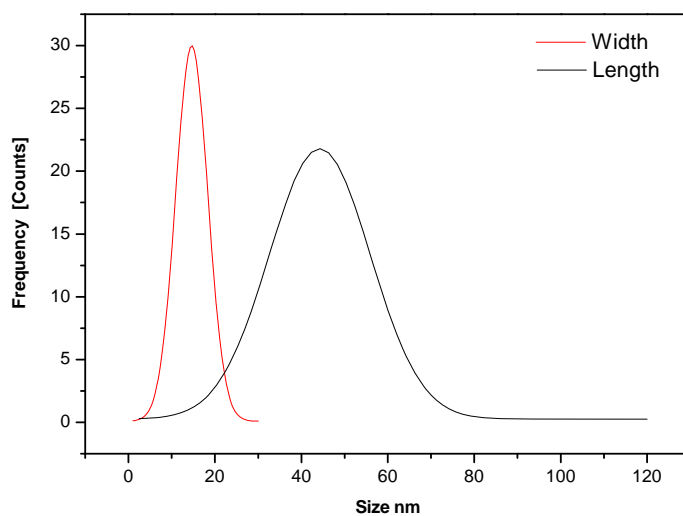
The main objective of the present study was to design a novel biodegradable nanocomposite nanofibers (NCNFs) scaffolds consisting of PVA/ Col with unidirectional aligned nano hydroxyapatite to mimic the nano structure of human long bone tissue.

### 4.4.1. Crystalline structure and morphology of HAp and the electrospun NCNFs

Fig. 40 shows a TEM micrograph of HAp nanoparticles, in which the morphology of the individual HAp nanoparticles was clearly revealed to be of rod-like shape. The image indicated that HAp consists of well defined crystalline rods have a width of 10 to 30 nm and lengths of 20 to 120 nm (see Fig. 41). Most striking feature obtained from TEM investigation was that all HAp nanorods exhibited nano porous morphology on the surface, which might be useful for cell anchorage sites, provide mechanical stability, also to provide interface to respond to physiological and biological changes and to remodel the ECM in order to integrate with the surrounding native tissue.



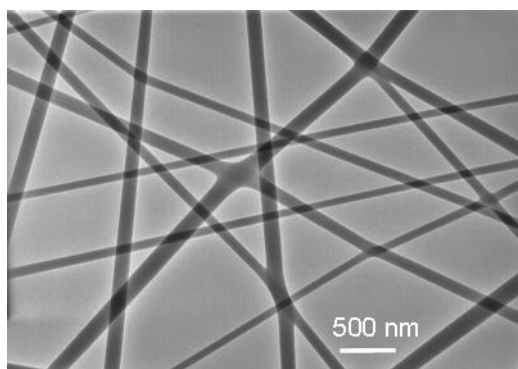
**Fig. 40.** TEM micrograph of HAp nanorods



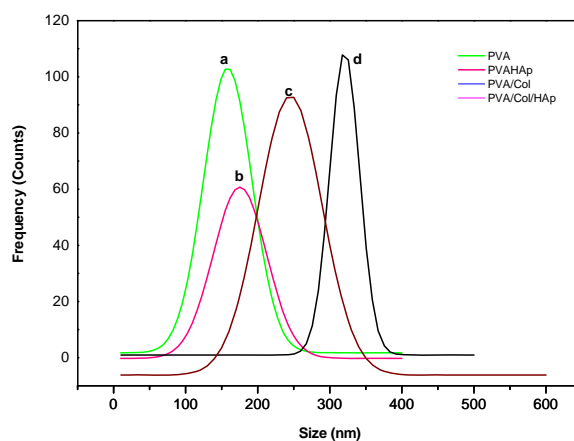
**Fig. 41.** Size diameters distribution of n- HAp nanorods

Fig. 42 shows a representative TEM micrograph of pure PVA nanofibers (NFs), which have a uniform structure without any sign of beads formation. In Fig. 43, which represents the average size diameters for all electrospun NFs, it is shown that PVA NFs has an average size diameter of  $\sim 160$  nm. The structure of electrospun PVA/n-HAp nanocomposites nanofibers (Fig. 44) showed that they have structures identical to those from pure PVA. However, a minor increase in the fiber average size occurred by addition of HAp nanorods; the average size diameter of the PVA/n-HAp NCNFs slightly increased to  $\sim 176$  nm. Nevertheless, the majority of diameter in both cases was in the range of 100 to 250 nm.

The typical internal morphology of the electrospun PVA containing n-HAp is shown in Fig. 44. It is clearly seen that the HAp nanoparticles are well distributed within the electrospun fibers, and of most interest a large number of HAp nanoparticles were preferentially oriented parallel to the longitudinal direction of the electrospun PVA.



**Fig. 42. TEM micrograph for electrospun PVA nanofibers**



**Fig. 43. Diameter distribution of (a) electrospun PVA, (b) PVA/n-HAp, (c) PVA/Col and (d) PVA/Col/n-HAp**

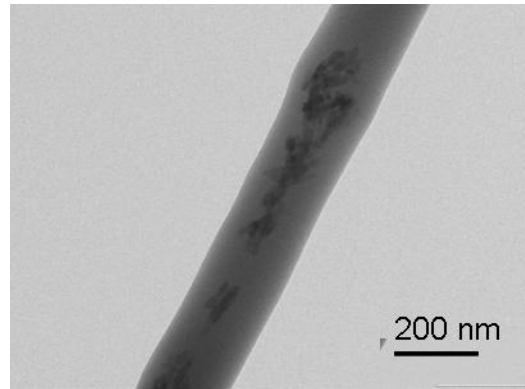


**Fig. 44.** TEM micrograph of electrospun PVA/n-HAp nanocomposite nanofiber

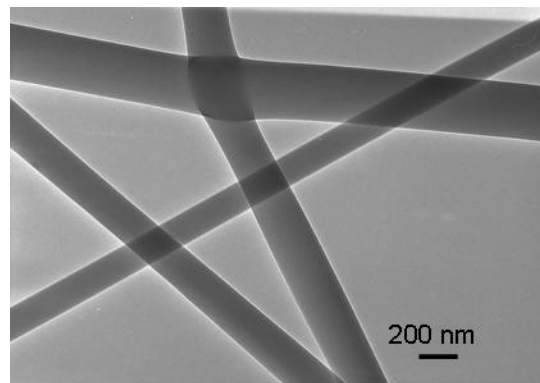
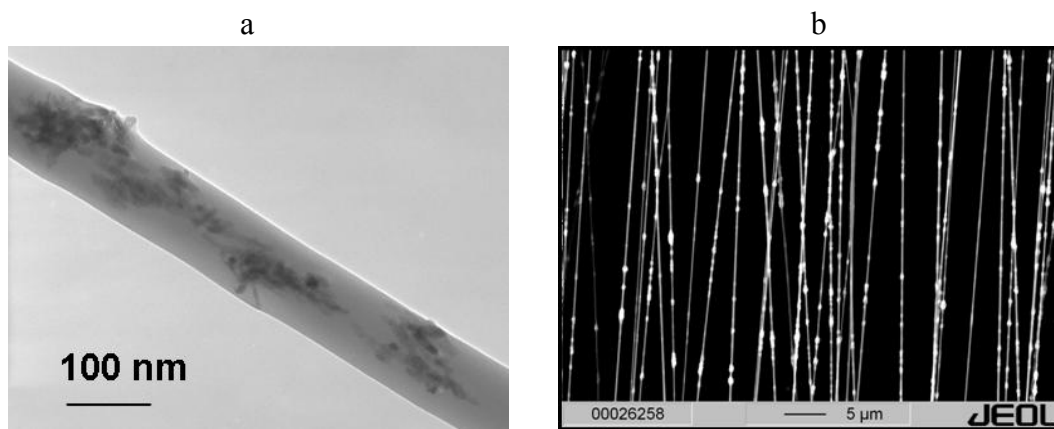


**Fig. 45.** TEM micrograph of electrospun PVA/Col nanofibers

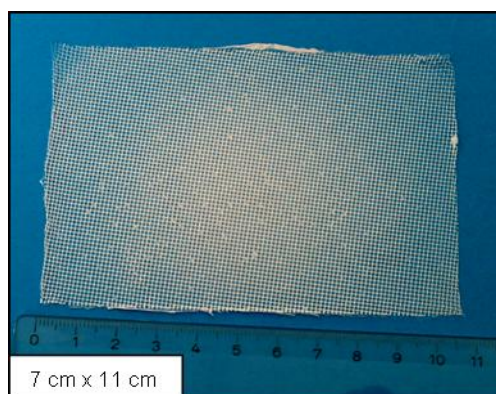
PVA/Col solution with and without n-HAp have been electrospun at the same conditions described above. It was shown in Fig. 45 that PVA/Col NFs are unchanged compared with PVA and PVA/HAp NCNFs, accompanied by increasing in the average size diameter (~ 245 nm). Furthermore, uniform NCNFs could be produced after incorporation of 5 wt % HAp nanorods to PVA/Col solution. The obtained NCNFs have the same homogeneity as the previous NFs without any beads formation (see Fig. 46 a). The average size diameter occur to be ~ 320 nm, and the majority of diameters in both cases is in the range of 100 to 530 nm.

Fig. 46 b shows the SEM back-scattered images of uniaxially aligned electrospun PVA/Col/n-HAp NCNFs. It is shown that the majority of n-HAp particles is arranged in the fiber direction (see Fig. 46 a). This nanoscale orientation resembles the orientation of HAp crystals in mineralized ECM and Col NFs of natural bone fibril<sup>133</sup>. Furthermore, aligned NFs represent an effective approach to control cell orientation and migration in

tissue engineering<sup>6</sup>. Fig. 47 shows the final electrospun PVA/Col/n-HAp NCNFs web scaffold (7 cm × 11 cm). This scaffold can be helpful for building 3-D structure for tissue engineering applications<sup>134</sup>.



**Fig. 46. TEM micrograph for electrospun (a) PVA/Col/n-HAp and (b) back scattered SEM micrograph for aligned electrospun PVA/Col/n-HAp**



**Fig. 47. Photograph of PVA/Col/n-HAp biocomposite nanofibrous scaffold**

### 4.4.2. FTIR measurements

FTIR spectroscopy was carried out to elucidate the presence of Col and HAp in the blended nanocomposite, to analyse any complex structural changes that might be occurred due to the blending and also to analyse the interaction (hydrogen bonding) between Col, HAp and PVA in the final NCNFs. The representative FTIR absorption spectrum of the pure HAp nanorods is shown in Fig. 48 and tabulated in Table 6. A broad band observed starts from about  $3700\text{ cm}^{-1}$  to  $2500\text{ cm}^{-1}$  and is centred at about  $3297\text{ cm}^{-1}$ , which could be attributed to the stretching mode of  $\text{OH}^-$  ions. In addition, two distinct bands were observed at  $3576\text{ cm}^{-1}$  and  $1639\text{ cm}^{-1}$ , which arose from the stretching mode and the bending mode

of H<sub>2</sub>O molecules, respectively. Furthermore, some other impurity ions were also identified by the peaks appeared in the range of 1490 cm<sup>-1</sup> to 1410 cm<sup>-1</sup>, which were attributed to components of the stretching mode of a trace amount of CO<sub>3</sub><sup>-2</sup> groups presented in HAp.

The phosphate ions PO<sub>4</sub><sup>-3</sup> are the principal molecular components of HAp giving to the IR absorbance in the region of 550 cm<sup>-1</sup> to 1200 cm<sup>-1</sup>. The HAp characteristic peaks appear at 962 cm<sup>-1</sup>, 1019 cm<sup>-1</sup> and 1088 cm<sup>-1</sup> correspond to the stretching vibration of PO<sub>4</sub><sup>-3</sup> and peak at 599 cm<sup>-1</sup> corresponds to the deformation vibrations of PO<sub>4</sub><sup>-3</sup>.

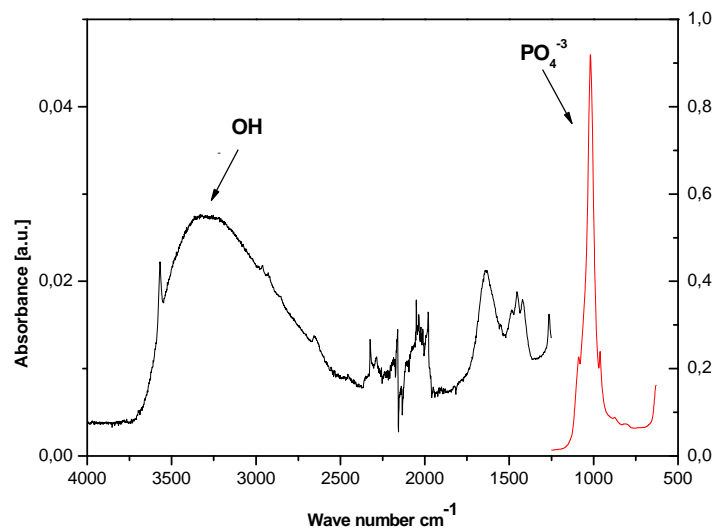


Fig. 48. FTIR spectra of n-HAp nanorods

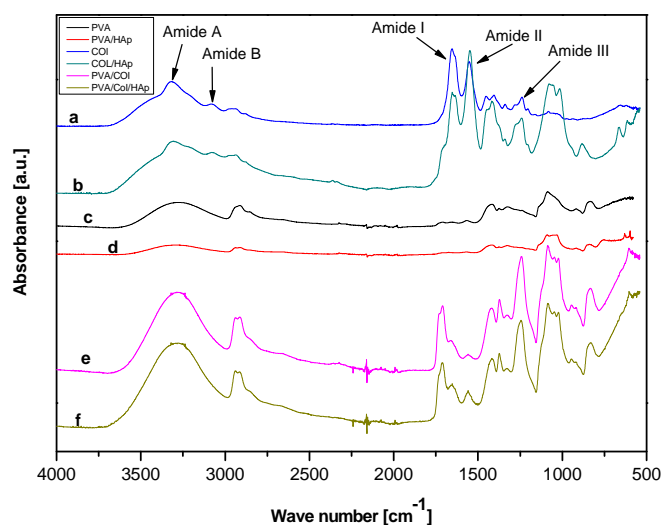


Fig. 49. FTIR spectra for solutions of (a) Col, (b) Col/n-HAp and electrospun fibers of (c) PVA, (d) PVA/n-HAp, (e) PVA/Col and (f) PVA/Col/n-HAp

**Table. 6. Assignments of FTIR absorption bands of pure polymers and electrospun nanofibers**

Peaks for Solution (cm <sup>-1</sup> )			Peaks for Electrospun Nanofibers (cm <sup>-1</sup> )				Assignment
Col	HAp	Col/HAp	PVA	PVA/HAp	PVA/Col	PVA/Col/HAp	
	3567						stretching and bending mode of H <sub>2</sub> O (water)
3312							amide A, N-H stretching and O-H stretching
	3316		3278	3296			Stretching of OH
3076							amide B, C-H stretching
2949		2940	2935	2939	2923	2927	asymmetric stretching of CH <sub>2</sub>
			2914	2911			symmetric stretching of CH <sub>2</sub>
			1711	1717	1710	1713	stretching of CO
			1657	1674			O=H, C=C
1653		1654			1657	1656	amide I, C=O stretching
	1638			shoulder			stretching and bending mode of H <sub>2</sub> O (water)
1552		1549			1556	1554	amide II, N-H bending and C-N stretching
1450	1421	1413		1421		1416	impurities (CO <sub>2</sub> <sup>-3</sup> )
1404		1413	1418	1418	1422	1416	O-H, C-H bending, γ(CH <sub>2</sub> ), δ(OH)
1341		1341	1374	1378	1372	1373	CH <sub>2</sub> wagging
			1326	1325	1327	1325	δ(OH) with CH wagging
1240		1240			1243	1246	amide III, CN stretching and N-H bending
			1241	1240			C-O-C
			1143	shoulder			stretching of CO(crystalline sequence of PVA)
1079			1087		1083	1083	stretching of CC and bending of OH(amorphous sequence of PVA)
	1088	1078		1092		1083	symmetric stretching of PO <sub>4</sub> <sup>-3</sup>
	1019	1016		1033		1019	symmetric stretching of PO <sub>4</sub> <sup>-3</sup>
	962	884		962		941	symmetric stretching of PO <sub>4</sub> <sup>-3</sup>
			917	920	914	918	bending of CH <sub>2</sub>
			831	838	836	828	rocking of CH <sub>2</sub>
	599						PO <sub>4</sub> <sup>-3</sup> deformation vibration

Typical FTIR spectra of pure PVA NFs and PVA/n-HAp NCNFs are shown in Fig. 49 and tabulated in Table. 6. As it seen in the characteristic absorption bands of PVA occur at  $3278\text{ cm}^{-1}$  (stretching of OH),  $2935\text{ cm}^{-1}$  (asymmetric stretching of  $\text{CH}_2$ ),  $2906\text{ cm}^{-1}$  (symmetric stretching of  $\text{CH}_2$ ),  $1417\text{ cm}^{-1}$  (wagging of  $\text{CH}_2$  and bending of OH),  $1143\text{ cm}^{-1}$  (stretching of CO from crystalline sequence of PVA),  $1088$  (stretching of CO and bending of OH from amorphous sequence of PVA),  $919\text{ cm}^{-1}$  (bending of  $\text{CH}_2$ ) and  $838\text{ cm}^{-1}$  (rocking of CH).

The FTIR spectrum of the electrospun PVA/n-HAp NCNFs after incorporating HAp nanorods onto the PVA solution, exhibited the characteristic absorption bands of PVA along with additional bands corresponding to the phosphate groups of n-HAp. The predominant broad absorption band associated with the OH stretching of PVA centered at  $3278\text{ cm}^{-1}$  shifted the higher wave number region ( $\nu_{\text{OH}} = 3296\text{ cm}^{-1}$ ). This result suggested that the hydrogen bonding became stronger in the electrospun PVA/n-HAp than that of in pure PVA as well as in the electrospun PVA fibers due to the increase in the number of OH groups by adding of HAp. In addition, the major absorption band of  $\text{PO}_4^{3-}$  stretching appearing at  $1019\text{ cm}^{-1}$  in HAp's spectrum, moved to  $1033\text{ cm}^{-1}$ . This shift might be attributed to the interactions between PVA molecules and n-HAp particles. Furthermore, the overall PVA crystallinity decreased by loading of n-HAp within the electrospun fibers, which was clearly evidenced by weakening of the crystalline band at  $1143\text{ cm}^{-1}$ .

It is of interest to note here that the absorption bands associated with  $\text{H}_2\text{O}$  molecules distinctly appeared at  $3576\text{ cm}^{-1}$  and  $1638\text{ cm}^{-1}$  in the spectrum of n-HAp. The higher peak at  $3576\text{ cm}^{-1}$  was completely missing in the electrospun fibers of PVA/n-HAp NCNFs, while the peak at  $1638\text{ cm}^{-1}$  still exists in the spectrum in spite of a large extent of reduction in its intensity.

In conjunction with the TGA results we confirmed that the former band at  $3576\text{ cm}^{-1}$  was identified with the loosely physisorbed water at the surface of HAp nanorods, whereas the latter arose from the chemisorbed molecular water within the HAp lattice.

The characteristic peaks of Col (Fig. 49 and Table. 6), appears at  $3312\text{ cm}^{-1}$  (amide A, N-H stretching and O-H stretching),  $3078\text{ cm}^{-1}$  (amide B, C-H stretching),  $1654\text{ cm}^{-1}$  (amide I, C=O stretching),  $1552\text{ cm}^{-1}$  (amide II, N-H bending and C-N stretching) and  $1240\text{ cm}^{-1}$  (amide III, CN stretching and N-H bending)<sup>135, 136</sup>. Col/n-HAp composite spectrum showed the peaks for amide A, amide B, amide I, amide II and amide III without any significant shifts for Col characteristic peaks. Furthermore, the characteristic peaks for HAp in Col/n-HAp composite appeared also at the same wave numbers for pure HAp

without any significant shifts. PVA/Col NFs spectrum showed that the amide A band shifted to lower frequencies than in collagen and the amide B band disappeared, because the amide B band was observed only for Col/PVA blend weight ratio (99:1)<sup>135</sup>. Besides, it displayed a moderate peak at 2923 cm<sup>-1</sup> resulting from the acetic acid solvent. The peaks of amide I, II and III bands displayed at the same wave numbers for pure Col. The spectra of PVA/Col/n-HAp NCNFs, show a small decrement for amide A compared with pure Col, and absence of amide B (due to the high amount of PVA)<sup>135</sup>. Amide I, II and III appears without any significant shifts, as well as the characteristic peaks for HAp in the NCNFs compared with pure HAp.

FTIR results demonstrate that Col can be successfully electrospun in combination with water soluble PVA and nano hydroxyapatite without any structural change of Type I Col. Furthermore, there was strong intermolecular hydrogen bonding between the molecules in the electrospun PVA/Col/n-HAp biocomposite NFs due to the presence of large number of OH groups.

### 4.4.3. DSC measurements

DSC measurements have been done to investigate the thermal behaviour of the electrospun NCNFs, such as melting, crystallization and formation of crystalline structure. To characterize thermal properties of all samples in the present work, the second heating run of DSC was taken into account. The results from DSC and the characteristics observed for pure polymers and the prepared NCNFs are shown in Fig. 50 and summarized in Table 7.

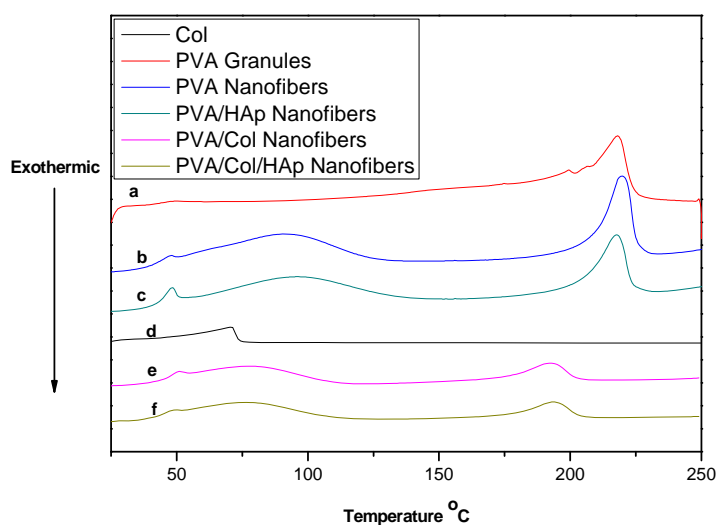


**Fig. 50. (a) DSC curves for PVA granules, (b) electrospun PVA, (c) PVA/n-HAp, (d) Col, (e) PVA/Col and (f) PVA/Col/n-HAp**

DSC for PVA granules in Fig. 50 showed the first endothermic peak at 49.8 °C, which is corresponding to the glass transition temperature ( $T_g$ ). The glass transition temperature decreased to reach 48.3 °C for electrospun PVA. The decrease in glass transition temperature can be attributed to the very large surface to volume ratio of the electrospun membranes having air as the plasticizer<sup>137</sup>. By addition of HAp nanorods onto PVA NFs, an increment of  $T_g$  occurred to reach ~ 50.3 °C, this increment could be attributed to the segmental motions of the polymer chains which were greatly constricted by the strong interactions between them through the hydrogen bonds. The second endothermic peaks ( $T_m$ ) for PVA granule, PVA NFs and PVA/n-HAp NCNFs appeared at ~ 218 °C, 219 °C and ~ 216 °C respectively, which were attributed to the melting of the crystalline phase of PVA<sup>138</sup>.

**Table 7. DSC and the characteristics observed for the pure and electrospun polymer nanofibers.**

Sample name	$T_g$ (°C)	$T_d$ (°C)	$T_m$ (°C)	$T_c$ (°C)	$\Delta H_m$ (j/g)	Crystallinity (%)
PVA granules	49.86	--	218	179	65.3	47
PVA fiber	48.3	--	219	190	61.4	44
PVA/n-HAp fiber	50.3	--	216	187	57.8	42
Col Soln	30.86	70.90	70.90	----	36.13	----
PVA/Col	50.96	78.71	192.39	93.4	41.22	29.74
PVA/Col/n-HAp	49.32	76.82	193.73	100.47	38.42	25.36

It is observed that the melting temperature ( $T_m$ ) in the pure PVA granules and electrospun PVA NFs was almost the same, but the melting temperature shifted slightly to the lower value after addition of HAp nanorods in case of PVA/n-HAp NCNFs compared with others. A decrease in the enthalpy of fusion and the melting temperature suggested that the crystallinity and perfection of the crystal structure were reduced by addition of n-HAp.

The DSC for type I Col is shown in Fig. 50. A shoulder endothermic event has been observed at 30.86 °C which is corresponding to the water bonded to molecules and unfolding of the triple helical structure in diluted acetic acid<sup>139</sup>. Furthermore a strong endothermic event has been showed at 70.8 °C ( $T_m$ ) with enthalpy of fusion (36.13 J/g), corresponded to the maximum temperature at which there was complete denaturation of the Col samples.

The DSC measurements for PVA/Col NFs with and without n-HAp (Fig. 50 and Table. 7) showed three main thermal phenomena. A shoulder peak observed at 50.7 °C, which is corresponding to glass transition of PVA, this increment also attributed to the strong interactions between the molecules through the hydrogen bonds. A broad peak at 78.2 °C corresponding to Col denaturation and strong peak at  $T_m$  192.7 °C represents the melting of PVA. After incorporation of n-HAp to PVA/Col NFs, the glass transition ( $T_g$ ) for PVA decreased to 49 °C, the denaturation of Col occurred at 77.6 and the melting of PVA occurred at 194 °C. Beatrice et al. proved that Col denaturation endotherm in PVA/Col blend shifted to higher temperature with increasing PVA content<sup>140</sup>.

By calculating the degree of crystallinity ( $X_c$ ) from the equation (1), it is found that  $X_c$  for the PVA granule is ~ 47 %, which is considered as semi crystalline polymers, but the degree of crystallinity decreased to 44 % after the electrospinning. This decrement is attributed to the reason of the strong electrostatic potential applied to a capillary which causes the jet ejection from a capillary tip with a high elongation flow rate. The polymer chains will be stretched in the electrostatic direction and the solvent will evaporate simultaneously within a very short time scale that generally leads to a lowering of the temperature (like quenching) and thereby the development of crystallinity is considerably hindered to form perfect crystalline structure. As a consequence, the molecules in the electrospun fibers exhibit a little bit decrement in the degree of crystallinity. The further decrease in crystallinity (42 %) which is observed for PVA/n-HAp NCNFs, attributed to the effect of hydroxyl groups presented on the surface of HAp nanorods which serve as heterogeneous nucleation sites for PVA crystallization<sup>64</sup>. Furthermore, the interactions between PVA and HAp nanoparticles via hydrogen bonds induce defects in a crystalline phase in PVA. As a consequence, the decrease of the melting temperature results<sup>141</sup>.

It is interesting to observe that degree of crystallinity for PVA/Col NFs decreased to 29.7 %. This decrease attributed to the strong hydrogen bonds occurred between Col, HAp and PVA (see Fig. 51). Col, which is a hydrogen donor, should form hydrogen bonds with the hydroxyl group of PVA even in small amount of Col<sup>135</sup>. By incorporation of HAp



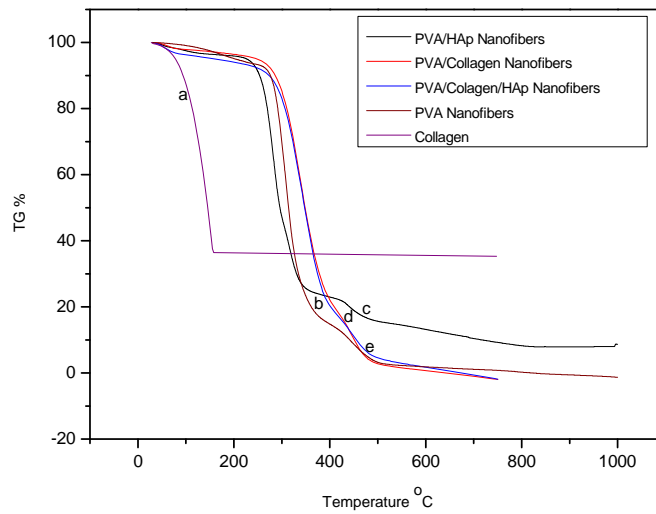


**Fig. 52. TGA thermogram for (a) Col, (b) electrospun PVA, (c) PVA/n-HAp, (d) PVA/Col and (e) PVA/Col/n-HAp**

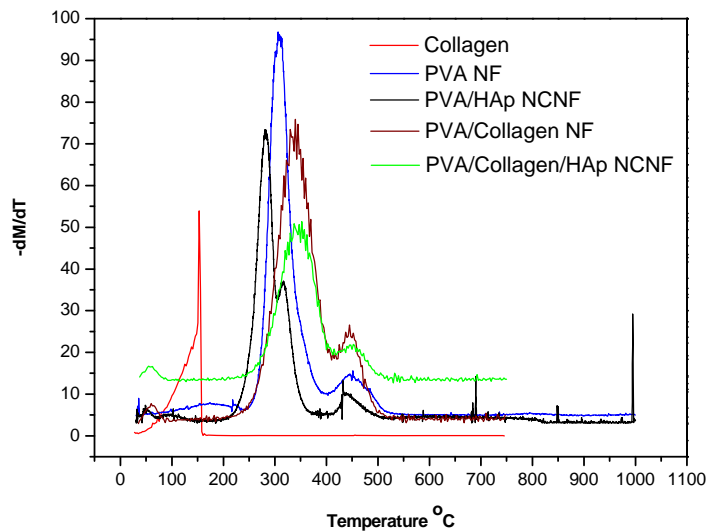


**Fig. 53. First order derivatives TGA for (a) Col, (b) electrospun PVA, (c) PVA/n-HAp, (d) PVA/Col and (e) PVA/Col/n-HAp**

Fig. 53 shows the first order derivatives of TGA (DTGA) for all samples, refers to the temperatures at which the maximum decrease of mass occurs. It is observed that DTGA for Col has a maximum peak at  $\sim 150$  °C, which is attributed to the water bound in Col. The temperature at the maximum mass loss rate for PVA NFs and PVA/n-HAp NCNFs are 308 °C and 281°C respectively, which indicated that the decomposition of the PVA side chains

was occurred readily before to the main chains. The maximum mass loss rate of the electrospun PVA/n-HAp NCNFs further shifted to a lower temperature compared with that of the electrospun pure PVA. It is interesting to note here that in the first derivative of the electrospun fibers of PVA/n-HAp NCNFs exhibited a distinctive peak at 316 °C, which was not appeared in TGA curve. To identify this peak we dried the electrospun PVA/n-HAp NC fibers in air at 85 °C for 8h, then cooled in a desiccators and TGA was carried out again. This peak completely disappeared in the DTGA curve of the dried electrospun PVA/n-HAp NCNFs fibers. This result clearly indicated that the peak at 316 °C arises from the loss of lattice water which may be “structural” water or water trapped within HAp nanorods. This result is consistent with data of Rootare and Craig for the chemisorbed water layer<sup>144</sup>. The maximum mass loss rate of the electrospun fibers of PVA/Col shifted to a higher temperature 338 °C compared with that of the electrospun pure PVA, which was attributed to the strong hydrogen bonds between Col and PVA. Furthermore, incorporation of n-HAp onto PVA/Col NFs increased the maximum mass loss rate to a higher temperature (345 °C) compared to other. This is attributed to increasing the number of hydrogen bonds between Col and n-HAp with PVA. Over ~600 °C, all TGA diagrams became flat and mainly the inorganic residue (i.e. HAp nanorods) remained. From the amounts of the residue at 800 °C, the inorganic contents of the electrospun PVA/n-HAp NCNFs was estimated to about 7.5 wt%.

The results shown here provide the possibility of producing a new 3-D biocomposite NFs scaffold for potential bone graft applications, which has biocompatibility and composition similar to that of bone. Microscopic photographs showed that PVA/Col/n-HAp biocomposite NFs had a similar nanostructure to bone in which the nano rod-shape HAp crystals were aligned along PVA/Col NFs. The alignment of n-HAp, Col and PVA was self-assembled by strong hydrogen bonding interaction between them. PVA/Col/n-HAp NCNFs scaffold (7 cm × 11cm), has a porous structure with a controllable pore size and shape, the pore sizes are in the range of 650 μm with porosity of 49.5 %.

In conclusion, the most striking properties of electrospun PVA/Col/n-HAp biocomposite NFs scaffold are not only the composition but also mimicking the hierarchical structure of ECM and mineral organization in bone at the nanoscale level which might be open up a wide variety of future applications for higher bioactive bone graft materials especially for non load-bearing bone tissue engineering.

### **4.5. Nanofibers from blends of polyvinyl alcohol and polyhydroxy butyrate as potential scaffolds material for tissue engineering of skin**

Skin is the largest organ of the human body which provides many different functions including protection against heat, injury and infections<sup>145</sup>. Therefore, failure or complete loss of the skin is incompatible with sustained life. Basically, skin built up of two main layers, the superficial one called epidermis layer which is formed from keratinocytes, providing a barrier against infection and moisture loss. Below the epidermis lies the dermis layer, formed primarily from fibroblasts cells. The dermal layer is responsible for the elasticity and mechanical integrity of the skin<sup>146</sup>. Epidermal substitutes emerged in the 1980s<sup>147</sup> and provide a source of advanced therapies for burn victims and healing of chronic or deep wounds and diabetes related ulcers<sup>146, 148, 149</sup>. However this epidermal sheets have certain disadvantages like fragility and poor take rates<sup>150</sup>. Hence, a lot of attempts have been made by different groups to generate many types of skin substitutes<sup>151, 152</sup>. They developed different scaffolds with varied compositions and structures to meet the primary goal of the restoration of native skin functions. Some of these scaffolds provide temporary coverage and others act as a permanent skin replacement<sup>152</sup>. For this purpose, the ideal tissue-engineered skin should as closely as possible approximate the skin in structure and function. Therefore, some essential characteristics should be taken into consideration when creating a scaffold for skin tissue engineering in order to heal the wound properly<sup>153-155</sup>. For this reason the material for dermal equivalents should promote adhesion, growth and function of fibroblasts, while the epidermal should solely promote keratinocytes and inhibit colonization with fibroblasts. One of the most important features of the scaffold is its high surface area which helps to improves cell attachment, proliferation and migration<sup>146, 153</sup>. Electrospun polymeric nanofibers have great interests in tissue engineering because of their nanostructure which mimics the native extracellular matrix (ECM)<sup>156</sup>. Moreover, electrospun nanofibers have desirable features as skin substitute materials, such as high surface area to volume ratio, and high porosity which is efficient for nutrient delivery, fluid absorption and excretion of the metabolic wastes<sup>122</sup>.

Over the past years, attentions have been focused on the production and potential applications of Polyhydroxyalkanoates (PHAs) and their copolymers<sup>157, 158</sup>. Poly-3-hydroxybutyrate (PHB) is probably the most common type of PHAs. It has been demonstrated that PHB is biodegradable and biocompatible thermo-plastic polymer with a high degree of crystallinity, displaying properties similar to polypropylene<sup>159</sup>. Because of the biodegradability, biocompatibility, optical activity and piezoelectricity of PHB<sup>160, 161</sup>,

it has been evaluated as a suitable material for a wide variety of medical applications including but not limited to controlled release system, surgical sutures, wound dressing, orthopedic uses, bone tissue engineering and skin substitute material<sup>161-163</sup>. Currently the main problem which limits the widespread utilization of PHB, is its high crystallinity and brittleness<sup>83</sup>. An approach to improve its physical and mechanical properties can be made through blending PHB with flexible and/or plasticizer polymers<sup>52, 164</sup>. Several reports showed that PHB is miscible with poly(ethylene oxide) (PEO)<sup>165</sup>, poly(vinyl acetate) (PVAc)<sup>166</sup>, poly(vinyl chloride) (PVC)<sup>167</sup>, and poly(vinylidene fluoride) (PVdF)<sup>168</sup>.

Polyvinyl alcohol (PVA) is a water-soluble synthetic polymer used in a wide range of industrial, commercial, food and medical applications<sup>169</sup>. It is a hydrophilic, semi-crystalline polymer with a good chemical and thermal stability<sup>170</sup>. Furthermore, it is a biodegradable, non toxic, non-immunogenic and non-carcinogenic polymer with excellent mechanical properties<sup>171, 172</sup>. Because of the excellent properties of PVA, many attempts have been devoted to prepare miscible films from PVA/PHB blends<sup>173, 174</sup>. The hybrid polymers showed a partial miscibility of the two components in the amorphous region<sup>175</sup>. Moreover, they adopt low crystallinity for both PVA and PHB in the blend film<sup>176</sup>. In addition, PVA significantly improved the mechanical properties of the blends and exhibited a faster degradation of the blend compared to pure PHB<sup>177</sup>.

Mixing both phases of PVA and PHB at the macromolecular region is not so easy by using the solution casting method, because PVA is more hydrophilic than PHB. Nevertheless, electrospun PVA/PHB nanofibers have not been reported heretofore. Herein, the aim of the present work was to fabricate nanofibrous scaffolds from PVA/PHB blend and to investigate their miscibility in the macromolecular region. Then, the nanofiber scaffolds composed of hydrophilic/hydrophobic components could be useful for culturing both HaCaT and fibroblasts cells for potential application as a skin substitute material, since HaCaT might prefer more hydrophilic substrate and fibroblasts don't. To these end physical properties of nanofibers from PVA/PHB blends of different ratio were studied, while the biocompatibility of nanofibers mats was studied with human fibroblasts and keratinocytes (HaCaT) cell line. Results are reported herein.

### 4.5.1. Morphology of electrospun PVA/PHB blended nanofibers

Fig. 54 shows the morphology of electrospun pure PVA, PHB and PVA/PHB (50/50). It is shown that PHB, PVA/PHB (50/50) nanofibers have a uniform structure without any sign of beads formation. In addition, the average size diameter of PHB is about 680 nm and PVA/PHB (50/50) is about 615 nm (see Fig. 55). Nevertheless, the majority of fiber diameters in both cases were in the range of 200–1100 nm. On the other hand, increasing PVA fraction more than 50 wt% in the blend resulted in a non-homogenous structure with small beads and ribbon like morphology. Pure PVA also showed non-homogenous fibers with a ribbon like structure, because of using HFIP as a solvent. In this study we have chosen only the homogenous fibers structures (blends with PVA fraction up to 50 %) to study the possibility of using them as scaffolds for skin tissue engineering.

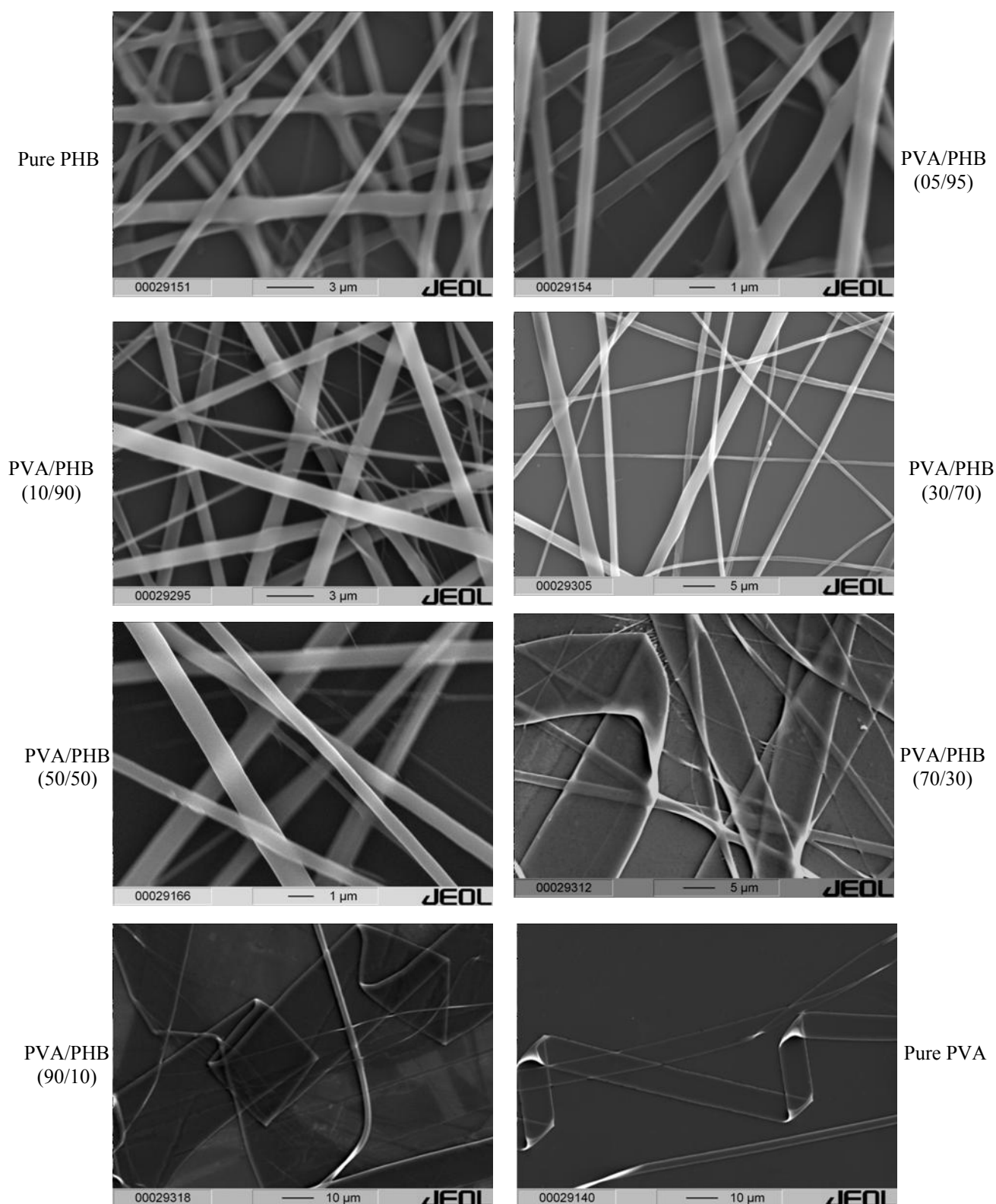
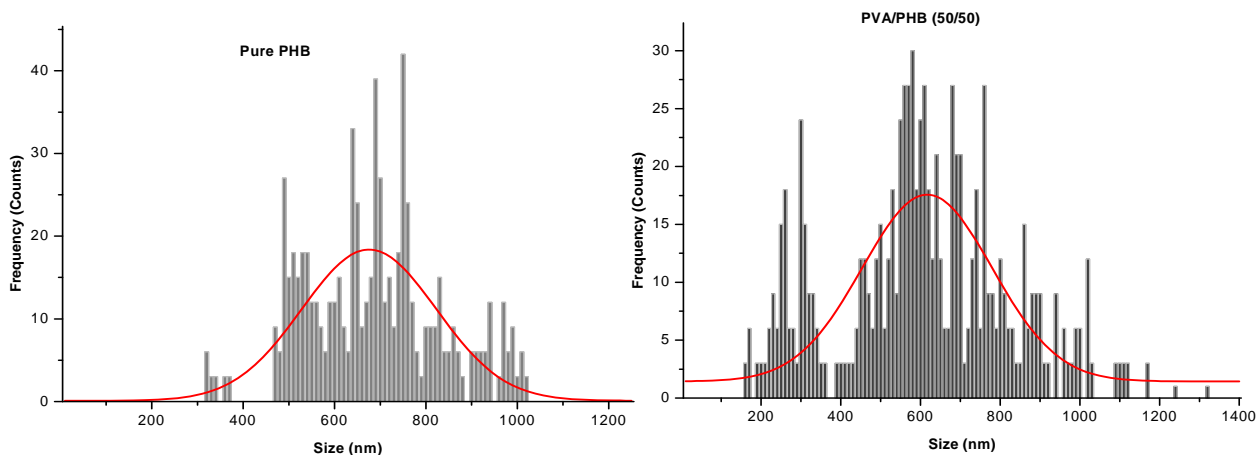


Fig. 54. SEM micrographs of the electrospun fibers of (a) pure PHB, (b) PVA/PHB (50/50) and (c) pure PVA using HFIP as a solvent for both polymers



**Fig. 55. Fiber diameter distribution of electrospun mats of (a) pure PHB and (b) PVA/PHB (50/50) blend nanofibers**

### 4.5.2. Phase morphology characterization of electrospun PVA/PHB

It is known from previous studies with blend polymers that PVA fraction appears as a darker area while the PHB fraction remains non-stained<sup>54</sup>. Therefore, to obtain information about miscibility or segregation of both polymers after electrospinning, nanofibers of PVA/PHB (50/50) were stained with OsO<sub>4</sub> vapors for 4 days in order to give good contrast during TEM inspection. As shown in Fig. 56, the fibers were found to have a relatively smooth surface with a homogenous distribution of both PHB and PVA fractions in the blend nanofibers at the macromolecular level. Moreover, the internal morphology of the nanofiber showed no visible phase segregation or porosity. This can be considered as a sign of good compatibility and miscibility of the two polymers in the blend<sup>178</sup>. On the other hand, changing electrospinning parameters leads to production of fibers in the micron range. These thicker fibers (with diameter more than 1.5  $\mu\text{m}$ ) showed phase separation between the two polymers (see Fig. 57). The non homogeneity of the thicker fibers can be related to the tendency of PVA to be agglomerated on the fiber surface making micro-phase separation<sup>179</sup>. This result revealed that the reduction of the fibers diameters increases the molecular distribution of the polymers in the blend.

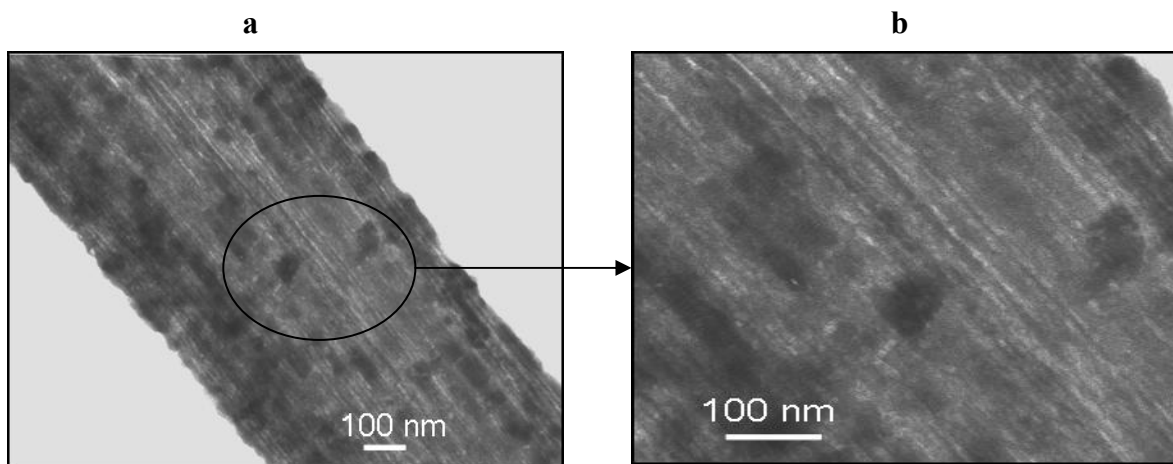


**Fig. 56.** TEM micrograph of chemically stained PVA/PHB (50/50) nanofibers, stained with OsO<sub>4</sub> vapor for 4 days (a, b) in a lower and higher magnification (fibers have an average diameter less than 1.5 μm)

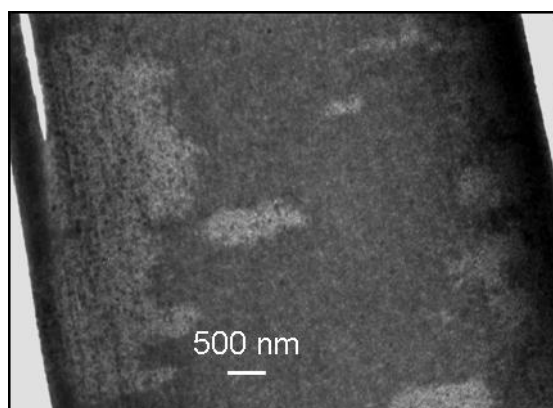


**Fig. 57.** TEM micrograph of chemically stained PVA/PHB (50/50) nanofibers, stained with OsO<sub>4</sub> vapor for 4 days (fibers have an average diameter more than 1.5 μm)

### 4.5.3. Water contact angle (WCA) measurements

Films of PVA, PHB and their blends prepared by spin-coating were used for WCA measurements. The static values were tabulated in Table 8 and merged with zeta potential values. It is shown that pure PHB exhibited less hydrophilic surface with WCA of about 70°. However, addition of PVA to the PHB gradually decreased the values of WCA for the blend films. PVA/PHB (50/50) showed a more hydrophilic surface because of the segregation of PVA fraction on the surface of the blend film. Moreover, PVA/PHB blend films containing 30 and 50 wt% PVA were found to have similar water contact angle of

about 41°. This might be related to the surface being covered and saturated with PVA molecules. Ikejima et al revealed by ATR-FTIR spectroscopy that the surface of films of PVA/PHB blends was more hydrophilic than that of only PHB films, because of the preferential accumulation of PVA fraction at the surface<sup>180</sup>.

**Table. 8. Water contact angle, zeta potential and pH values at zero charge for spin coated films of PHB, PVA and their blend with different compositions**

Sample name	WCA (°)	Zeta potential at pH 7.54 (mv)	pH (point of zero charge)
Pure PHB	70	- 16	6.9
PVA/PHB (05/95)	62	- 12.6	6.5
PVA/PHB (10/90)	54.8	- 6.9	5.9
PVA/PHB (30/70)	41.7	-2.3	5.6
PVA/PHB (50/50)	41	-2.1	5.1
Pure PVA	37.3	—	—

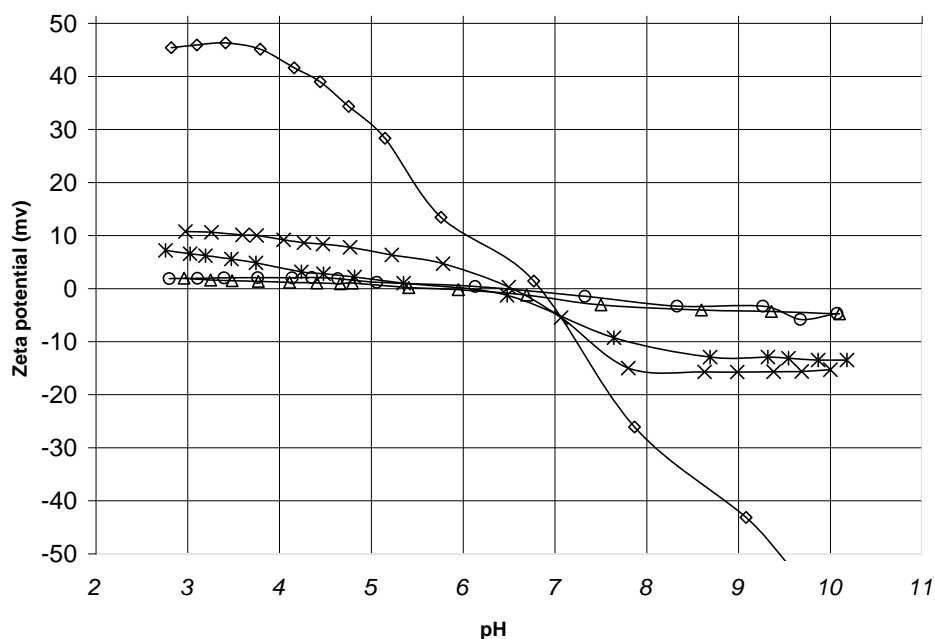


Fig. 58. Zeta potential vs. pH for films of (□) pure PHB, (×) PVA/PHB (05/95), (\*) PVA/PHB (10/90), (Δ) PVA/PHB (30/70) and (○) PVA/PHB (50/50)

#### 4.5.4. Zeta potential

Zeta potential is related to the quantity and dissociation of charged groups on the material surface and dependent on ionic strength and pH value of electrolyte solutions. Thereby, increasing or decreasing in the surface charged groups will result in a higher or lower zeta potential value<sup>72</sup>. Results of zeta potential measurements in dependence of pH value for different blend compositions were presented in Fig. 58, and summarized in Table 8. It is shown that pure PHB has a zeta potential of about 45mV at extreme acidic pH. On the contrary, at alkaline pH, the PHB molecules tend to adsorb hydroxyl ion and become negatively charged (~ -42 mV). It was reported previously that hydroxyl ion preferentially adsorb onto aqueous-hydrophobic interfaces resulting in a net negative surface charge density<sup>181</sup>. On the other hand, addition of a small amount of PVA(5 wt %) to PHB resulted in a significant decrease in zeta potential values for the blend films, and these values further decreased by increasing PVA fraction. This decrement in potential is a reflection of decrease of the number of surface charges attributable to the presence of PVA molecules<sup>182</sup>. Furthermore, zeta potentials for films with PVA content of 30 and 50 wt% were almost the same, which can be another sign showing that the PVA molecules becomes saturated

on the surface of the film and that the hydroxyl groups are the reason of the decrease in zeta-potential and water contact angle.

Zeta potential values for all the compositions were found to be negative at pH 7.5 (biological pH). However, the negative magnitude decreased gradually by increasing the PVA fraction, due to the presence the hydroxyl groups (Table 8). Altankov et al. demonstrated that the hydroxyl polar groups (OH) diminish the negative magnitude of zeta potential while the carboxylic group (COOH) increased it <sup>183</sup>. Moreover, the iso electric point of the samples was in the acidic range and shifted to a lower pH region by increasing PVA fraction compared with pure PHB. Such decrement is attributed to the specific adsorption of anions (hydroxyl ions ) <sup>184</sup>. Based on the WCA and zeta potential results, it can be concluded that PVA molecules are concentrated on the surface of the film and the hydroxyl groups play a role in changing surface charge properties.

**Table. 9. Assignments of FTIR absorption bands for electrospun pure PVA, pure PHB and PVA/PHB (50/50) blend nanofibers**

Peaks for electrospun nanofibers ( $\text{cm}^{-1}$ )			Assignment
PVA	PHB	PVA/PHB (50/50)	
3278		3311.70	Stretching of OH
	2976		C-CH <sub>3</sub>
2912.82	2936.18	2941.38	Asymmetric stretching of CH <sub>2</sub>
	2871		CH stretching
	1720	1723.23	C=O carbonyl group stretching Vibration of the crystalline carbonyl group
1714.36	1687		Stretching of C=O (Acetate group) (Crystalline)
1656			O=H, C=C
1556.21			C=C end group
	1452.30	1454.57	Asymmetric deformation of CH <sub>3</sub>
1417			O-H, C-H bending, $\gamma(\text{CH}_2)$ , $\delta(\text{OH})$
	1380.24	1381.24	Symmetric wagging of CH <sub>3</sub>
1374			C-H bending or CH <sub>2</sub> wagging
1326.70			C-O-H bending
	1276.67	1284.23	Symmetric C-O-C stretching
	1258.92	1263.14	Symmetric C-O-C stretching + C-H deformation
1233.61			C-O-C (Acetate group)
	1227.44	shoulder	C-O-C stretching
	1180.40	1182.67	Asymmetric C-O-C stretching
	1130.11	1130.43	Symmetric stretching vibration of C-O-C group
	1100.90	1198.96	Symmetric C-O-C stretching
1089.92			Stretching of C-O and bending of OH(amorphous sequence of PVA)
	1057.10	1058	C-O stretching and CH <sub>2</sub> rocking
	980.85	shoulder	C-C stretching (Crystalline)
918.66			Bending of CH <sub>2</sub>
831.87		828.03	Rocking of CH <sub>2</sub>

### 4.5.5. Fourier transform infrared spectroscopy (FTIR)

FTIR measurements have been performed to analyze the structural changes that might be occurred upon blending, as well as the interactions between (OH) groups of PVA and (C=O) groups of PHB, which consequently affect on the miscibility and crystallinity of the blend nanofibers. The absorption peaks of the observed frequencies and their assignments were summarized in Table 9. Results obtained showed that the most evident characteristic bands for PHB and PVA were the carbonyl and hydroxyl group bands centered at  $\sim 1720$   $\text{cm}^{-1}$  and  $\sim 3278$   $\text{cm}^{-1}$ , respectively. These two molecular vibrations are important in infrared range absorption peaks; the investigation of these peaks in the blend gives important information about the intermolecular interaction (e.g., hydrogen bond) between two polymers in the blend and their compatibility<sup>173</sup>. The other characteristic bands for PHB were observed at  $\sim 1276$ ,  $\sim 1180$  and  $\sim 1057$   $\text{cm}^{-1}$  which can be assigned to the ester groups of the polymer<sup>185</sup>. The bands centered at 980, 1227, 1276 and 1720  $\text{cm}^{-1}$  were shown to arise from the crystalline phase of PHB. On the other hand, pure PVA nanofibers showed two bands centered at 1714 and 1089  $\text{cm}^{-1}$  which are corresponding to C–O of the remaining acetyl groups present on the partially hydrolyzed PVA back bone<sup>186</sup>.

The sensitivity of FTIR spectrum to crystallization of PHB has been investigated by Bloembergen et al.<sup>85</sup>. Moreover, analyzing the spectra of FTIR would give crucial evidences on both crystallization and miscibility of the blend polymers<sup>187</sup>. In the present study, the electrospun PVA/PHB (50/50) blend nanofibers showed an increment in the crystalline related carbonyl group bands of PHB to  $\sim 1723$  and 1284  $\text{cm}^{-1}$  (see Table 9). The increment of carbonyl band order can be attributed to the absence of an ordered structure (hydrogen-bonding effects are reduced) and thereby the wave number of absorbance will be increase<sup>87</sup>. Furthermore, the intensity of bands observed at 980, 1227  $\text{cm}^{-1}$  were decreased in the blend PVA/PHB (50/50) fibers. In addition, the absorption band of PVA hydroxyl group shifted to a higher frequency at  $\sim 3311$   $\text{cm}^{-1}$ , due to the presence of intermolecular hydrogen bonding interaction between the two polymers<sup>188</sup>. Moreover, in the pure PHB nanofibers, a crystalline related peak such as peak at  $\sim 2976$   $\text{cm}^{-1}$  for  $\text{CH}_3$  asymmetric and symmetric stretching was disappeared in the blend fibers, which can be assumed as a sign of depression of crystallization of PHB by addition of PVA. Likewise, this phenomenon can be verified also by the disappearance of the band centered at  $\sim 2871$   $\text{cm}^{-1}$  (CH stretching of PHB) and band at  $\sim 1687$   $\text{cm}^{-1}$  (stretching of C=O of PHB). Besides, the crystalline related peaks at 1417 and 1326  $\text{cm}^{-1}$  in pure PVA were disappeared in the blend fibers (Table 9), which can be a sign of interaction of the carbonyl groups of

PHB with hydroxyl groups of PVA. Thereby, restrictions of these bands were obtained and disappearance of wagging and bending movement of the hydroxyl groups were observed. The FTIR results revealed that the crystallinity of electrospun PVA/PHB (50/50) nanofibers was suppressed compared with pure PHB. Such decrement of the total crystallinity is very important factor for acceleration of the fibers degradation and also for decreasing the brittleness and improving the mechanical properties of the nanofibers scaffolds. The intermolecular hydrogen bonds between C=O groups of PHB and OH groups of PVA found in the blend PVA/PHB (50/50) fibers are considered to be an evidence for the miscibility of the polymers.

### 4.5.6. Differential scanning calorimetry (DSC)

The second heating scans of DSC for PVA granules, PHB powder, electrospun PVA, PHB and their blend nanofibers with different ratios were taken into consideration and the data were given in Table 10. Results obtained show that PVA granules exhibit a first endothermic peak at  $\sim 41.7$  °C, which is corresponding to the glass transition temperature ( $T_g$ ). Furthermore, crystallization temperature ( $T_c$ ) and melting temperature ( $T_m$ ) of PVA granules were observed at  $\sim 179$  and  $\sim 218$  °C, respectively. The  $T_g$  of PVA nanofibers was found to be  $\sim 48.3$  °C with a slightly increment after electrospinning. Similarly, electrospun PVA nanofibers exhibit a slightly increment in  $T_c$  and  $T_m$  peaks to  $\sim 190$  and  $\sim 219$  °C, respectively. These increments indicated that the oriented PVA chains are highly confined in the electrospun fibers. Thus, the molecular orientation limits the chain mobility and thereby  $T_g$ ,  $T_c$  and  $T_m$  values were increased<sup>137</sup>. Likewise, an increment of  $T_c$ ,  $T_m$  and degree of crystallinity were observed for the electrospun PHB nanofibers compared with PHB powder. Increasing degree of crystallinity for PHB fibers can be attributed to the orientation of polymer molecules in the fiber direction during electrospinning. It was reported previously that electrospinning improves the degree of crystallinity and aligns the molecules in the direction of the fiber axis<sup>89</sup>. On the other hand,  $T_g$  of PHB and their blends with PVA were not detectable because of the high crystallinity of PHB. Xing et al. suggested that  $T_g$  of the blends must be between glass transition temperatures of the two polymers<sup>174</sup>. Furthermore, neat PHB exhibited cold crystallization peak at  $\sim 76$  °C suggesting that PHB crystallizes more rapidly at a lower temperature compared with PVA. In addition, PHB exhibited double melting peaks at  $\sim 147$  and  $\sim 159$  °C. The double or multiple melting behavior of PHB can be attributed to secondary crystallization (melting–recrystallisation–remelting), which can occur during the melting process as well as during

storage at room temperatures<sup>88, 189</sup>. Furthermore, in the electrospun PHB and their blends with PVA, cold crystallization of PHB was observed which normally takes place above  $T_g$  of the blend where crystallizable polymer chains have enough segmental mobility to crystallize. The crystallinity of both PVA and PHB were reduced by the blending (even with 5wt % PVA) due to some specific interactions between them (e.g., hydrogen bonds). The interaction between PVA and PHB occurs only in the amorphous phase, whereas the crystalline fractions of both components do not influence each other. Another factor other than hydrogen bonds which lowers the degree of crystallinity of PHB is the difference in the molecular mobility between PHB and PVA. The difference in the glass transition temperature between PVA and PHB ( $\sim 60\text{-}80\text{ }^\circ\text{C}$ ) influences the degree of crystallinity of their blends. The 'glassy' environment of PVA are trapped the molecules of PHB in the amorphous phase and hindered their required mobility for crystallization, resulted in a lower degree of crystallinity. Therefore, the influence of PVA on the crystallinity of PHB can be considered as a proof for good miscibility (compatibility) of the two polymers. In literature, PHB has been found to be partially miscible with PVA and in the amorphous region<sup>180</sup>. Moreover, Yoshie et al. found that PVA/PHB blend is compatible only when the blend contains a large amount of PVA<sup>175</sup>. A similar behavior has been observed previously for the blends of PHB in blends with chitin and chitosan<sup>84</sup>. The DSC results revealed that blending PVA with PHB suppressed the crystallinity of both polymers in the blend fibers. In addition, there was an interaction between both polymers in the electrospun PVA/PHB blend fibers. Such interaction can be considered as a sign of miscibility of the two polymers in the macromolecular region.

### 4.5.7. TGA and first order derivatives of TGA

Fig. 59 shows typical TGA thermograms indicating the weight loss as a function of temperature for the electrospun PVA, PHB and their blends with different ratios. It is observed that TGA thermograms for all samples exhibited major weight loss stages ( $\sim 4\text{ wt}\%$ ) at  $30\text{-}220\text{ }^\circ\text{C}$ , which is refers to the weakly physisorbtion of water. Furthermore, the as spun PHB nanofibers showed higher thermal stability than PHB powder. In case of PHB powder, the main decomposition ( $\sim 93\text{ wt}\%$ ) occurs at  $\sim 280\text{ }^\circ\text{C}$ , while the thermal degradation of PHB nanofibers ( $\sim 89\%$ ) occurs at  $\sim 290\text{ }^\circ\text{C}$ . The thermal stability of the electrospun PHB nanofibers can be attributed to its high crystallinity and orientation of the polymer molecules in the fiber direction during electrospinning compared to PHB powder

<sup>89</sup>. On the other hand, thermal decomposition of PVA occurs at 400 °C (~81 %) which indicated that PVA is more thermally stable than PHB:

First order derivatives of TGA (DTGA) curves, showing weight loss over temperature change (-dM/dT) vs. temperature, was calculated and drawn for all samples (Fig .60). DTGA refers to the temperatures where maximum mass decomposition occurred. The results showed that the temperature at which the maximum decomposition of PHB powder and electrospun PHB nanofibers occurs at 275 and 281°C, respectively. In PVA nanofibers, the maximum decomposition occurred at 308 °C, indicated that PVA more thermally stable than PHB as demonstrated above. In the blend nanofibers containing PVA up to 10 wt %, the thermal stability decreased, due to the lower degree of crystallinity and hydrogen bonds interaction between them. Increasing PVA content up to 50 wt %, two decomposition temperatures were observed. Furthermore, the decomposition temperature of both polymers in the blend nanofibers will be decreased by increasing PVA contents. Lowering the decomposition temperature can be considered as a sign of good compatibility of the two polymers as confirmed also with TEM, DSC and FTIR results.

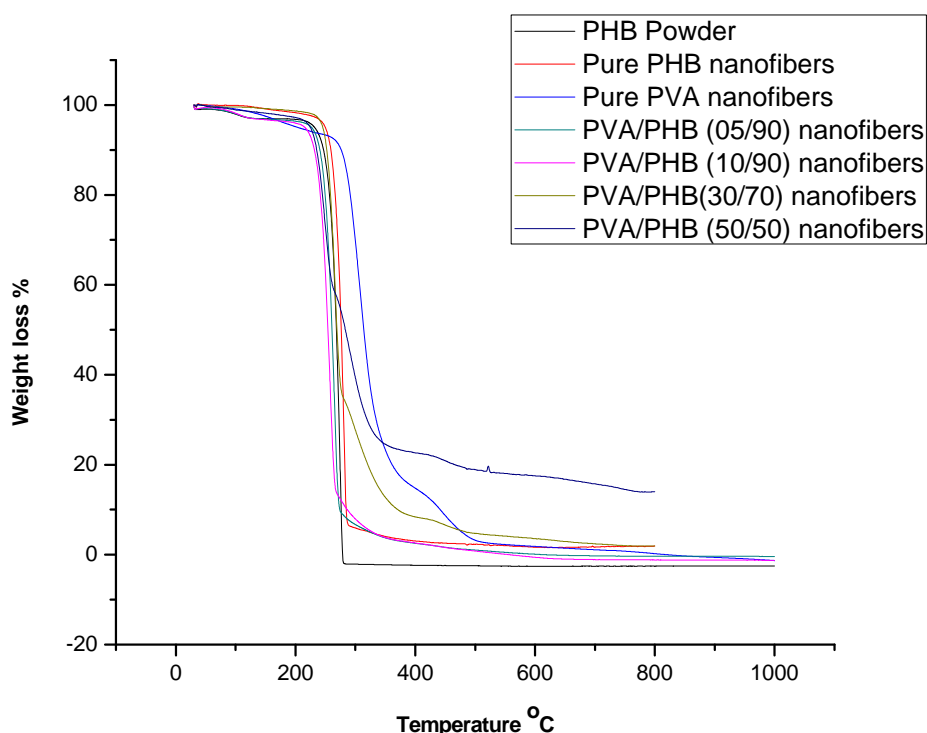


**Fig. 59.** TGA thermograms for electrospun pure PVA, pure PHB and their blends with different ratios

**Table. 10.DSC data and the characteristics observed for PVA granules, PHB powder, electrospun PVA, PHB and their blend nanofibers with different compositions**

Sample	T <sub>m1</sub> (°C)	T <sub>m2</sub> (°C)	T <sub>c</sub> First crystallization temperature	ΔH m (j.g <sup>-1</sup> )	Crystallinity (%)
PVA granules	218	----	179	65.3	47
PVA Nanofibers	219	----	190	61.4	44
PHB Powder	147.2	159.68	76.1	97	66.43
PHB Nanofibers	152.2	164.50	81.4	98.5	67.46
PVA/PHB (05/95)	134.9	152.19	65.4	84	60.56**
PVA/PHB (10/90)	133.4	151.59	82.3	74	56.31**
PVA/PHB (30/70)	116.6	134.34 144.15 186.51*	161.9	53.5	52.34**
PVA/PHB (50/50)	102	122.26 135.29 186.15*	159.6	24	32.87**

---

\* T<sub>m</sub> for PVA fraction

\*\* Crystallinity of PHB fraction in the blend nanofibers

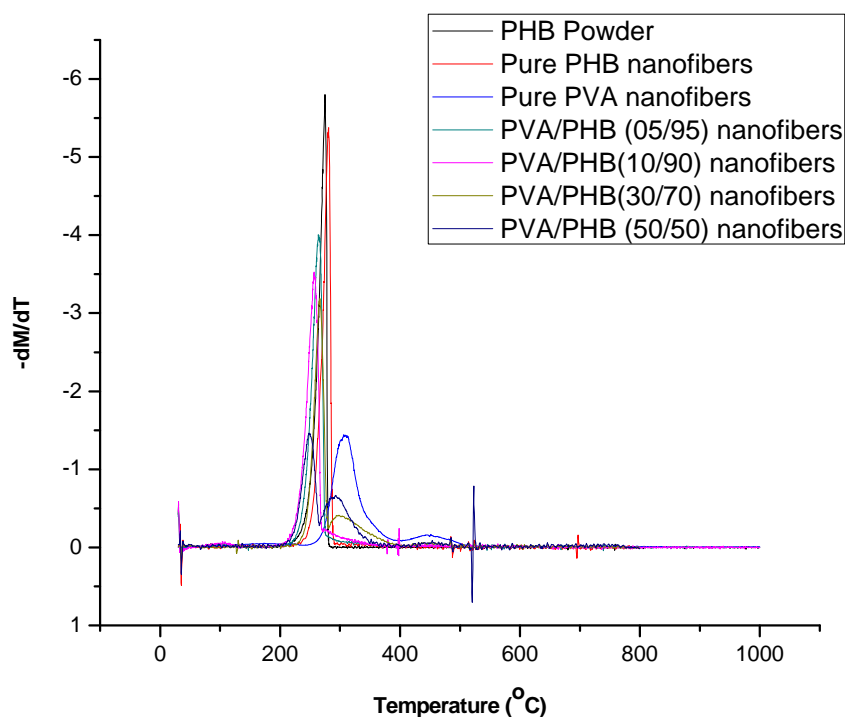
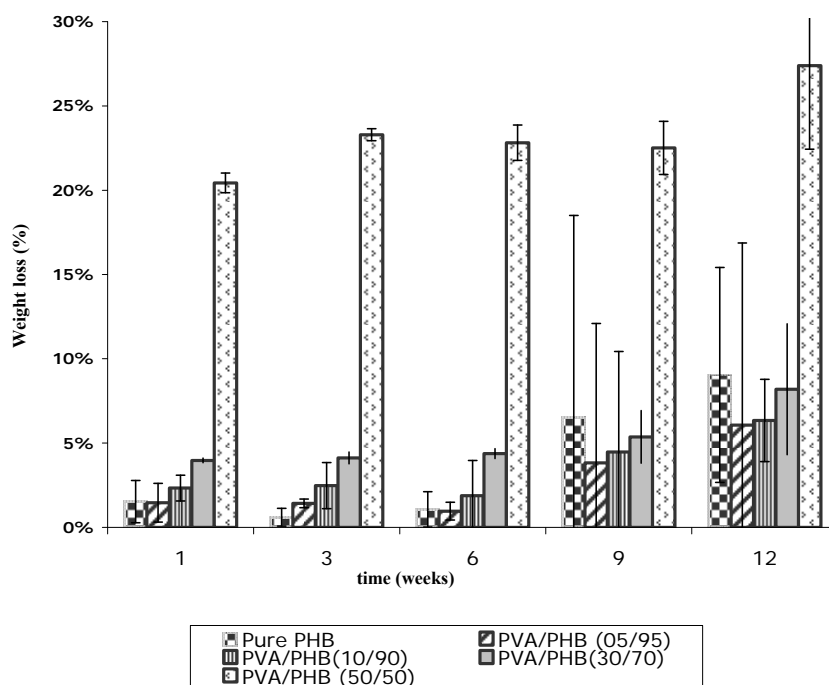


Fig. 60. DTGA thermograms for electrospun pure PVA, pure PHB and their blends with different ratios

#### 4.5.7. In vitro degradation of electrospun PVA/PHB nanofibrous scaffold

PHB and PVA were reported as biodegradable polymers<sup>190, 191</sup>, but PHB has a rather low degradation rate due to its high crystallinity<sup>90</sup>. However, the hydrolytic degradation of PHB has been investigated by several researchers and results have provided contradictory findings. While some authors have reported that PHB degrades through surface erosion<sup>192-194</sup>, others have reported the random bulk hydrolysis of ester bonds in the polymer chain<sup>195-197</sup>. Fig. 61 shows the hydrolytic degradation of electrospun PHB and PVA/PHB nanofibers mats with different PVA fractions. It was found that all electrospun fibers were partially degradable and they began to degrade one week after starting the test. Furthermore, they showed a remarkable degradation over time, but the degradation was significant only for the nanofibers mats contain PVA-rich composition. Moreover, significant degradation of pure PHB nanofibers occurred after 9 weeks. PHB nanofibers containing 30 and 50 wt % PVA showed degradation after 12 weeks of ~ 8 % and ~ 28 % weight loss, respectively. However, pure PHB nanofibers showed ~ 9% weight loss after 12 weeks which is higher than PVA/PHB nanofibers containing 30% PVA. This can be

attributed to the different degradation mechanism in pure PHB nanofibers and PVA containing one<sup>171</sup>. The accelerated degradation rate of PVA/PHB nanofibers mats (contains 30 and 50 wt % PVA) is mainly due to the lower degree of crystallinity of the final blend nanofibers. Previous reports demonstrated the biodegradation behaviors of PVA/PHB blend films and they concluded that the biodegradation profile depends strongly on the water solubility of the PVA components<sup>177, 198</sup>. The degradation results showed that PVA accelerates the degradation of PHB. In addition, the degradation of PVA/PHB blend nanofibers was dependent on the PVA fraction.



**Fig. 61.** Degradation of electrospun nanofibrous mats of PHB, PVA/PHB (05/95), PVA/PHB (10/90), PVA/PHB (30/70) and PVA/PHB (50/50), degradation were measured by weighting the nanofibers scaffolds after degradation in phosphate-buffered saline within 3 months

### 4.5.9. Adhesion and proliferation of epidermal and dermal cells on the nanofibers

#### ▪ HaCaT cells

Fig. 62 and 63 showed the qualitative and quantitative measurements of HaCaT cells adhesion and growth on the electrospun PHB and its blends with different PVA fractions. It is shown that HaCaT cells attached and grew well on pure PHB nanofibers. Moreover, the surface coverage after 7 days was almost the same as the control surface (TCP). Peschel et al. suggested that the surface hydrophobicity might have a negative effect on HaCaT cell growth<sup>199</sup>. However, it has been shown previously that PHB nanofibers mimic the nanostructure of the native ECM and this characteristic may overcome the possible negative effect of less hydrophilic PHB on the behavior of HaCaT cells<sup>81, 82</sup>. On the other hand, addition of 5wt % PVA resulted in a significant decrease in the number of viable HaCaT cells. However, it is somehow difficult to explain such decrement of the viable cells number on the 5% PVA containing scaffolds. On the contrary, increasing PVA fraction exhibited an increment in the number of viable cells on the nanofibers scaffolds. Such increment of the viable cells was attributed to the saturation of PVA on the surface, as was found by surface analysis (water contact angle and zeta potential measurements). As discussed previously, HaCaT cells prefer more hydrophilic surfaces, and increasing PVA content (hydrophilicity), resulted in a good adhesion and proliferation of the HaCaT cells on the nanofibers scaffolds<sup>199</sup>.

In all, HaCaT cells showed highest proliferation on electrospun pure PHB nanofibers (comparable to tissue culture polystyrene) and relatively good adhesion and proliferation on high PVA containing scaffolds after 1 and 2 weeks, promising further proliferation and growth in longer incubation time.

HaCaT cells distribution and growth

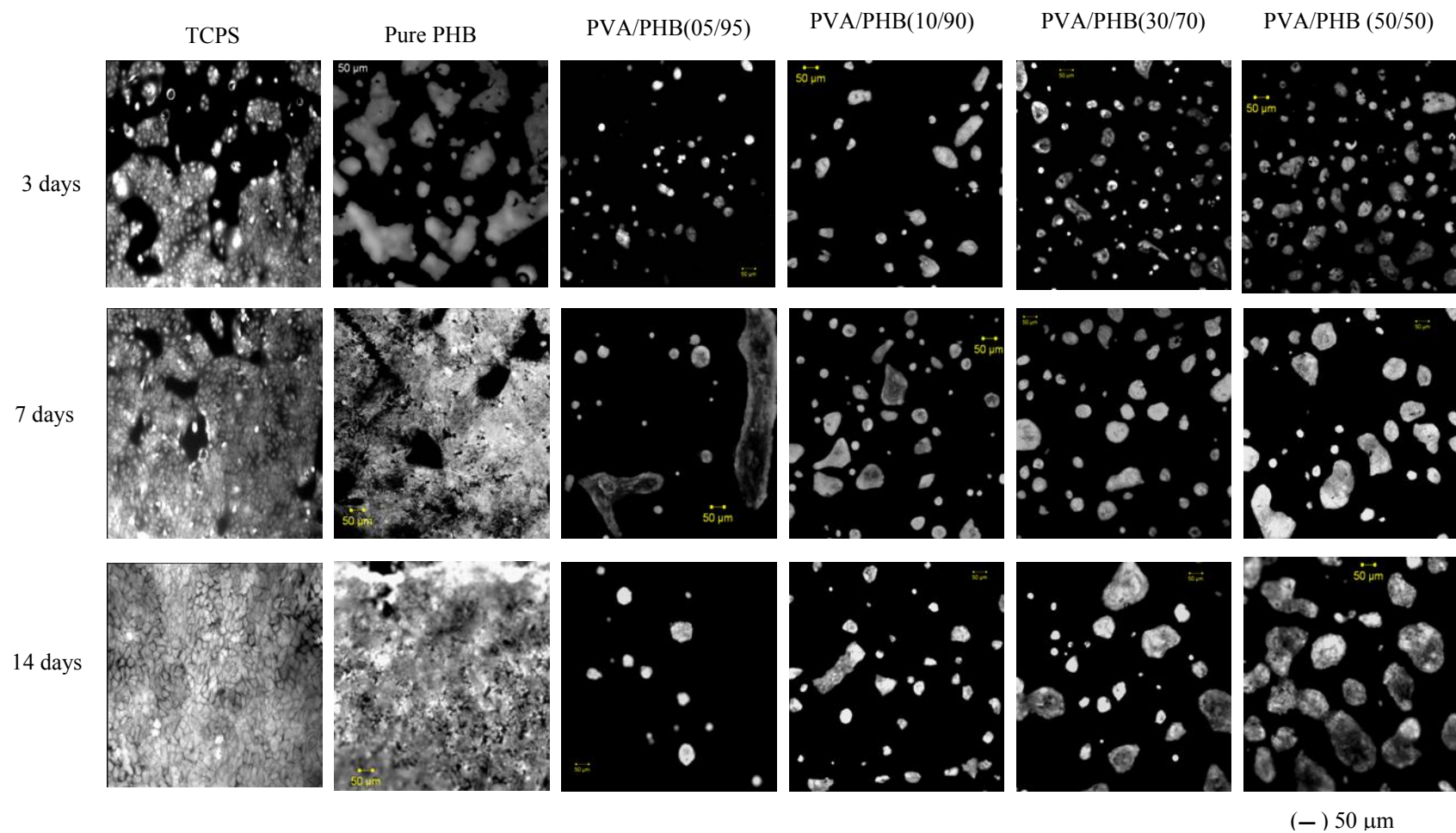
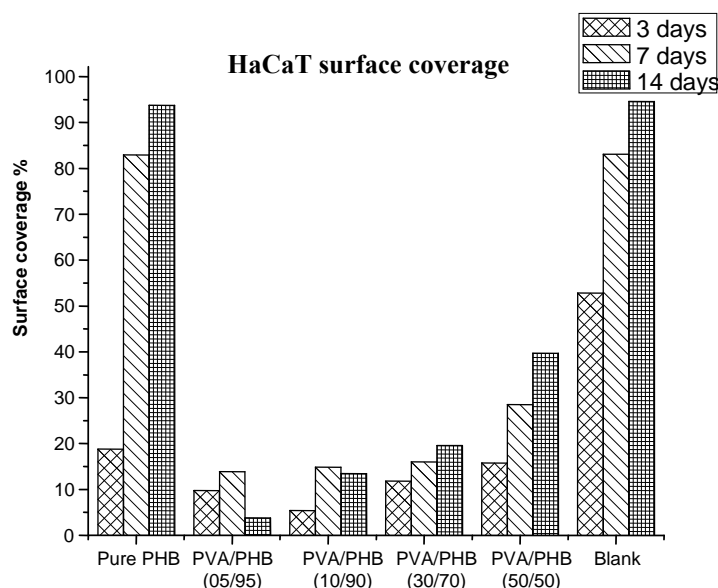


Fig. 62. HaCaT cell growth on the electrospun PVA/PHB nanofibers scaffolds with different blend compositions after 3, 7 and 14 days

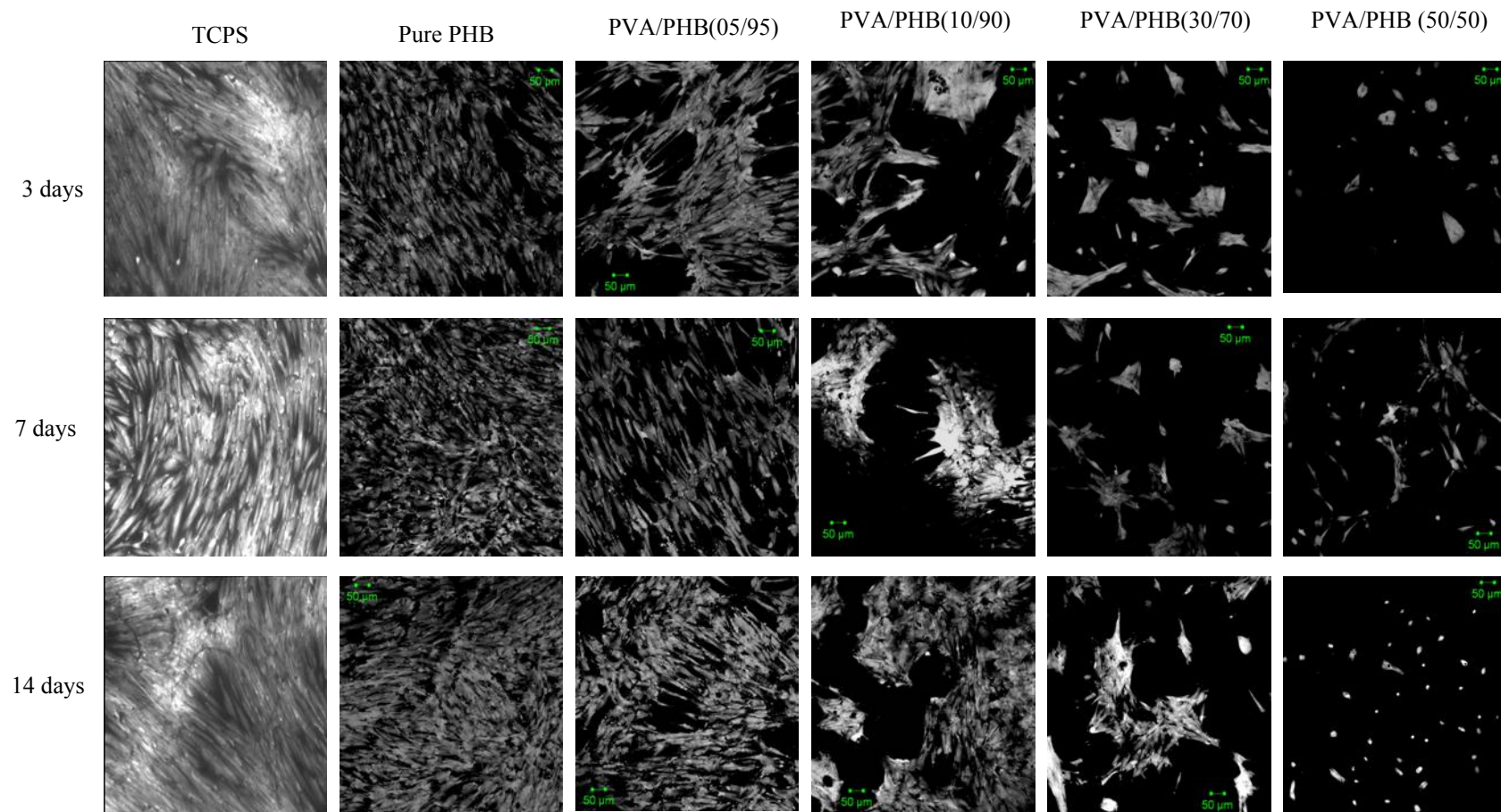


**Fig. 63. HaCaT cells surface coverage on the electrospun PVA/PHB nanofibers scaffolds with different blend compositions after 3, 7 and 14 days**

▪ **Dermal fibroblasts cells**

Qualitative and quantitative measurements of the adhesion and growth of dermal fibroblast were presented in Fig.64 and 65. It is shows that increasing PVA content of the nanofibers scaffolds has a negative impact on attachment and proliferation of the fibroblasts cells. It was reported previously that the hydrophilicity of the substrate had a negative effect on the fibroblasts proliferation and function and better cellular interaction was found on intermediate wettable surfaces <sup>183</sup>. Decreasing amount of fibroblasts living cells by increasing substrate hydrophilicity can be related to the high water uptake of PVA, probably reducing adsorption of attachment proteins <sup>200</sup>. On the other hand, water uptake for PVA/PHB blend nanofibers has a small unfavourable impact on HaCaT cells because they have a tight connection and have cell-cell signaling with neighboring cell. It was only necessary that some of them find and attach to the few anchorage sites available on highly hydrophilic surface, then other cells can attach to these cells and further cell-cell communication and their proliferation can follow <sup>201</sup>. Here again, PHB nanofibers were found to have highest fibroblasts adhesion and proliferation compared to other blend compositions. Nanofibers mats with 5-10 % PVA content were also found to promote cell adhesion and proliferation (although inferior to pure PHB mats).

Fibroblast morphology and growth



(—) 50 μm

Fig. 64. Dermal fibroblast growth on the electrospun PVA/PHB nanofibers scaffolds with different blend compositions after 3, 7 and 14 days

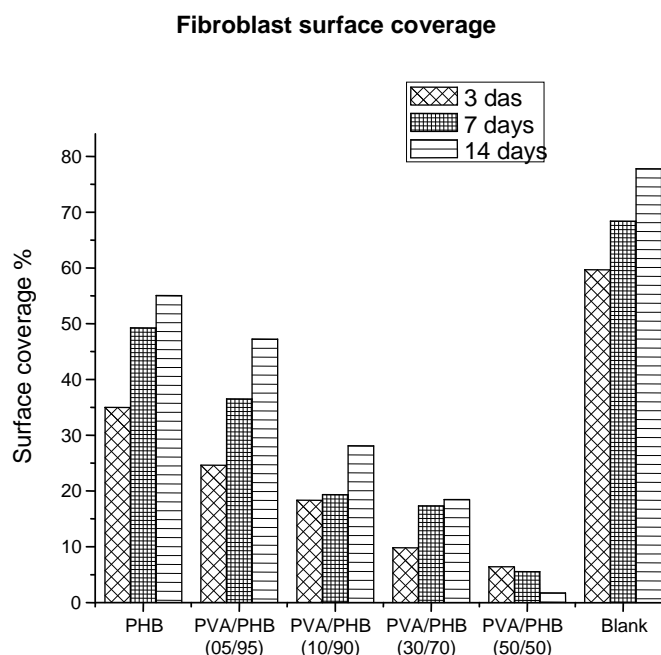


**Fig. 65. Dermal fibroblast cells surface coverage on the electrospun PVA/PHB nanofibers scaffolds with different blend compositions after 3, 7 and 14 days**

To conclude, biocompatible PVA/PHB blend nanofibers with different compositions were prepared by electrospinning techniques for future applications in skin tissue engineering. Morphological characterization, crystallization behavior, degradation rate and cell culture investigations were studied for the blend nanofibers. The average fibres diameter of the as spun PHB and PVA/PHB (50/50) blend nanofibers were at  $\sim 680$  and  $620$  nm, respectively. The nanostructure of the prepared nanofibers scaffolds was found to be mimicking the structure of the native ECM. It was found that PVA and PHB connected in the macromolecular region through hydrogen bonds. The hydrogen bonding interaction between hydroxyl group of PVA and carbonyl group of PHB leads to the miscibility of both polymers in the amorphous phase. Furthermore, PVA suppressed the crystallinity of PHB and the degree of crystallinity of PHB decreased by increasing PVA fraction. In addition, PHB nanofibers and their blends with PVA were found to be degradable in a simulated body fluid and the degradation increased by increasing PVA content. Water solubility of PVA fraction was found to affect the degradation of whole blend nanofibers. The cell culture results demonstrated that the moderately hydrophobic surface of pure PHB nanofibers promoted highest cell adhesion and proliferation for both HaCaT and

fibroblasts cells. Increasing PVA fraction had a negative impact on fibroblasts cell adhesion and growth which is in agreement with the literature. Adhesion and growth of HaCaT cells was hindered by addition of 5 wt% PVA. However, the adhesion and growth of HaCaT were increased again by further increasing PVA fraction in the blend nanofibers. The obtained PVA/PHB nanofibers blend could be a good candidate for fabrication and designing of bi-layer nanofibers scaffold. The top layer could be composed from PVA/PHB blend fibers with more hydrophilic polymers to enhance the adhesion, proliferation and growth of HaCaT cells. The dermal equivalent could be fabricated from pure PHB to promote fibroblast adhesion and growth. Such kind of this bi-layer scaffold not only mimics the morphological structure of native ECM of the skin, but also mimics its composition (epidermal and dermal cells). It might be helpful to fabricate 3-D scaffolds for skin tissue engineering application.



### 5. Summary and conclusions

Nanofibers have unique properties compared to other conventional fibrous structures because of their extremely high surface area to mass ratio. This makes nanofibers ideal materials for use in widespread applications particularly as scaffolds for biomedical uses. In the present work, varieties of novel polymeric micro and nanofibers have been fabricated using electrospinning method to provide new materials for biomedical applications (see Table.11). Detailed studies of the changes in physico-chemical properties that take place during the fabrication of the polymeric materials have been investigated. FTIR, DSC and TGA measurements were performed to analyze the structural changes that might be occurred upon blending, as well as the macromolecular interactions in the blend fibers which consequently affect on the crystallinity and mechanical properties of the nanofiber scaffolds. In addition, morphology of the obtained fibers and their phase behaviour at the nanoscale range has been investigated by SEM, ESEM and TEM inspections. Furthermore, the obtained fibers have been investigated in details to check their potential for biomedical applications (such as tissue engineering and dentistry).

The macromolecular orientation and molecular mobility of the brittle polystyrene (PS) has been enhanced by electrospinning. Electrospun PS nanofibers transformed from brittle to ductile material and its micromechanical deformation found to be mainly dependent on the fiber diameter: decreasing diameter of the electrospun fibers enhances their mechanical properties. Thus, the increased ductility of very thin PS fibers could be used to produce ductile PS networks for different applications.

Electrospun PMMA/EVA blend nanofibers have been prepared to generate macromolecular interaction between soft liner (EVA) and heat-cured (PMMA) denture base for dentistry applications. The blend nanofibers were used as an interface between denture base and liner during processing. Morphology using SEM, TEM, and mechanical properties of the adhered dentures has been measured. The results demonstrated that the large surface area to volume ratio of the electrospun PMMA/EVA nanofibers significantly improves the bond strength between denture base and liner materials. The nanofibers are not themselves sticky, but the millions of nano contacts from the same polymers (e.g., hydrogen bonds and van der Waals forces) work together to adhere the two polymers. This method might open a new door to enhance the contact between polymers with low adhesion that can be used for a wide range of applications especially in dentistry applications (denture and mouth guards).

## Summary and conclusions

**Table. 11. Summary of all prepared and investigated electrospun fibers**

Polymer	Solvent	Diameter of the obtained fibers	Morphology	Potential applications
PLLA	CHCl <sub>3</sub>	~ 500 nm – 3 μm	Porous structure	Drug delivery
PEI	CHCl <sub>3</sub>	~ 5 μm	Ribbon-like structure	Artificial organs
PEI	NMP	~ 500 nm – 2 μm	Bead structure	Artificial organs
PET/γ-Fe <sub>2</sub> O <sub>3</sub>	CHCl <sub>3</sub>	~ 1 – 5 μm	Twisted structure	Smart textiles
PEO/γ-Fe <sub>2</sub> O <sub>3</sub>	CHCl <sub>3</sub>	~ 300 nm – 1.5 μm	Helical structure	Smart textiles
PEI/EVA	NMP	~ 200 nm – 1.2 μm	Rough surface	Wound healing
CTS	TFA/DCM	~ 150 nm – 800 nm	Smooth surface	Skin substitutes
PHB	HFIP	~ 200 nm – 800 nm	Smooth surface	Bone regeneration
PHB/CTS	HFIP/TFA	~ 150 – 600 nm	Smooth surface	Tissue engineering
PS	THF/CHCl <sub>3</sub>	~ 200 – 800 nm	Smooth surface	Filter media
PVA	Distilled water	~ 150 – 500 nm	Smooth surface	Tissue engineering
PVA/Col	Distilled water/Acetic acid	~ 200 – 600 nm	Smooth surface	Tissue engineering
PVA/n-HAP	Distilled water	~ 200 – 600 nm	Smooth surface	Bone regeneration
PVA/Col/n-HAp	Distilled water/Acetic acid	~ 200 – 800 nm	Smooth surface	Bone regeneration
PMMA/EVA	CHCl <sub>3</sub> /DMF	~ 150 – 600 nm	Smooth surface	Dentistry application
PVA/PHB	HFIP	~ 200 – 1.2 μm	Smooth surface	Skin substitute

A new nanofibrous scaffold composed of PVA/Col/n-HAp has been prepared for bone tissue engineering applications. The most striking physiochemical feature of the electrospun PVA/Col/n-HAp composite nanofibers was that the n-HAp nanorods were preferentially oriented parallel to the longitudinal direction of the electrospun PVA/Col matrix as confirmed by TEM. In addition, the electrospun PVA/Col as matrix and n-HAp nanorods as inorganic phase strongly interact through hydrogen bonds within the electrospun PVA/Col/n-HAp nanocomposite fibers. The strong bonding in the nanocomposite nanofibers due to the presence of a great extent of OH groups in the PVA, Col and the HAp nanorods leads to a significant decrement in the degree of crystallinity, and thereby increasing their degradation rate. This feature bears strong resemblance to the nanostructure of mineralized hard tissues serving as building block of bone. The hybrid

## Summary and conclusions

---

electrospun PVA/Col/n-HAp nanocomposite nanofibers shown in the present work provides great potential for the fabrication of bio-mimicking mineralized hard tissues suitable for bone regeneration.

Electrospun hydrophilic/hydrophobic (PVA/PHB) nanofibers scaffolds have been prepared to mimic the ECM of the human skin tissue in order to facilitate the treatment of burns, chronic and diabetes related ulcers. Generally, skin substitutes were engineered by culturing keratinocytes and dermal fibroblasts cells in vitro. Since keratinocytes might prefer more hydrophilic substrate and fibroblasts don't, blend containing hydrophilic and hydrophobic components could be useful to fabricate nanofibrous scaffolds for future application in skin tissue engineering. Miscibility and morphological properties of the polymer blends in the nanofibers were studied using FTIR, SEM, TEM and DSC. It was found that PVA and PHB are miscible with a good compatibility in the blend nanofibers at the macromolecular region. In addition, DSC revealed that the crystallinity of PHB in the blend nanofibers is suppressed when the proportion of PVA is increased. Furthermore, the degradation was found to be dependent on the PVA fraction. The PVA-rich blend nanofibers degrade to greater extents than pure PHB fibers. On the other hand, cell culture experiments were conducted with a human keratinocyte cell line (HaCaT) and dermal fibroblast on the electrospun PHB and PVA/PHB nanofibrous scaffolds. Both cell types showed maximum adhesion and proliferation when cultured on pure PHB fibers. Addition of 5 wt % PVA to pure PHB inhibits the growth of HaCaT cells. However, the cell viability increased again by increasing the PVA fraction. PVA/PHB (50/50) showed a relatively good adhesion and proliferation of HaCaT cells after two weeks incubation promising further incubation. Selectivity could be achieved by fabricating a bilayer scaffold with a PVA/PHB (50/50) blend composition on top as support for keratinocytes, while the layer beneath would be composed of pure PHB or PVA/PHB (10/90) that favors growth of fibroblasts. The results indicated that the as spun PVA/PHB blend nanofibrous scaffolds might be a good candidate for fabricating bi-layered scaffolds for culturing epidermal and dermal cells for skin tissue engineering.

In all, the physico-chemical properties of the polymeric fibers and nanocomposite fibers can be controlled by changing electrospinning parameters, as well as by blending them with other polymers to match the desired application.

## Summary and conclusions

**Table 12. Overview on the kind of the work novelty, e.g, the type of the polymer used to produce nanofibers, obtained morphology, applications, new effect and combination of non-compatible polymers.**

Electrospun fibers	Novelty type	Applications	Remarks
PLLA/PEO	Using new polymers	Drug delivery and tissue engineering	Asran et al. <i>Macromol. Symp</i> (2010): 294-I, 153–161.
PET/ $\gamma$ -Fe <sub>2</sub> O <sub>3</sub>	Using new polymers	Tissue engineering	Asran et al. ( <i>in Press</i> )
PEI/EVA	Using new polymers	Drug delivery and tissue engineering	Asran et al. ( <i>in Press</i> )
PHB/CTS	Using new polymers and combining these polymers at the macromolecular region	Skin tissue engineering	Asran et al. ( <i>in Press</i> )
PVA/Col	Using new polymers and mimicking the ECM of bone	Bone tissue engineering	Asran et al. <i>Polymer</i> (2010): 51, 868–876 & <i>Bioinsp. Biomim.</i> (2008): 3, 046003 (12pp)
PVA/n-HAP	Using new polymers polymers and mimicking the ECM of bone	Bone tissue engineering	<i>Deutsches Patent</i>
PVA/Col/n-HAp	Using new polymers and mimicking the ECM of bone	Bone tissue engineering	Asran et al. <i>Biomacromolecules</i> (2010) 11, 3413–3421
PMMA/EVA	Combining the non-compatible polymers at the macromolecular region	Dentistry (denture and mouth guards)	Asran et al. <i>J Appl Polymer Sci</i> (accepted manuscript)
PVA/PHB	Using new polymers and mimicking the ECM of skin	Skin tissue engineering	Asran et al. ( <i>in Press</i> )
PS	Transition of PS from brittle to ductile	Material science and filter applications	Asran et al. ( <i>in press</i> )
PEI nanofibers	Obtaining a ribbon-like and bead structure from this polymer	Tissue engineering	Asran et al. ( <i>in Press</i> )
PEO/ $\gamma$ -Fe <sub>2</sub> O <sub>3</sub>	Obtaining a twisted structure from this polymer	Tissue engineering	Asran et al. <i>Biomacromolecules</i> (2010): 11, 3413–3421
CTS	Using a new solvent	Tissue engineering	Asran et al. <i>Macromol. Symp</i> (2010): 294-I, 153–161

### 6. References

1. Feynman R. There's Plenty of Room at the Bottom: An invitation to Enter a New Field of Physics. Talk at the Annual Meeting of the American Physical Society; 1959.
2. Jotterand F, Whitman AG, Lambert PJ, Dyson OF, Akula SM. Applications of Nanotechnology in the Biomedical Sciences: Small Materials, Big Impacts, and Unknown Consequences. In: Spicker SF, Engelhardt HT, Wildes SJKW, Agich GJ, Capaldi N, Erde E, et al., editors. Emerging Conceptual, Ethical and Policy Issues in Bionanotechnology. Netherlands: Springer; 2008. p. 117-30.
3. Huang ZM, Zhang YZ, Kotaki M, Ramakrishna S. A review on polymer nanofibers by electrospinning and their applications in nanocomposites. *Composites Science and Technology* 2003;63(15):2223-53.
4. Zhang Y, Venugopal JR, El-Turki A, Ramakrishna S, Su B, Lim CT. Electrospun biomimetic nanocomposite nanofibers of hydroxyapatite/chitosan for bone tissue engineering. *Biomaterials* 2008;29(32):4314-22.
5. Yang F, Murugan R, Wang S, Ramakrishna S. Electrospinning of nano/micro scale poly(L-lactic acid) aligned fibers and their potential in neural tissue engineering. *Biomaterials* 2005;26(15):2603-10.
6. Xu CY, Inai R, Kotaki M, Ramakrishna S. Aligned biodegradable nanofibrous structure: a potential scaffold for blood vessel engineering. *Biomaterials* 2004;25:877-86.
7. Venugopal J, Vadgama P, Kumar TSS, Ramakrishna S. Biocomposite nanofibres and osteoblasts for bone tissue engineering. *Nanotechnology* 2007;18(5):055101.
8. Greiner A, Wendorff Joachim H. Electrospinning: A Fascinating Method for the Preparation of Ultrathin Fibers. *Angewandte Chemie International Edition* 2007;46(30):5670-703.
9. Reneker DH, Chun I. Nanometre diameter fibres of polymer, produced by electrospinning. *Nanotechnology* 1996;7(3):216-23.
10. Taniguchi N. On the Basic Concept of "Nano-Technology". *Proc. Intl. Conf. Prod. Eng.* London: British Society of Precision Engineering; 1974.
11. Drexler KE. Molecular engineering: An approach to the development of general capabilities for molecular manipulation. *Proceedings of the National Academy of Sciences of the United States of America* 1981;78(9):5275-78.

## References

---

12. Drexler KE. Engines of Creation: The Coming Era of Nanotechnology. New York: Anchor; 1986.
13. Hullavarad NV, Hullavarad SS, Karulkar PC. Cadmium sulphide (CdS) nanotechnology: synthesis and applications. *J Nanosci Nanotechnol* 2008;8(7):3272-99.
14. Ramakrishna S, Fujihara K, Teo W-E, Lim T-C, Ma Z. An Introduction to Electrospinning and Nanofibers. Singapore: World Scientific Publishing Co Pte Ltd 2005.
15. Fang J, Niu H, Lin T, Wang X. Applications of electrospun nanofibers. *Chinese Science Bulletin* 2008;53(15):2265-86.
16. Ramakrishna S, Fujihara K, Teo W-E, Yong T, Ma Z, Ramaseshan R. Electrospun nanofibers: solving global issues. *Materials Today* 2006;9(3):40-50.
17. Xing XB, Wang YQ, Li BJ. Nanofiber drawing and nanodevice assembly in poly(trimethylene terephthalate). *Optics Express* 2008;16(14):10815-22.
18. Hulteen JC, Chen HX, Chambliss CK, Martin CR. Template synthesis of carbon nanotubule and nanofiber arrays. *Nanostructured Materials* 1997;9(1-8):133-36.
19. Liu X, Ma PX. Phase separation, pore structure, and properties of nanofibrous gelatin scaffolds. *Biomaterials* 2009;30(25):4094-103.
20. Sargeant TD, Guler MO, Oppenheimer SM, Mata A, Satcher RL, Dunand DC, et al. Hybrid bone implants: Self-assembly of peptide amphiphile nanofibers within porous titanium. *Biomaterials* 2008;29(2):161-71.
21. Goddard WA, Lyshevski SE, Goddard WA, Brenner DW, Iafrate GJ. Handbook of Nanoscience, Engineering, and Technology. New York: Taylor & Francis, Inc; 2007.
22. Formhals A, inventor. Process and apparatus for preparing artificial threads. US patent 1975504. 1934.
23. Hohman MM, Shin M, Rutledge G, Brenner MP. Electrospinning and electrically forced jets. I. Stability theory. *Physics of Fluids* 2001;13(8):2201-20.
24. Shao C, Kim H-Y, Gong J, Ding B, Lee D-R, Park S-J. Fiber mats of poly(vinyl alcohol)/silica composite via electrospinning. *Materials Letters* 2003;57(9-10):1579-84.
25. Barhate RS, Ramakrishna S. Nanofibrous filtering media: Filtration problems and solutions from tiny materials. *Journal of Membrane Science* 2007;296(1-2):1-8.

## References

---

26. Choi SW, Jo SM, Lee WS, Kim YR. An electrospun poly(vinylidene fluoride) nanofibrous membrane and its battery applications. *Advanced Materials* 2003;15(23):2027-32.
27. Krishnan J, Kotaki M, Yanzhong Z, Xiumei M, Ramakrishna S. Recent Advances in Polymer Nanofibers. *Journal of Nanoscience and Nanotechnology* 2004;4:52-65.
28. Zeng J, Yang L, Liang Q, Zhang X, Guan H, Xu X, et al. Influence of the drug compatibility with polymer solution on the release kinetics of electrospun fiber formulation. *Journal of Controlled Release* 2005;105(1-2):43-51.
29. Khil M-S, Cha D-I, Kim H-Y, Kim I-S, Bhattarai N. Electrospun nanofibrous polyurethane membrane as wound dressing. *Journal of Biomedical Materials Research Part B: Applied Biomaterials* 2003;67B(2):675-79.
30. Buttafoco L, Kolkman NG, Poot AA, Dijkstra PJ, Vermes I, Feijen J. Electrospinning collagen and elastin for tissue engineering small diameter blood vessels. *Journal of Controlled Release* 2005;101(1-3):322-24.
31. Saslow WM. *Electricity, Magnetism, and Light*. New York: Academic Press; 2002.
32. Cooley JF, inventor. Apparatus for electrically dispersing fluids. US patent 692631. 1902.
33. Morton WJ, inventor. Method of dispersing fluids. US patent 705691. 1902.
34. Formhals A, inventor. Spinner for Synthetic Fibers. US patent 2,349,950. 1944.
35. Norton CL, inventor. Method of and apparatus for producing fibrous or filamentary material. US patent 2048651. 1936.
36. Melcher JR, Taylor GI. Electrohydrodynamics: A Review of the Role of Interfacial Shear Stresses. *Annual Review of Fluid Mechanics* 1969;1(1): 111-46.
37. Doshi J, Reneker DH. Electrospinning process and applications of electrospun fibers. *J. Electrostat* 1995;35:151-60.
38. Reneker DH, Yarin AL, Fong H, Koombhongse S. Bending instability of electrically charged liquid jets of polymer solutions in electrospinning. *Journal of Applied Physics* 2000;87(9):4531-47.
39. Zhang YZ, Feng Y, Huang Z-M, Ramakrishna S, Lim CT. Fabrication of porous electrospun nanofibres. *Nanotechnology* 2006;17(3):901-08.
40. Koombhongse S, Liu W, Reneker DH. Flat polymer ribbons and other shapes by electrospinning. *Journal of Polymer Science Part B: Polymer Physics* 2001;39(21):2598-606.

## References

---

41. McCann JT, Chen JIL, Li D, Ye Z-G, Xia Y. Electrospinning of polycrystalline barium titanate nanofibers with controllable morphology and alignment. *Chemical Physics Letters* 2006;424(1-3):162-66.
42. Kessick R, Tepper G. Microscale polymeric helical structures produced by electrospinning. *Applied Physics Letters* 2004;84(23):4807-09.
43. Sun Z, Zussman E, Yarin AL, Wendorff JH, Greiner A. Compound Core-Shell Polymer Nanofibers by Co-Electrospinning. *Advanced Materials* 2003;15(22):1929-32.
44. Fong H, Chun I, Reneker DH. Beaded nanofibers formed during electrospinning. *Polymer* 1999;40(16):4585-92.
45. Yao C, Li X, Song T. Electrospinning and crosslinking of zein nanofiber mats. *Journal of Applied Polymer Science* 2007;103(1):380-85.
46. Tan EPS, Lim CT. Mechanical characterization of nanofibers - A review. *Composites Science and Technology* 2006;66(9):1102-11.
47. Li WJ, Danielson KG, Alexander PG, Tuan RS. Biological response of chondrocytes cultured in three-dimensional nanofibrous poly(epsilon-caprolactone) scaffolds. *Journal of Biomedical Materials Research Part A* 2003;67A(4):1105-14.
48. Gosiewska A, Rezanian A, Dhanaraj S, Vyakarnam M, Zhou J, Burtis D, et al. Development of a three-dimensional transmigration assay for testing cell-polymer interactions for tissue engineering applications. *Tissue Engineering* 2001;7(3):267-77.
49. Li W-J, Laurencin CT, Caterson EJ, Tuan RS, Ko FK. Electrospun nanofibrous structure: A novel scaffold for tissue engineering. *Journal of Biomedical Materials Research* 2002;60(4):613-21.
50. Li WJ, Mauck RL, Cooper JA, Yuan XN, Tuan RS. Engineering controllable anisotropy in electrospun biodegradable nanofibrous scaffolds for musculoskeletal tissue engineering. *Journal of Biomechanics* 2007;40(8):1686-93.
51. Teo WE, Ramakrishna S. A review on electrospinning design and nanofibre assemblies. *Nanotechnology* 2006;17(14):R89-R106.
52. Lucia HI-M, Julio RB, Rodrigo CB. Mechanical and thermal properties of poly(3-hydroxybutyrate) blends with starch and starch derivatives. *Macromolecular Symposia* 2003;197(1):77-88.
53. Bates FS. Polymer-Polymer Phase-Behavior. *Science* 1991;251(4996):898-905.
54. Michler GH. *Electron Microscopy of Polymers*. Berlin: Springer; 2008.

## References

---

55. Peng P, Chen Y-Z, Gao Y-F, Yu J, Guo Z-X. Phase morphology and mechanical properties of the electrospun polyoxymethylene/polyurethane blend fiber mats. *Journal of Polymer Science Part B: Polymer Physics* 2009;47(19):1853-59.
56. Chunyi T, Pingping C, Haiqing L. Cocontinuous cellulose acetate/polyurethane composite nanofiber fabricated through electrospinning. *Polymer Engineering & Science* 2008;48(7):1296-303.
57. Xin Y, Huang ZH, Li WW, Jiang ZJ, Tong YB, Wang C. Core-sheath functional polymer nanofibers prepared by co-electro spinning. *European Polymer Journal* 2008;44(4):1040-45.
58. Crosby AJ, Lee J-Y. Polymer Nanocomposites: The “Nano” Effect on Mechanical Properties. *Polymer Reviews* 2007;47(2):217 - 29.
59. Zheng Y, Zheng Y, Ning R. Effects of nanoparticles SiO<sub>2</sub> on the performance of nanocomposites. *Materials Letters* 2003;57(19):2940-44.
60. Teng S-H, Lee E-J, Wang P, Kim H-E. Collagen/hydroxyapatite composite nanofibers by electrospinning. *Materials Letters* 2008;62(17-18):3055-58.
61. Asran AS, Henning S, Michler GH. Polyvinyl alcohol-collagen-hydroxyapatite biocomposite nanofibrous scaffold: Mimicking the key features of natural bone at the nanoscale level. *Polymer* 2010;51(4):868-76.
62. Fratzl P. Biomimetic materials research: what can we really learn from nature's structural materials? *J R Soc Interface* 2007;4(15):637-42.
63. Bar-Cohen Y. Biomimetics-using nature to inspire human innovation. *Bioinspiration & Biomimetics* 2006;1(1):P1-P12.
64. Nayar S, Pramanick AK, Sharma BK, Das G, Kumar BR, Sinha A. Biomimetically synthesized polymer-hydroxyapatite sheet like nano-composite. *Mater Sci: Mater Med* 2008;19:301-04.
65. Fratzl P, Weinkamer R. Hierarchical Structure and Repair of Bone: Deformation, Remodelling, Healing. *Self healing materials: an alternative approach to 20 centuries of materials science*. Berlin: Springer; 2008. p. 323-35.
66. Ghasemi-Mobarakeh L, Semnani D, Morshed M. A novel method for porosity measurement of various surface layers of nanofibers mat using image analysis for tissue engineering applications. *Journal of Applied Polymer Science* 2007;106(4):2536-42.

## References

---

67. Barham PJ, Keller A, Otun EL, Holmes PA. Crystallization and morphology of a bacterial thermoplastic: poly-3-hydroxybutyrate. *Journal of Materials Science* 1984;19:2781-94.
68. Tubbs RK. Melting point and heat of fusion of poly(vinyl alcohol). *J Polym Sci A* 1965;3(12):4181 - 89.
69. Colette S, Bridgette AB. Fourier Transform Infrared Spectroscopy: A Molecular Approach to an Organismal Question. *Journal of Phycology* 2001;37(2):197-99.
70. Quinteiro Rodríguez MP. Fourier Transform Infrared (FTIR) Technology for the Identification of Organisms. *Clinical Microbiology Newsletter* 2000;22(8):57-61.
71. Kansiz M, Domínguez-Vidal A, McNaughton D, Lendl B. Fourier-transform infrared (FTIR) spectroscopy for monitoring and determining the degree of crystallisation of polyhydroxyalkanoates (PHAs). *Analytical and Bioanalytical Chemistry* 2007;388(5):1207-13.
72. Müller RH, Davis SS, Illum L, Mark E. Particle Charge and Surface Hydrophobicity of Colloidal Drug Carriers In: G. Gregoriadis JSaGP, editor. *Targeting of Drugs with Synthetic Systems* Plenum, New York; 1986. p. 239-63
73. Jarusuwannapoom T, Hongrojjanawiwat W, Jitjaicham S, Wannatong L, Nithitanakul M, Pattamaprom C, et al. Effect of solvents on electro-spinnability of polystyrene solutions and morphological appearance of resulting electrospun polystyrene fibers. *European Polymer Journal* 2005;41(3):409-21.
74. Zhao BH, Lee IS, Han IH, Park JC, Chung SM. Effects of surface morphology on human osteosarcoma cell response. *Current Applied Physics* 2007;7(Supplement 1):e6-e10.
75. Asran AS, Salama M, Popescu C, Michler GH. Solvent Influences the Morphology and Mechanical Properties of Electrospun Poly(L-lactic acid) Scaffold for Tissue Engineering Applications. *Macromolecular Symposia* 2010;294(1):153-61.
76. Hyon SH. Biodegradable poly (lactic acid) microspheres for drug delivery systems. *Yonsei Med J* 2000;41(6):720-34.
77. Seifert B, Mihanetzis G, Groth T, Albrecht W, Richau K, Missirlis Y, et al. Polyetherimide: a new membrane-forming polymer for biomedical applications. *Artif Organs* 2002;26(2):189-99.
78. Shi C, Zhu Y, Ran X, Wang M, Su Y, Cheng T. Therapeutic potential of chitosan and its derivatives in regenerative medicine. *J Surg Res* 2006;133(2):185-92.

## References

---

79. Jiang T, Kumbar SG, Nair LS, Laurencin CT. Biologically active chitosan systems for tissue engineering and regenerative medicine. *Curr Top Med Chem* 2008;8(4):354-64.
80. Jayakumar R, Prabakaran M, Nair SV, Tamura H. Novel chitin and chitosan nanofibers in biomedical applications. *Biotechnology Advances* 2010;28(1):142-50.
81. Sombatmankhong K, Sanchavanakit N, Pavasant P, Supaphol P. Bone scaffolds from electrospun fiber mats of poly(3-hydroxybutyrate), poly(3-hydroxybutyrate-co-3-hydroxyvalerate) and their blend. *Polymer* 2007;48(5):1419-27.
82. Li XT, Zhang Y, Chen GQ. Nanofibrous polyhydroxyalkanoate matrices as cell growth supporting materials. *Biomaterials* 2008;29(27):3720-28.
83. Reis KC, Pereira J, Smith AC, Carvalho CWP, Wellner N, Yakimets I. Characterization of polyhydroxybutyrate-hydroxyvalerate (PHB-HV)/maize starch blend films. *Journal of Food Engineering* 2008;89(4):361-69.
84. Ikejima T, Inoue Y. Crystallization behavior and environmental biodegradability of the blend films of poly(3-hydroxybutyric acid) with chitin and chitosan. *Carbohydrate Polymers* 2000; 41( 4):351-56.
85. Bloembergen S, Holden DA, Hamer GK, Bluhm TL, Marchessault RH. Studies of composition and crystallinity of bacterial poly( $\beta$ -hydroxybutyrate-co- $\beta$ -hydroxyvalerate). *Macromolecules* 1986;19(11):2865-71.
86. Tetsuya I, Kaoru Y, Yoshio I. Thermal properties and crystallization behavior of poly(3-hydroxybutyric acid) in blends with chitin and chitosan. *Macromolecular Chemistry and Physics* 1999;200(2):413-21.
87. Xu J, Guo B, Yan R, Wu Q, Chen G, Zhang Z. In situ FTIR study on melting and crystallization of polyhydroxyalkanoates. *Polymer* 2002;43(25):6893-99.
88. Gunaratne LMWK, Shanks RA. Melting and thermal history of poly(hydroxybutyrate-co-hydroxyvalerate) using step-scan DSC. *Thermochimica Acta* 2005;430(1-2):183-90.
89. Wong S-C, Baji A, Leng S. Effect of fiber diameter on tensile properties of electrospun poly( $\epsilon$ -caprolactone). *Polymer* 2008;49(21):4713-22.
90. Renard E, Walls M, Guerin P, Langlois V. Hydrolytic degradation of blends of polyhydroxyalkanoates and functionalized polyhydroxyalkanoates. *Polymer Degradation and Stability* 2004;85(2):779-87.
91. Spyros A, Kimmich R, Briese BH, Jendrossek D.  $^1\text{H}$  NMR Imaging Study of Enzymatic Degradation in Poly(3-hydroxybutyrate) and Poly(3-hydroxybutyrate-co-

## References

---

- 3-hydroxyvalerate). Evidence for Preferential Degradation of the Amorphous Phase by PHB Depolymerase B from *Pseudomonas lemoignei*. *Macromolecules* 1997;30(26):8218-25.
92. Carlisle CR, Coulais C, Namboothiry M, Carroll DL, Hantgan RR, Guthold M. The mechanical properties of individual, electrospun fibrinogen fibers. *Biomaterials* 2009;30(6):1205-13.
93. Brody AL, Marsh KS. Packaging Technology. In: Brody AL, Marsh KS, editors. *The Wiley Encyclopedia of Packaging Technology*. New York: John Wiley & Sons; 1997. p. 1-12, 449-50 and 768-71.
94. Robertson GL. *Food Packaging, Principles and Practices*. New York: Marcel Dekker Inc; 1992. p. 34-36.
95. Kim G-T, Hwang Y-J, Ahn Y-C, Shin H-S, Lee J-K, Sung C-M. The morphology of electrospun polystyrene fibers. *Korean Journal of Chemical Engineering* 2005;22(1):147-53.
96. Moon S, Choi J, Farris RJ. Highly porous polyacrylonitrile/polystyrene nanofibers by electrospinning. *Fibers and Polymers* 2008;9(3):276-80.
97. Kausch HH. *Crazing in Polymers (Advances in Polymer Science, Vols 91/92)*. Berlin: Springer 1990.
98. Michler GH. *Kunststoff-Mikromechanik: Morphologie, Deformations- und Bruchmechanismen*. München: Carl Hanser; 1992.
99. Donald AM, Kramer EJ. Craze Microstructure and Molecular Entanglements in Polystyrene-Poly(Phenylene Oxide) Blends. *Polymer* 1982;23(3):461-65.
100. Kramer EJ. Craze Fibril Formation and Breakdown. *Polymer Engineering and Science* 1984;24(10):761-69.
101. Michler GH, Kausch HH, Adhikari R. Modeling of thin layer yielding in polymers. *Journal of Macromolecular Science Part B-Physics* 2006;45(5):727-39.
102. Sulkowski WW, Wolinska A, Szolysik B, Bajdur WM, Sulkowska A. Preparation and properties of flocculants derived from polystyrene waste. *Polymer Degradation and Stability* 2005;90:272-80.
103. An H, Shin C, Chase GG. Ion exchanger using electrospun polystyrene nanofibers. *Journal of Membrane Science* 2006;283(1-2):84-87.
104. Prime D, Paul S. Electrical and morphological properties of polystyrene thin films for organic electronic applications. *Vacuum* 2010;84(10):1240-43.

## References

---

105. Kuznetsov V, Sheremet'ev S. Sensing elements of optical sensors based on polystyrene with covalently immobilized reagents. *Journal of Analytical Chemistry* 2007;62(3):270-78.
106. Byun J-W, Kim J-U, Chung W-J, Lee Y-S. Surface-Grafted Polystyrene Beads with Comb-Like Poly(ethylene glycol) Chains: Preparation and Biological Application. *Macromolecular Bioscience* 2004;4(5):512-19.
107. Westerman B, Stringfellow PM, Eccleston JA. Beneficial effects of air inclusions on the performance of ethylene vinyl acetate (EVA) mouthguard material. *British Journal of Sports Medicine* 2002;36(1):51-53.
108. Newsome PRH, Tran DC, Cooke MS. The role of the mouthguard in the prevention of sports-related dental injuries: a review. *International Journal of Paediatric Dentistry* 2001;11(6):396-404.
109. Badel T, Jerolimov V, Panduric J, Carek V. Custom-made mouthguards and prevention of orofacial injuries in sports. *Acta Med Croatica* 2007;61 Suppl 1:9-14.
110. Gould TE, Piland SG, Shin J, Hoyle CE, Nazarenko S. Characterization of mouthguard materials: Physical and mechanical properties of commercialized products. *Dental Materials* 2009;25(6):771-80.
111. Braden M, Wright PS, Parker S. Soft lining materials--a review. *Eur J Prosthodont Restor Dent* 1995;3(4):163-74.
112. Whitters CJ, Strang R, Brown D, Clarke RL, Curtis RV, Hatton PV, et al. Dental materials: 1997 literature review. *Journal of Dentistry* 1999;27(6):401-35.
113. Frazer RQ, Byron RT, Osborne PB, West KP. PMMA: an essential material in medicine and dentistry. *J Long Term Eff Med Implants* 2005;15(6):629-39.
114. Jones JD. A qualitative comparison of various record base materials. *J Prosthet Dent* 1983;49(1):130-32.
115. Elias CN, Henriques FQ. Effect of thermocycling on the tensile and shear bond strengths of three soft liners to a denture base resin. *J Appl Oral Sci* 2007;15(1):18-23.
116. Kawano F, Dootz ER, Koran A, Craig RG. Comparison of bond strength of six soft denture liners to denture base resin. *The Journal of Prosthetic Dentistry* 1992;68(2):368-71.
117. Hristov I, Pavlov B, Ivanova D, Georgieva I. A comparative study on the bonding strength between the denture base and the relining materials. *Journal of IMAB-Annual Proceeding (Scientific Papers)* 2006;book 2:27-28.

## References

---

118. Dette K-E, Michler GH, Hey J, Asran AS, Arnold C, inventors. Verfahren zur Herstellung eines dauerhaften Verbundes zwischen Ethylenevinylacetat (EVA) als Weichplastmaterial und Polymethylmethacrylate (PMMA) für herausnehmbaren Zahnersatz. US patent DE 10 2010 007 956. 1. 2010.
119. Rose FRAJ, Oreffo ROC. Bone Tissue Engineering: Hope vs Hype. *Biochemical and Biophysical Research Communications* 2002;292(1):1-7.
120. Ahlborg HG, Johnell O, Turner CH, Rannevik G, Karlsson MK. Bone loss and bone size after menopause. *N Engl J Med* 2003;349(4):327-34.
121. Kao ST, Scott DD. A review of bone substitutes. *Oral Maxillofac Surg Clin North Am* 2007;19(4):513-21.
122. Venugopal J, Low S, Choon AT, Ramakrishna S. Interaction of cells and nanofiber scaffolds in tissue engineering. *J Biomed Mater Res B Appl Biomater* 2008;84(1):34-48.
123. Wahl DA, Czernuszka JT. Collagen-hydroxyapatite composites for hard tissue repair. *Eur Cell Mater* 2006;11:43-56.
124. Kikuchi M, Itoh S, Ichinose S, Shinomiya K, Tanaka J. Self-organization mechanism in a bone-like hydroxyapatite/collagen nanocomposite synthesized in vitro and its biological reaction in vivo. *Biomaterials* 2001;22(13):1705-11.
125. Jansen EJP, Sladek REJ, Bahar H, Yaffe A, Gijbels MJ, Kuijjer R, et al. Hydrophobicity as a design criterion for polymer scaffolds in bone tissue engineering. *Biomaterials* 2005;26(21):4423-31.
126. Krumova M, López D, Benavente R, Mijangos C, Pereña JM. Effect of crosslinking on the mechanical and thermal properties of poly(vinyl alcohol). *Polymer* 2000;41(26):9265-72.
127. Hyon S-H, Cha W-I, Ikada Y, Kita M, Ogura Y, Honda Y. Poly(vinyl alcohol) hydrogels as soft contact lens material. *Journal of Biomaterials Science, Polymer Edition* 1994;5:397-406.
128. Juang JH, Bonner-Weir S, Ogawa Y, Vacanti JP, Weir GC. Outcome of subcutaneous islet transplantation improved by polymer device. *Transplantation* 1996;61(11):1557-61.
129. Thanoo BC, Sunny MC, Jayakrishnan A. Controlled release of oral drugs from cross-linked polyvinyl alcohol microspheres. *J-Pharm-Pharmacol* 1993;45:16–20.

## References

---

130. Sirousazar M, Yari M. Dehydration kinetics of polyvinyl alcohol hydrogel wound dressings during wound healing process. *Chinese Journal of Polymer Science* 2010;28(4):573-80.
131. Kobayashi M, Oka M. Composite device for attachment of polyvinyl alcohol-hydrogel to underlying bone. *Artif Organs* 2004;28(8):734-8.
132. Kobayashi M, Toguchida J, Oka M. Preliminary study of polyvinyl alcohol-hydrogel (PVA-H) artificial meniscus. *Biomaterials* 2003;24(4):639-47.
133. Du C, Cui FZ, Zhu XD, Groot Kd. Three-dimensional nano-HAp/Co matrix loading with osteogenic cells in organ culture. *J Biomed Mater Res* 1999;44(Part A):407-15.
134. Jayarama Reddy V, Yanzhong Z, Seeram R. In Vitro Culture of Human Dermal Fibroblasts on Electrospun Polycaprolactone Collagen Nanofibrous Membrane. *Artificial Organs* 2006;30(6):440-46.
135. Sionkowska A, Skopinska J, Wisniewski M. Photochemical stability of Collagen/poly (vinyl alcohol) blends. *Polymer Degradation and Stability* 2004;83:117-25.
136. Jackson M, Choo L, Watson P, Halliday W, Mantsch H. Beware of connective tissue proteins: assignment and implications of Col absorptions in infrared spectra of human tissues. *Biochim Biophys Acta* 1995;1270:1-6.
137. Zong X, Kima K, Fangb D, Rana S, Hsiaoa BS, Chu. B. Structure and process relationship of electrospun bioabsorbable nanofiber membranes. *Polymer* 2002;43:4403-12.
138. Buckley CP, Kovacs AJ. In: Hall IH, editor. *Structure of Crystalline Polymers*. London: Elsevier Applied Science Publishers; 1984.
139. Persikov AV, Xu Y, Brodsky B. Equilibrium thermal transitions of Collagen model peptides *Protein Sci* 2004;13:893-902.
140. Beatrice S, Mariastella S. Viscoelastic and thermal properties of Co/poly(vinyl alcohol) blends. *Biomaterials* 1995;16:785-92.
141. Pramanik N, Biswas SK, Pramanik P. Synthesis and Characterization of Hydroxyapatite/ Poly(Vinyl Alcohol Phosphate) Nanocomposite Biomaterials. *Int. J. Appl. Ceram. Technol* 2008;5:20-28
142. Puett D. DTA and Heats of Hydration of Some Polypeptides. *Biopolymers* 1967;5:327-30.
143. Chikako N, Takeo S, Toshio Y, Masataka S. The effects of chromium compounds on PVA-coated AN and GAP binder pyrolysis, and PVA-coated AN/GAP propellant combustion. *Fuel* 1998;77:321-26.

## References

---

144. Rootare HM, Craig RG. Free Surface Energy Change for Water Adsorbed on Hydroxyapatite. *J Dent Res* 1977;56:744-47.
145. Balasubramani M, Kumar TR, Babu M. Skin substitutes: a review. *Burns* 2001;27(5):534-44.
146. Metcalfe AD, Ferguson MWJ. Tissue engineering of replacement skin: the crossroads of biomaterials, wound healing, embryonic development, stem cells and regeneration. *J R Soc Interface* 2007; 4(14):413-37.
147. Hata K-i. Current issues regarding skin substitutes using living cells as industrial materials. *Journal of Artificial Organs* 2007;10(3):129-32.
148. van der Veen VC, van der Wal MBA, van Leeuwen MCE, Ulrich MMW, Middelkoop E. Biological background of dermal substitutes. *Burns* 2009;36(3):305-21.
149. Gibbs S, van den Hoogenband HM, Kirtschig G, Richters CD, Spiekstra SW, Breetveld M, et al. Autologous full-thickness skin substitute for healing chronic wounds. *British Journal of Dermatology* 2006;155(2):267-74.
150. Lee KH. Tissue-engineered human living skin substitutes: development and clinical application. *Yonsei Med J* 2000;41(6):774-9.
151. Shores JT, Gabriel A, Gupta S. Skin substitutes and alternatives: a review. *Adv Skin Wound Care* 2007;20(9):493-508.
152. Pham C, Greenwood J, Cleland H, Woodruff P, Maddern G. Bioengineered skin substitutes for the management of burns: a systematic review. *Burns* 2007;33(8):946-57.
153. Sheridan RL, Morgan JR, Cusick JL, Petras LM, Lydon MM, Tompkins RG. Initial experience with a composite autologous skin substitute. *Burns* 2001;27(5):421-24.
154. Hu Y, Grainger DW, Winn SR, Hollinger JO. Fabrication of poly(alpha-hydroxy acid) foam scaffolds using multiple solvent systems. *Journal of Biomedical Materials Research* 2001;59(3):563-72.
155. Li W-J, Cooper JJA, Mauck RL, Tuan RS. Fabrication and characterization of six electrospun poly([alpha]-hydroxy ester)-based fibrous scaffolds for tissue engineering applications. *Acta Biomaterialia* 2006;2(4):377-85.
156. He W, Yong T, Teo WE, Ma Z, Ramakrishna S. Fabrication and Endothelialization of Collagen-Blended Biodegradable Polymer Nanofibers: Potential Vascular Graft for Blood Vessel Tissue Engineering. *Tissue Engineering* 2005;11(9-10):1574-88.

## References

---

157. Müller H-M, Seebach D. Poly(hydroxyalkanoates): A Fifth Class of Physiologically Important Organic Biopolymers? *Angewandte Chemie International Edition* 1993;32:477-502.
158. Philip S, Keshavarz T, Roy I. Polyhydroxyalkanoates: biodegradable polymers with a range of applications. *Journal of Chemical Technology & Biotechnology* 2007;82(3):233-47.
159. Harding KG, Dennis JS, von Blottnitz H, Harrison STL. Environmental analysis of plastic production processes: Comparing petroleum-based polypropylene and polyethylene with biologically-based poly-[beta]-hydroxybutyric acid using life cycle analysis. *Journal of Biotechnology* 2007;130(1):57-66.
160. Zhijiang C. Biocompatibility and Biodegradation of novel PHB porous substrates with controlled multi-pore size by emulsion templates method. *J Mater Sci: Mater Med* 2006;17:1297-303.
161. Chen G-Q, Wu Q. The application of polyhydroxyalkanoates as tissue engineering materials. *Biomaterials* 2005;26(33):6565-78.
162. Galego N, Rosza C, Sanchez R, Fung J, Vazquez A, Tomas J. Characterization and application of poly( $\beta$ -hydroxyalkanoates) family as composite biomaterials. *Polym Test* 2000;19:485-92.
163. Wu Q, Wang Y, Chen GQ. Medical application of microbial biopolyesters polyhydroxyalkanoates. *Artif Cells Blood Substit Immobil Biotechnol* 2009;37(1):1-12.
164. Songling X, Rongcong L, Linping W, Kaitian X, Guo-Qiang C. Blending and characterizations of microbial poly(3-hydroxybutyrate) with dendrimers. *Journal of Applied Polymer Science* 2006;102(4):3782-90.
165. Avella M, Martuscelli E. Poly-D(-)(3-hydroxybutyrate)/poly(ethylene oxide) blends: phase diagram, thermal and crystallization behaviour. *Polymer* 1988;29(11):1731-37.
166. Greco P, Martuscelli E. Crystallization and thermal behavior of poly(D(-)-3-hydroxybutyrate)-based blends. *Polymer* 1989;30(8):1475-83.
167. McCarthy SP, Gross R. *Proceedings of Environmentally Degradable Polymers: Technical, Business, and Public Perspectives*. Chelmsford, MA 1991.
168. Kaito A, Li Y, Shimomura M, Nojima S. Oriented lamellar structures in uniaxially drawn films of poly(vinylidene fluoride) and poly(3-hydroxybutyrate) blends studied

## References

---

- by small-angle X-ray scattering measurements. *Journal of Polymer Science Part B: Polymer Physics* 2009;47(4):381-92.
169. Chen J, Zhang Y, Du G-C, Hua Z-Z, Zhu Y. Biodegradation of polyvinyl alcohol by a mixed microbial culture. *Enzyme and Microbial Technology* 2007; 40( 7):1686-91.
170. Koski A, Yim K, Shivkumar S. Effect of molecular weight on fibrous PVA produced by electrospinning. *Mater. Lett* 2004; 58 (3-4):493-97.
171. Chiellini E, Corti A, D'Antone S, Solaro R. Biodegradation of poly (vinyl alcohol) based materials. *Progress in Polymer Science* 2003;28(6):963-1014.
172. Paradossi G, Cavalieri F, Chiessi E, Spagnoli C, Cowman M. Poly(vinyl alcohol) as versatile biomaterial for potential biomedical applications. *J Mater Sci Mater Med* 2003;14(8):687-91.
173. Zhao L, Tsuchiya K, Inoue Y. Fully-Biodegradable Poly(3-hydroxybutyrate)/Poly(vinyl alcohol) Blend Films with Compositional Gradient. *Macromol. Biosci* 2004;4(8):699-705.
174. Xing P, Ai X, Dong L, Feng Z. Miscibility and Crystallization of Poly(3-hydroxybutyrate)/Poly(vinyl acetate-co-vinyl alcohol) Blends. *Macromolecules* 1998; 31 (20): 6898-907.
175. Yoshie N, Azuma Y, Sakurai M, Inoue Y. Crystallization and compatibility of poly(vinyl alcohol)/poly(3-hydroxybutyrate) blends: Influence of blend composition and tacticity of poly(vinyl alcohol). *Journal of Applied Polymer Science* 1995;56(1):17-24.
176. Azuma Y, Yoshie N, Sakurai M, Inoue Y, Chûjô R. Thermal behaviour and miscibility of poly(3-hydroxybutyrate)/poly(vinyl alcohol) blends. *Polymer* 1992;33(22):4763-67.
177. Ikejima T, Yoshie N, Inoue Y. Influence of tacticity and molecular weight of poly(vinyl alcohol) on crystallization and biodegradation of poly(3-hydroxybutyric acid)/poly(vinyl alcohol) blend films. *Polymer Degradation and Stability* 1999;66(2):263-70.
178. Xie J, Li X, Xia Y. Putting Electrospun Nanofibers to Work for Biomedical Research. *Macromol Rapid Commun* 2008;29(22):1775-92.
179. Ma M, Krikorian V, Yu JH, Thomas EL, Rutledge GC. Electrospun polymer nanofibers with internal periodic structure obtained by microphase separation of cylindrically confined block copolymers. *Nano Lett* 2006;6(12):2969-72.

## References

---

180. Ikejima T, Cao A, Yoshie N, Inoue Y. Surface composition and biodegradability of poly(3-hydroxybutyric acid)/poly(vinyl alcohol) blend films. *Polymer Degradation and Stability* 1998;62(3): 463-69.
181. Tandon V, Bhagavatula SK, Nelson WC, Kirby BJ. zeta potential and electroosmotic mobility in microfluidic devices fabricated from hydrophobic polymers: 1. The origins of charge. *Electrophoresis* 2008;29(5):1092-101.
182. Isci S, Unlu CH, Atici O, Gungor N. Rheology and structure of aqueous bentonite-polyvinyl alcohol dispersions. *Bulletin of Materials Science* 2006;29(5):449-56.
183. Altankov G, Richau K, Groth T. The role of surface zeta potential and substratum chemistry for regulation of dermal fibroblasts interaction. *Materialwissenschaft und Werkstofftechnik* 2003;34(12):1120-28.
184. Somasundaran P, Hubbard A. *Encyclopedia of Surface and Colloid Science*. New York: CRC Press; 2006.
185. Kecskemeti G, Smausz T, Kresz N, Toth Z, Hopp B, Chrisey D, et al. Pulsed laser deposition of polyhydroxybutyrate biodegradable polymer thin films using ArF excimer laser. *Applied Surface Science* 2006;253(3):1185-89.
186. Andrade G, Barbosa-Stancioli EF, Mansur AAP, Vasconcelos WL, Mansur HS. Design of novel hybrid organic–inorganic nanostructured biomaterials for immunoassay applications *Biomed. Mater* 2006;1:221–34.
187. Guo L, Sato H, Hashimoto T, Ozaki Y. FTIR Study on Hydrogen-Bonding Interactions in Biodegradable Polymer Blends of Poly(3-hydroxybutyrate) and Poly(4-vinylphenol). *Macromolecules* 2010;43(8):3897-902.
188. Yi JZ, Goh SH. Miscibility and interactions in poly(n-propyl methacrylate)/poly(vinyl alcohol) blends. *Polymer* 2005;46(21):9170-75.
189. El-Hadi A, Schnabel R, Straube E, Müller G, Henning S. Correlation between degree of crystallinity, morphology, glass temperature, mechanical properties and biodegradation of poly (3-hydroxyalkanoate) PHAs and their blends. *Polymer Testing* 2002;21(6): 613-733.
190. Roberto S, Andrea C, Emo C. Biodegradation of poly(vinyl alcohol) with different molecular weights and degree of hydrolysis. *Polymers for Advanced Technologies* 2000;11(8-12):873-78.
191. Freier T, Kunze C, Nischan C, Kramer S, Sternberg K, Saß M, et al. In vitro and in vivo degradation studies for development of a biodegradable patch based on poly(3-hydroxybutyrate). *Biomaterials* 2002;23(13):2649-57.

## References

---

192. Majid MIA, Ismail J, Few LL, Tan CF. The degradation kinetics of poly(3-hydroxybutyrate) under non-aqueous and aqueous conditions. *European Polymer Journal* 2002;38(4):837-39.
193. Tsuji H, Suzuyoshi K. Environmental degradation of biodegradable polyesters 2. Poly(epsilon-caprolactone), poly [(R)-3-hydroxybutyrate], and poly(L-lactide) films in natural dynamic seawater. *Polymer Degradation and Stability* 2002;75(2):357-65.
194. Naira LS, Laurencin CT. Biodegradable polymers as biomaterials. *Prog. Polym. Sci* 2007;32(8-9):762-98.
195. Scott G. *Degradable polymers: principles and applications*. Dordrecht: Kluwer Academic Publishers; 2002.
196. Holland SJ, Jolly AM, Yasin M, Tighe BJ. Polymers for biodegradable medical devices. II. Hydroxybutyrate-hydroxyvalerate copolymers: hydrolytic degradation studies. *Biomaterials* 1987;8(4):289-95.
197. Loh XJ, Goh SH, Li J. Hydrolytic degradation and protein release studies of thermogelling polyurethane copolymers consisting of poly[(R)-3-hydroxybutyrate], poly(ethylene glycol), and poly(propylene glycol). *Biomaterials* 2007;28(28):4113-23.
198. Ikejima T, Inoue Y. Experimental approaches to generate compositional gradients in the fully biodegradable polymer blend system based on poly(3-hydroxybutyric acid). *Macromolecular Chemistry and Physics* 2000;201(14):1598-604.
199. Peschel G, Dahse HM, Konrad A, Wieland GD, Mueller PJ, Martin DP, et al. Growth of keratinocytes on porous films of poly(3-hydroxybutyrate) and poly(4-hydroxybutyrate) blended with hyaluronic acid and chitosan. *J Biomed Mater Res A* 2008;85(4):1072-81.
200. Groth T, Seifert B, Malsch G, Albrecht W, Paul D, Kostadinova A, et al. Interaction of human skin fibroblasts with moderate wettable polyacrylonitrile-copolymer membranes. *J Biomed Mater Res* 2002;61(2):290-300.
201. Ren Q, Kari C, Quadros MRD, Burd R, McCue P, Dicker AP, et al. Malignant Transformation of Immortalized HaCaT Keratinocytes through Deregulated Nuclear Factor k B Signaling. *Cancer Res* 2006;66(10):5209-15.

## List of publications

### *Articles*

1. G. H. Michler, A. Sh. Asran, G.-M. Kim. Nanofibres-Preparation, Morphology, Mechanical and Biomedical Properties. **5<sup>th</sup> International Conference of Textile Research Division**, 6 – 8 April (2008). Cairo, Egypt.
2. Gyeong-Man Kim, Ashraf Sh Asran, Georg H Michler, Paul Simon and Jeong-Sook Kim. Electrospun PVA/HAp nanocomposite nanofibers: biomimetics of mineralized hard tissues at a lower level of complexity. **Bioinsp. Biomim.** **3** (2008) 046003 (1-12).
3. G.H. Michler, A. Sh. Asran, G.M. Kim, V. Seydewitz. Nanofibers from polymer nanocomposites by electro static spinning process. **6<sup>th</sup> International Conference of Textile Research Division**, 5 – 7 April (2009). Cairo, Egypt.
4. A. Sh Asran, S Henning, G H Michler. Polyvinyl alcohol–collagen–hydroxyapatite biocomposite nanofibrous scaffold: Mimicking the key features of natural bone at the nanoscale level. **Polymer** 2010; 51(4):868-876.
5. A. Sh. Asran, M. Salama, C. Popescu, G.H. Michler. Solvent Influences the Morphology and Mechanical Properties of Electrospun Poly(L-lactic acid) Scaffold for Tissue Engineering Applications. **Macromolecular Symposia**, Volume 294, Issue 1, pages 153–161, 2010.
6. Khashayar Razghandi. Electrospinning of PVA-PHB blend nanofibers as a scaffold for skin tissue engineering. **Master Thesis**. Supporvised by : Prof. Dr. Thomas Groth, Prof. Dr. Goerg H. Michler and M.Sc Ashraf Sh. Asran. Martin-Luther-University Halle-Wittenberg, Institute of Pharmacy. January 2010.
7. A. Sh. Asran, V. Seydewitz, G.H. Michler. Micromechanical properties and ductile behaviour of electrospun polystyrene nanofibers. **Journal of Applied Polymer Science**, 2010 (In press)
8. Ashraf Sh. Asran, Kashayar Razghandi, Neha Aggarwal, Goerg H. Michler, T Groth. Nanofibers from Blends of Polyvinyl Alcohol and Polyhydroxy Butyrate As Potential Scaffold Material for Tissue Engineering of Skin. **Biomacromolecules**, 2010, 11 (12), pp 3413–3421.
9. Ashraf Sh. Asran and Goerg H. Michler. Morphological and thermal analysis of electrospun polyhydroxy butyrate/chitosan blend nanofibers as a scaffold for tissue engineering applications. 2010 (**in press**).

10. K.-E. Dette, G.H. Michler, J. Hey, A. Sh. Asran and Chr. Arnold. **Deutsch Patent.**“Verfahren zur Herstellung eines dauerhaften Verbundes zwischen Ethylenevinylacetat (EVA) als Weichplastmaterial und Polymethylmethacrylate (PMMA) für herausnehmbaren Zahnersatz“ Aktenzeichen DE 10 2010 007 956. 1.

### *Oral lectures*

1. G.-M. Kim, A. Sh. Asran, G.H. Michler. Polymer nanofibres for biomedical applications, 12<sup>th</sup> Symposium "Nanostructured Biomaterials: Characterization and Properties" Lutherstadt Wittenberg, Germany., 10 - 11 Mai 2007.
2. G.-M. Kim, A. Sh. Asran, G. H. Michler. Biomimetics based on polymer nanocomposite nanofibers via electrospinning technique. The international conference Bio meets Nano and IT Halle/S. 4-5 Dec 2007.
3. G. H. Michler, A. Sh. Asran, G.-M. Kim. Nanofibres-Preparation, Morphology, Mechanical and Biomedical Properties. 5<sup>th</sup> International Conference of Textile Research Division. April 6 – 8 (2008). Cairo, Egypt.
4. G. H. Michler, A. Sh. Asran. Nanofibers from polymer nanocomposites by electrostatic spinning process. 6<sup>th</sup> International Conference of Textile Research Division. April 5 – 7 (2009). Cairo, Egypt.
5. A. Sh. Asran, V. Seydewitz, G. H. Michler. Mechanical transitions in electrospun polymer nanofibers. 13<sup>th</sup> Symposium on "Layered Nanostructures: Polymers with Improved Properties". Wittenberg, Saxony Anhalt, Germany, 12-13 May 2009.
6. A. Sh. Asran, G. H. Michler. Polymer Nanofibres: Preparation and Properties. 12<sup>th</sup> International and Interdisciplinary Symposium. Biomaterials and Biomechanics: Fundamentals and Clinical Applications March 17-19, 2010.
7. A. Sh. Asran, V. Seydewitz, G. H. Michler. Mechanical properties of electrospun nanofibers. 14<sup>th</sup> Symposium Electron Microscopy in Materials Science "Nanostructured Polymers / Nanocomposites" 18 - 19 May 2010, Francke Foundations, Halle (Saale), Germany.
8. G. H. Michler, A. Sh. Asran. Electrospun nanofibers for material science and medical applications. 7<sup>th</sup> International Conference of Textile Research Division. October 10 – 12 (2010). Cairo, Egypt.

## *Posters*

1. H. Schneider, G.-M. Kim, A. Sh. Asran, M. Busch, H. Jentsch, G. H. Michler. Resin-based Composite Restorations on Human Molars with Polymer Nanofiber-reinforced Adhesive Layer, 12th Symposium "Nanostructured Biomaterials: Characterization and Properties" Lutherstadt Wittenberg, Germany, 10 - 11 Mai 2007.
2. A. Sh. Asran, G.-M. Kim, G.H. Michler. Bioactive polymerfibers prepared by electrospinning for biomedical applications, 12th Symposium "Nanostructured Biomaterials: Characterization and Properties" Lutherstadt Wittenberg, Germany, 10 - 11 Mai 2007.
3. A. Sh. Asran, G.-M. Kim, G.H. Michler. Biocompatible electrospun fibers for tissue scaffolds and drug delivery systems. 15 Jähriges Bestehen des IPW, Merseburg die Festveranstaltung anlässlich des 15 jährigen Bestehens des IPW statt, 11. Juni 2007.
4. G.M. Kim, A. Sh. Asran, G. H. Michler. Prospective of Polyme Nanofibers Produced by Electrospinning Process. Soft meets Hard-Structure and Properties under Confinement International Workshop, LEUCOREA Lutherstadt Wittenberg, Germany. 12-13 September 2007.
5. A. Sh. Asran, G.-M. Kim, G.H. Michler. Preparation of polylactic acid composite fibers via electrospinning technique as scaffolds for tissue engineering. The international conference Bio meets Nano and IT Halle (Saale), Germany, 4-5 Dec 2007.
6. A. Sh. Asran, M. Salama, C. Popescu, G.H. Michler. Solvent influences on the morphology and crystallinity of electrospun poly (L-lactic acid) as a biomaterial for tissue engineering applications. 13th Internationale Fachtagung "Polymerwerkstoffe P2008" Halle (Saale), 24. - 26. September 2008.
7. A. Sh. Asran , G.H. Michler. Morphological study of electrospun Polyetherimide nanofibers as a scaffold for potential applications in regenerative medicine. 13th Symposium on "Layered Nanostructures: Polymers with Improved Properties". Wittenberg, Saxony Anhalt, Germany, 12-13 May 2009.
8. A Sh Asran, S Henning, G H Michler. Bio-inspired nanofibers nanocomposite for bone tissue engineering. 12<sup>th</sup> International and Interdisciplinary Symposium. Biomaterials and Biomechanics: Fundamentals and Clinical Applications University Duisburg-Essen, Germany March 17-19, 2010.

## Curriculum Vitae

Ashraf Sh Asran, Ph.D. Student

---

Allgemeine Werkstoffwissenschaften  
Martin-Luther-Universität Halle-Wittenberg  
Institut für Physik  
D-06099 Halle (Saale)



### **Contact information**

Tel. +49 (0)345 55 25405

Fax. +49 (0) 345 55 27149

E-mail: [ashraf.abdel-sayed@physik.uni-halle.de](mailto:ashraf.abdel-sayed@physik.uni-halle.de)

Mailing address:

Abdel Sayed, Ashraf Shaban Asran

Martin-Luther-Universität Halle-Wittenberg

Institute für Physik

von-Danckelmann-Platz 3

D-06120 Halle (Saale)

### **Professional experience**

**12/2006-present**

**Ph.D Scholarchip**

Martin-Luther-Universität Halle-Wittenberg  
Institute of Physics  
Group of General Material Science

**8/2004 – 12-2006**

**Assistant Researcher**

National Research Center,  
El-Bohous St., 12311 Dokki, Giza, Egypt.

**5/2003 - 8/2004**

**Research Assistant**

National Research Center,  
El-Bohous St., 12311 Dokki, Giza, Egypt.

## **Educational background**

**12/2006-present**

**Ph.D in Material Science**

Martin-Luther-Universität Halle-Wittenberg

Institut für Physik

Dissertation: Electrostatic spinning of nanofibers and nanocomposites polymeric materials: Fabrication, physicochemical characterization and biomedical applications

Supervised by

Prof. Dr. rer. nat. habil. Goerg H. Michler

Telefon: (+49) 0345 / 55 25401 oder 25400

Fax: (+49) 0345 / 55 27149

E-Mail: goerg.michler@physik.uni-halle.de

**10/2001- 6/2004**

**M.Sc. Applied Chemistry**

Al Azhar University, Department of Chemistry, Faculty of Science, Egypt.

Thesis: Preparation, Characterization and Utilization of Some Water Soluble Polymers

Note: All Subjects in B.Sc. and M.Sc was in English Language.

**10/1995-5/1999**

**B.Sc. in Special Chemistry**

Al Azhar University, Department of Chemistry, Faculty of Science, Egypt.

General Estimation of “Very good”.

## **Profile**

Integrated background in Organic chemistry with comprehensive research experience in polymers science; preparation, characterization and their biomedical applications. Mr. Asran participated in a research project in Egypt to develop the medical textile industry, which is entitled “Road Map”. In addition, Mr Asran participated in a research project entitled (Cellulose/Chitosan Nano Fiber Blends in Medical Care Application), Co-Operation between National Research Centre & Textile College at North Carolina State University. Furthermore, Mr Asran participated in DAAD project for preservation and conservation of archaeological antiques as project assistance. The project is entitled “Nanotechnology-based processes for conservation and preservation of archaeological antiques (Flax, Wool, Papyrus or Wood) made from natural polymers”.

## **Achievements**

One of the organizing committee of the “ 1<sup>st</sup>, 2<sup>nd</sup> and 3<sup>rd</sup> “ International Conference of Textile Research Division” National Research Center, Cairo, Egypt. (2004, 2005 and 2006).

## **Personal Activities**

- Member of Egyptian Syndicate of Scientific professions
- Member of Institut für Polymerwerkstoffe e.V. (IPW)

## **Personal**

- Highly adaptable, geographically flexible.

## **Other skills**

Languages:

Fluent in English (Spoken & Writing)

Germany: **Niveaustufe B1**, Goethe Institutes, Cairo.

**Computer: International Computer Driving Licence (Windows, Office, Internet, Photoshop, Image analysis software, OriginLab).**

## **Training course**

- Analytical Chemistry (HPLC, IR, G.C Mass, Atomic Absorption, BOD, COD, Water Analysis, Biological Analysis).
- Electron microscopy ( SEM, TEM)
- Culturing the human cells